Current Awareness Bulletin

of

SCHOLARLY ARTICLES PUBLISHED

BY

Faculty, Students and Alumni

~ April 2012 ~

DELHI TECHNOLOGICAL UNIVERSITY CENTRAL LIBRARY
(formerly Delhi College of Engineering, Bawana Road, DELHI)

PREFACE

This is the first Current Awareness Bulletin Service started by Delhi Technological University Library. The aim of the bulletin is to compile, preserve and disseminate information published by the Faculty, Students and Alumni for mutual benefits. The bulletin also aims to propagate the intellectual contribution of DTU as a whole to the academia. It contains information resources available in the internet in the form of articles, reports, presentation published in international journals, websites, etc. by the faculty and students of Delhi Technological University in the field of science and technology. The publication of Faculty and Students which are not covered in this bulletin may be because of the reason that either the full text was not accessible or could not be searched by the search engine used by the library for this purpose. To make the bulletin more comprehensive, the learned faculty and Students may provide their uncovered publication to the library either through email or in CD, etc.

This issue contains the information published during April 2012. The arrangement of the contents is alphabetical wise starting from A-Z. The Full text of the article which is either subscribed by the University or available in the web has been provided in this Bulletin.

CONTENTS

*Faculty
@Students/Research Scholars
Alumni

Indian Pacing Electrophysiol. J. 2012;12(2):xx-xx Point of View

A Case for Pharmacogenomics in Management of Cardiac Arrhythmias

Article awaiting publication date, not to be archived or cited

Gaurav Kandoi1, Anjali Nanda2, Vinod Scaria4, Sridhar Sivasubbu3

1Department of Biotechnology, Delhi Technological University, Shahbad Daulatpur, Main Bawana Road, Delhi, India,.
2International Institute of Health Management Research, Plot no. 3, Sector 18A, Phase-II, Dwarka, New Delhi - 110075.
3Genomics and Molecular Medicine, CSIR Institute of Genomics and Integrative Biology, Mall Road, Delhi 100 007, India.
4GN Ramachandran Knowledge Center for Genome Informatics, CSIR Institute of Genomics and Integrative Biology, Mall Road, Delhi 100 007, India.

Address for Correspondence: Dr. Vinod Scaria, GN Ramachandran Knowledge Center for Genome Informatics, CSIR Institute of Genomics and Integrative Biology, Mall Road, Delhi 100 007, India. E-mail: vinods/at/igib.res.in

Financial Support: CSIR India.

Conflict of Interest: None.

Abstract

Disorders of the cardiac rhythm are quite prevalent in clinical practice. Though the variability in drug response between individuals has been extensively studied, this information has not been widely used in clinical practice. Rapid advances in the field of pharmacogenomics have provided us with crucial insights on inter-individual genetic variability and its impact on drug metabolism and action. Technologies for faster and cheaper genetic testing and even personal genome sequencing would enable clinicians to optimize prescription based on the genetic makeup of the individual, which would open up new avenues in the area of personalized medicine. We have systematically looked at literature evidence on pharmacogenomics markers for anti-arrhythmic agents from the OpenPGx consortium collection and reason the applicability of genetics in the management of arrhythmia. We also discuss potential issues that need to be resolved before personalized pharmacogenomics becomes a reality in regular clinical practice.

Keywords: Arrhythmia, Pharmacogenomics, Personal genome, Genetic testing, Adverse drug reactions

Arrhythmias or disorders of the cardiac rhythm are not uncommon in clinical settings and one of the major causes of mortality and morbidity. Atrial Fibrillation is supposed to be rare in young healthy individuals unless without underlying cardiac pathology [1], while prevalent in the elderly and affects roughly around 2-5 Million individuals in the United States alone [2]. Ventricular fibrillation has a smaller incidence of close to 0.4 million [3]. Ventricular tachy-arrhythmias contribute significantly to the morbidity and mortality in patients with underlying coronary artery disease. It has been estimated that close to a half of deaths due to coronary artery disease is caused by ventricular arrhythmias [4]. Apart from the genetic and underlying cardiac disease as causes of cardiac rhythm abnormalities, a number of therapeutic agents, including drugs not directly used in the therapy of cardiac rhythm abnormalities have now been implicated to cause significant prolongation of QT interval and a form of ventricular arrhythmia, torsades de pointes, which is potentially fatal [5]. Recent reports also point to cardiac arrhythmias as one of the top causes for drug withdrawal and failure of clinical trials [6].

No major study on the incidence of arrhythmias or adverse drug reactions to anti-arrhythmic drugs throughout India has been performed. The lack of adequate epidemiological data in this important area has been highlighted in recent publications [4]. According to a report of arrhythmia care in India, published in 2002, the prevalence of patients with arrhythmias in the country is around 2 million [7]. Studies have also pointed to the high prevalence of asymptomatic arrhythmias in elderly patients [8]. According to the reports from the National pharmacovigilance programme, several cases of adverse drug reactions to anti-arrhythmic agents have been reported from people across India. Verapamil and Amiodarone have been reported to cause Steven Johnsons syndrome. Atenolol has been similarly reported to have adverse drug events like fatigue, cough and edema in a study conducted in South India [9]. Similar studies have shown Atenolol to be associated with around 4-5% of total adverse drug reactions reported.

Individuals vary widely in their response to therapeutic agents, and a large component of this variability is modulated through the genetic makeup of the individual. Apart from the variability in response, genetic variations are also now known to contribute significantly to Adverse Drug Reactions (ADRs). One of the earliest contributions to understanding of genomics of external agents have stemmed from the observations of the British physician Garrod, who proposed that defects in enzymatic pathways in unusual diseases of metabolism could produce unusual sensitivity to chemical agents. Molecular genetic dissection of congenital conditions in humans has contributed immensely to the overall understanding of the genetics of heart rhythm. The field has now grown by leaps and bounds with the advent of modern tools and techniques, which enables dissecting genetic phenomena at single base-pair resolution. The advent of genomics technologies has paved the way to deciphering the molecular genetic mechanisms of variability in response to therapeutic agents. This variability could be caused by genetic variations, which modulate the pharmacokinetics or pharmacodynamics of the drug. This could involve variations in genes involved in drug transport/metabolism right up to variations in drug-targets and off-targets. The field of understanding genetic variability in the response to drugs has now emerged into a full-fledged branch of biology - pharmacogenomics with the potential to significantly improve disease management. The field has also offered novel clues towards understanding mechanisms and pathways, which involves therapeutic agents.

The last couple of decades have seen enormous improvements in the management of cardiac arrhythmias. Due to limited benefits and safety related concerns, very few drugs have been successful and have been commonly used in the treatment of arrhythmias. The field has also seen the emergence of newer classes of drugs which function by normalizing the channel activity rather than blocking them. According to the popular Singh Vaughan Williams classification schema, drugs are placed based on the

mechanism of action. The classification scheme has improved over time, presently including the miscellaneous class, which includes drugs which could not fit any of the previous classes. Recent years have seen a number of publications detailing the pharmacogenomics of anti-arrhythmic drugs [10-13]. Though many classes of anti-arrhythmic agents are not particularly used anymore currently in regular clinical practice except in special settings, the wealth of information on pharmacogenomics encompasses the commonly used classes of drugs as well. The Drugs and the genes involved in the pharmacogenomics of anti-arrhythmics and the respective references are summarized in Table 1.

Table 1. Summary of drugs, genes involved in the pharmacogenomics of anti-arrhythmic drugs.

Class of Drug	Drug Name	Genes with Pharmacogenomic markers	References
Class 1a	Quinidine	SCN5A	14
Class 1b	Lidocaine	SCN5A,SCN9A,SCN4A	15-17
Class 1b	Phenytoin	CYP2C9, CYP2C19, HLA-B, HLA-DR, HLA-C, EPHX1, SCN2A, SCN1A, ABCB1	18-26
Class 2	Atenolol	CACNA1C, GRK5, ADRB1, ADRB2, LDLR, APOB, EDN1, GNB3, GNAS, TGFB1, AGT, ACE, CYP11B2, AGTR1, ALAP	27-45
Class 2	Carvedilol	ADRB1,ADRB2	46-53
Class 3	Metoprolol	ADRB1, GRK5, GRK4 , CYP2D6, ADRB2	47,49,52,54-63
Class 3	Amiodarone	KCNH2	64
Class 3	Dofetilide	KCNH2	65
Class 4	Verapamil	CACNB2 , CACNA1C, NOS1AP , ADRB1 , ADRB2, KCNMB1, KCNH2	27,30,66-69
Class 5	Digoxin	ABCB1	70-77

Realizing the dream of personalized medicine is not without challenges and focused intervention. The major challenge in understanding the intricacies of genomic variations and deciphering the potential effects on pharmacokinetics and pharmacodynamics is the lack of of comprehensive models of drug metabolism and action for many drugs. Understanding and charting drug pathways is the first step towards this dream. A systems level understanding of the drug pathways would enable us to overlay genomic variations and offer smart guesses on drugs that could be involved. The drug pathways for many drugs are complicated, involving multiple and sometimes redundant mechanisms for drug transport, metabolism and targets. Deciphering the pathways is the first step towards understanding how genetic variation could potentially contribute to the changes in functionality of critical components of the drug pathway. In addition, it also provides crucial insights into the molecular mechanisms of drug-drug and drug-environment interactions and how genetic variations could modulate this phenomenon. A comprehensive outline of anti-arrhythmic drugs and their drug pathways are summarized in Figure 1.

Figure 1: Overview of the drug pathways for anti-arrhythmic drugs. The coloured drugs and edges represent drugs while the metabolizing enzymes are marked as solid circles. The transporters and targets are represented as solid triangles and rhomboids respectively.

Modeling a disease process or pathway is the next critical step in understanding the molecular mechanisms and the genetic architecture of disease processes. Animal models such as rodents and mammals have been used successfully for modeling cardiac arrhythmias. Recently advances include the application of newer model systems for understanding pharmacogenomics principles. Model organisms like zebrafish, which are easy to maintain and study, have been shown to be useful in modeling pharmacological principles and potential mode of action of many therapeutic agents.

The major area that would require focused attention in the immediate future is towards standardized efforts to collate pharmacogenomics data and evidence to enable meta-analysis, while at the same time be able to keep pace with the latest avalanche of evidence brought to light by high throughput genomics studies including Genome-wide associations studies (GWAS). Community led approaches like PharmGKB (www.pharmgkb.org) and crowd-sourcing approaches like OpenPGx (www.openpgx.org) are the possible way forward, and both approaches should be organized complementary to each other. Apart from the data, the second focus area is computational tools and resources that can handle the high-

throughput datasets. The availability of genome-wide scans as direct-to-consumer services has also provided an immense opportunity and challenge at the same time. With adequate computational tools and resources for interpretation of the data, this has the potential to lower the cost, while at the same time, widen the general acceptability of genetic testing. No healthcare intervention system is complete without adequate education and empowerment of the medical and paramedical professionals and the patients. For the success of widespread acceptability and application of pharmacogenomics testing for cardiac arrhythmias, appropriate focus and emphasis on awareness and healthcare education is essential.

These efforts should be complemented and supplemented by both systematic ways of collecting data and being able to analyze it to unravel emerging phenomena. This would necessitate creation of effective systems for systematic collection and sharing of clinical data, treatment protocols and outcome measures. This includes setting up of registries, which follow standard protocols, metadata and modes of data exchange. This also requires setting up collaborative and shared data resources and analytical approaches. In summary, seamless exchange of ideas, resources and knowhow between research laboratories and clinicians is essential to realize the dream of making pharmacogenomics based personalized medicine a reality.

Acknowledgements

The authors thank Dr. Shantanu Sengupta and Dr Mohd Faruq for reviewing the manuscript. Authors also thank Mr Jatin Talwar for discussions and visualization of data and Dr Yasha Hasija for comments and discussions. The authors acknowledge the OpenPGx (www.openpgx.org) consortium and community for data annotation from literature. This study is funded by CSIR India.

References

1. Domanski, Michael J.: The epidemiology of atrial fibrillation. Coronary Artery Disease 1995, 6:95-100.

2. Benjamin EJ, Wolf PA, D'Agostino RB, Silbershatz H, Kannel WB, Levy D.: Impact of atrial fibrillation on the risk of death: the Framingham Heart Study. Circulation 1998, 98:946-952.

3. Zheng, Z.J., Croft, J.B., Giles, W.H. & Mensah GA.: Sudden cardiac death in the United States, 1989 to 1998. Circulation 104, 2158–2163.

4. Naik, N., Yadav, R., Juneja, R.: Epidemiology of arrhythmias in India: How do we obtain reliable data? Current Science 2009, 97:411-16.

5. Nielsen J, Graff C, Kanters JK, Toft E, Taylor D, Meyer JM.: Assessing QT interval prolongation and its associated risks with antipsychotics. CNS Drugs. 2011, 25(6):473-90.

6. Crivellente, F: The Sooner the Better: utilising biomarkers to eliminate drug candidates with cardiotoxicity in preclinical development. Available at: http://www.ddw-online.com/s/summer-2011/p148216/the-sooner-the-better:-utilising-biomarkers-to-eliminate-drug-candidates-with-cardiotoxicity-in-preclinical-development.html

7. Lokhandwala Y.: Arrhythmia care in India-poised for the big leap. Indian Pacing Electrophysiol J. 2002, 2(1):1.

8. Singh, H and Gupta, G and Gupta, MS and Anand, JS and Aggarwal, R and Verma, RP.: A 24 hour holter study in asymptomatic elderly Indians. JIACM 2003, 4(4): 308-14.

9. Arulmani R, Rajendran SD, Suresh B.: Adverse drug reaction monitoring in a secondary care hospital in South India. Br J Clin Pharmacol. 2008 Feb;65(2):210-6.

10. Harkcom WT, Abbott GW.: Emerging concepts in the pharmacogenomics of arrhythmias: ion channel trafficking. Expert Rev Cardiovasc Ther. 2010, 8:1161-73.

11. Roden DM, Kannankeri PJ, Darbar D.: Arrhythmia pharmacogenomics: methodological considerations. Curr Pharm Des. 2009, 15:3734-41.

12. Clancy CE, Zhu ZI, Rudy Y.: Pharmacogenetics and anti-arrhythmic drug therapy: a theoretical investigation. Am J Physiol Heart Circ Physiol. 2007, 292:H66-75.

13. Darbar D, Roden DM.: Pharmacogenetics of antiarrhythmic therapy. Expert Opin Pharmacother. 2006, 7:1583-90.

14. Shuraih M, Ai T, Vatta M, Sohma Y, Merkle EM, Taylor E, Li Z, Xi Y, Razavi M, Towbin JA, Cheng J. : A common SCN5A variant alters the responsiveness of human sodium channels to class I antiarrhythmic agents. J Cardiovasc Electrophysiol. 2007 Apr;18(4):434-40. Epub 2007 Jan 10.

15. Barajas-Martínez HM, Hu D, Cordeiro JM, Wu Y, Kovacs RJ, Meltser H, Kui H, Elena B, Brugada R, Antzelevitch C, Dumaine R.: Lidocaine-induced Brugada syndrome phenotype linked to a novel double mutation in the cardiac sodium channel. Circ Res. 2008, 103:396-404.

16. Sheets PL, Jackson JO 2nd, Waxman SG, Dib-Hajj SD, Cummins TR.: A Nav1.7 channel mutation associated with hereditary erythromelalgia contributes to neuronal hyperexcitability and displays reduced lidocaine sensitivity. J Physiol. 2007, 581:1019-31.

17. Fan Z, George AL Jr, Kyle JW, Makielski JC.: Two human paramyotonia congenita mutations have opposite effects on lidocaine block of Na+ channels expressed in a mammalian cell line. J Physiol. 1996, 496:275-86.

18. Kesavan R, Narayan SK, Adithan C.: Influence of CYP2C9 and CYP2C19 genetic polymorphisms on phenytoin-induced neurological toxicity in Indian epileptic patients. Eur J Clin Pharmacol. 2010, 66:689-96.

19. Hung SI, Chung WH, Liu ZS, Chen CH, Hsih MS, Hui RC, Chu CY, Chen YT.: Common risk allele in aromatic antiepileptic-drug induced Stevens-Johnson syndrome and toxic epidermal necrolysis in Han Chinese. Pharmacogenomics. 2010, 11:349-56.

20. Azzato EM, Chen RA, Wacholder S, Chanock SJ, Klebanoff MA, Caporaso NE.: Maternal EPHX1 polymorphisms and risk of phenytoin-induced congenital malformations. Pharmacogenet Genomics. 2010, 20:58-63.

21. Chaudhry AS, Urban TJ, Lamba JK, Birnbaum AK, Remmel RP, Subramanian M, Strom S, You JH, Kasperaviciute D, Catarino CB, Radtke RA, Sisodiya SM, Goldstein DB, Schuetz EG.: CYP2C9*1B promoter polymorphisms, in linkage with CYP2C19*2, affect phenytoin autoinduction of clearance and maintenance dose. J Pharmacol Exp Ther. 2010, 332:599-611.

22. Kwan P, Poon WS, Ng HK, Kang DE, Wong V, Ng PW, Lui CH, Sin NC, Wong KS, Baum L.: Multidrug resistance in epilepsy and polymorphisms in the voltage-gated sodium channel genes SCN1A, SCN2A, and SCN3A: correlation among phenotype, genotype, and mRNA expression. Pharmacogenet Genomics. 2008, 18:989-98.

23. Locharernkul C, Loplumlert J, Limotai C, Korkij W, Desudchit T, Tongkobpetch S, Kangwanshiratada O, Hirankarn N, Suphapeetiporn K, Shotelersuk V.: Carbamazepine and phenytoin induced Stevens-Johnson syndrome is associated with HLA-B*1502 allele in Thai population. Epilepsia. 2008, 49:2087-91.

24. Man CB, Kwan P, Baum L, Yu E, Lau KM, Cheng AS, Ng MH.: Association between HLA-B*1502 allele and antiepileptic drug-induced cutaneous reactions in Han Chinese. Epilepsia. 2007, 48:1015-8.

25. Tate SK, Singh R, Hung CC, Tai JJ, Depondt C, Cavalleri GL, Sisodiya SM, Goldstein DB, Liou HH.: A common polymorphism in the SCN1A gene associates with phenytoin serum levels at maintenance dose. Pharmacogenet Genomics. 2006, 16:721-6.

26. Tate SK, Depondt C, Sisodiya SM, Cavalleri GL, Schorge S, Soranzo N, Thom M, Sen A, Shorvon SD, Sander JW, Wood NW, Goldstein DB.: Genetic predictors of the maximum doses patients receive during clinical use of the anti-epileptic drugs carbamazepine and phenytoin. Proc Natl Acad Sci U S A. 2005, 102:5507-12.

27. Beitelshees AL, Navare H, Wang D, Gong Y, Wessel J, Moss JI, Langaee TY, Cooper-DeHoff RM, Sadee W, Pepine CJ, Schork NJ, Johnson JA.: CACNA1C gene polymorphisms, cardiovascular disease outcomes, and treatment response. Circ Cardiovasc Genet. 2009, 2:362-70.
28.Kurnik D, Cunningham AJ, Sofowora GG, Kohli U, Li C, Friedman EA, Muszkat M, Menon UB, Wood AJ, Stein CM.: GRK5 Gln41Leu polymorphism is not associated with sensitivity to beta(1)-adrenergic blockade in humans. Pharmacogenomics. 2009, 10:1581-7.

29. Kurnik D, Li C, Sofowora GG, Friedman EA, Muszkat M, Xie HG, Harris PA, Williams SM, Nair UB, Wood AJ, Stein CM.: Beta-1-adrenoceptor genetic variants and ethnicity independently affect response to beta-blockade. Pharmacogenet Genomics. 2008, 18:895-902.

30. Pacanowski MA, Gong Y, Cooper-Dehoff RM, Schork NJ, Shriver MD, Langaee TY, Pepine CJ, Johnson JA; INVEST Investigators.: beta-adrenergic receptor gene polymorphisms and beta-blocker treatment outcomes in hypertension. Clin Pharmacol Ther. 2008, 84:715-21.

31. Iaccarino G, Izzo R, Trimarco V, Cipolletta E, Lanni F, Sorriento D, Iovino GL, Rozza F, De Luca N, Priante O, Di Renzo G, Trimarco B.: Beta2-adrenergic receptor polymorphisms and treatment-induced regression of left ventricular hypertrophy in hypertension. Clin Pharmacol Ther. 2006, 80:633-45.

32. Liljedahl U, Lind L, Kurland L, Berglund L, Kahan T, Syvänen AC.: Single nucleotide polymorphisms in the apolipoprotein B and low density lipoprotein receptor genes affect response to antihypertensive treatment. BMC Cardiovasc Disord. 2004, 4:16.

33. Karlsson J, Lind L, Hallberg P, Michaëlsson K, Kurland L, Kahan T, Malmqvist K, Ohman KP, Nyström F, Melhus H.: Beta1-adrenergic receptor gene polymorphisms and response to beta1-adrenergic receptor blockade in patients with essential hypertension. Clin Cardiol. 2004, 27:347-50.

34. Hallberg P, Karlsson J, Lind L, Michaëlsson K, Kurland L, Kahan T, Malmqvist K, Ohman KP, Nyström F, Liljedahl U, Syvänen AC, Melhus H.: Gender-specific association between preproendothelin-1 genotype and reduction of systolic blood pressure during antihypertensive treatment--results from the Swedish Irbesartan Left Ventricular Hypertrophy Investigation versus Atenolol (SILVHIA). Clin Cardiol. 2004, 27:287-90.

35. Filigheddu F, Reid JE, Troffa C, PinnaParpaglia P, Argiolas G, Testa A, Skolnick M, Glorioso N.: Genetic polymorphisms of the beta-adrenergic system: association with essential hypertension and response to beta-blockade. Pharmacogenomics J. 2004, 4:154-60.

36. Hallberg P, Lind L, Billberger K, Michaelsson K, Karlsson J, Kurland L, Kahan T, Malmqvist K, Ohman KP, Nyström F, Liljedahl U, Syvänen AC, Melhus H.: Transforming growth factor beta1 genotype and change in left ventricular mass during antihypertensive treatment--results from the Swedish Irbesartan Left Ventricular Hypertrophy Investigation versus Atenolol (SILVHIA). Clin Cardiol. 2004, 27:169-73.

37. Kurland L, Liljedahl U, Karlsson J, Kahan T, Malmqvist K, Melhus H, Syvänen AC, Lind L.: Angiotensinogen gene polymorphisms: relationship to blood pressure response to antihypertensive treatment. Results from the Swedish Irbesartan Left Ventricular Hypertrophy Investigation vs Atenolol (SILVHIA) trial. Am J Hypertens. 2004, 17:8-13.

38. Diez J, Laviades C, Orbe J, Zalba G, López B, González A, Mayor G, Páramo JA, Beloqui O.: The A1166C polymorphism of the AT1 receptor gene is associated with collagen type I synthesis and myocardial stiffness in hypertensives. J Hypertens. 2003, 21:2085-92.

39. Hallberg P, Lind L, Michaëlsson K, Kurland L, Kahan T, Malmqvist K, Ohman KP, Nyström F, Liljedahl U, Syvänen AC, Melhus H.: Adipocyte-derived leucine aminopeptidase genotype and response to antihypertensive therapy. BMC Cardiovasc Disord. 2003, 3:11.

40. Sofowora GG, Dishy V, Muszkat M, Xie HG, Kim RB, Harris PA, Prasad HC, Byrne DW, Nair UB, Wood AJ, Stein CM.: A common beta1-adrenergic receptor polymorphism (Arg389Gly) affects blood pressure response to beta-blockade. Clin Pharmacol Ther. 2003, 73:366-71.

41. Kurland L, Melhus H, Karlsson J, Kahan T, Malmqvist K, Ohman P, Nyström F, Hägg A, Lind L.: Aldosterone synthase (CYP11B2) -344 C/T polymorphism is related to antihypertensive response: result from the Swedish Irbesartan Left Ventricular Hypertrophy Investigation versus Atenolol (SILVHIA) trial. Am J Hypertens. 2002, 15:389-93.

42. Kurland L, Melhus H, Karlsson J, Kahan T, Malmqvist K, Ohman P, Nyström F, Hägg A, Lind L.: Polymorphisms in the angiotensinogen and angiotensin II type 1 receptor gene are related to change in left ventricular mass during antihypertensive treatment: results from the Swedish Irbesartan Left Ventricular Hypertrophy Investigation versus Atenolol (SILVHIA) trial. J Hypertens. 2002, 20:657-63.

43. O'Shaughnessy KM, Fu B, Dickerson C, Thurston D, Brown MJ.: The gain-of-function G389R variant of the beta1-adrenoceptor does not influence blood pressure or heart rate response to beta-blockade in hypertensive subjects. Clin Sci (Lond). 2000, 99:233-8.

44. Kurland L, Melhus H, Karlsson J, Kahan T, Malmqvist K, Ohman KP, Nyström F, Hägg A, Lind L; Swedish Irbesartan Left Ventricular Hypertrophy Investigation versus Atenolol (SILVHIA) Trial.: Angiotensin converting enzyme gene polymorphism predicts blood pressure response to angiotensin II receptor type 1 antagonist treatment in hypertensive patients. J Hypertens. 2001, 19:1783-7.

45. Dudley C, Keavney B, Casadei B, Conway J, Bird R, Ratcliffe P.: Prediction of patient responses to antihypertensive drugs using genetic polymorphisms: investigation of renin-angiotensin system genes. J Hypertens. 1996, 14:259-62.

46. Dudley C, Keavney B, Casadei B, Conway J, Bird R, Ratcliffe P.: Role of beta-adrenergic receptor gene polymorphisms in the long-term effects of beta-blockade with carvedilol in patients with chronic heart failure. Cardiovasc Drugs Ther. 2010, 24:49-60.

47. Cresci S, Kelly RJ, Cappola TP, Diwan A, Dries D, Kardia SL, Dorn GW 2nd.: Clinical and genetic modifiers of long-term survival in heart failure. J Am Coll Cardiol. 2009, 54:432-44.

48. Troncoso R, Moraga F, Chiong M, Roldán J, Bravo R, Valenzuela R, Díaz-Araya G, del Campo A, Sanhueza C, Rodriguez A, Vukasovic JL, Mellado R, Greig D, Castro PF, Lavandero S.: Gln(27)->Glubeta(2)-adrenergic receptor polymorphism in heart failure patients: differential clinical and oxidative response to carvedilol. Basic Clin Pharmacol Toxicol. 2009, 104:374-8.

49. Sehnert AJ, Daniels SE, Elashoff M, Wingrove JA, Burrow CR, Horne B, Muhlestein JB, Donahue M, Liggett SB, Anderson JL, Kraus WE.: Lack of association between adrenergic receptor genotypes and survival in heart failure patients treated with carvedilol or metoprolol. J Am Coll Cardiol. 2008, 52:644-51.

50. Chen L, Meyers D, Javorsky G, Burstow D, Lolekha P, Lucas M, Semmler AB, Savarimuthu SM, Fong KM, Yang IA, Atherton J, Galbraith AJ, Parsonage WA, Molenaar P.: Arg389Gly-beta1-adrenergic receptors determine improvement in left ventricular systolic function in nonischemic cardiomyopathy patients with heart failure after chronic treatment with carvedilol. Pharmacogenet Genomics. 2007, 17:941-9.

51. Mialet Perez J, Rathz DA, Petrashevskaya NN, Hahn HS, Wagoner LE, Schwartz A, Dorn GW, Liggett SB.: Beta 1-adrenergic receptor polymorphisms confer differential function and predisposition to heart failure. Nat Med. 2003, 9:1300-5.

52. Petersen M, Andersen JT, Hjelvang BR, Broedbaek K, Afzal S, Nyegaard M, Børglum AD, Stender S, Køber L, Torp-Pedersen C, Poulsen HE.: Association of beta-adrenergic receptor polymorphisms and mortality in carvedilol-treated chronic heart-failure patients. Br J Clin Pharmacol. 2011, 71:556-65.

53. Kaye DM, Smirk B, Williams C, Jennings G, Esler M, Holst D.: Beta-adrenoceptor genotype influences the response to carvedilol in patients with congestive heart failure. Pharmacogenetics. 2003, 13:379-82.

54. Bhatnagar V, O'Connor DT, Brophy VH, Schork NJ, Richard E, Salem RM, Nievergelt CM, Bakris GL, Middleton JP, Norris KC, Wright J, Hiremath L, Contreras G, Appel LJ, Lipkowitz MS; AASK Study Investigators.: G-protein-coupled receptor kinase 4 polymorphisms and blood pressure response to metoprolol among African Americans: sex-specificity and interactions. Am J Hypertens. 2009, 22:332-8.

55. Jin SK, Chung HJ, Chung MW, Kim JI, Kang JH, Woo SW, Bang S, Lee SH, Lee HJ, Roh J.: Influence of CYP2D6*10 on the pharmacokinetics of metoprolol in healthy Korean volunteers. J Clin Pharm Ther. 2008, 33:567-73.

56. Bijl MJ, Visser LE, van Schaik RH, Kors JA, Witteman JC, Hofman A, Vulto AG, van Gelder T, Stricker BH.: Genetic variation in the CYP2D6 gene is associated with a lower heart rate and blood pressure in beta-blocker users. Clin Pharmacol Ther. 2009, 85:45-50.

57. Lobmeyer MT, Gong Y, Terra SG, Beitelshees AL, Langaee TY, Pauly DF, Schofield RS, Hamilton KK, Herbert Patterson J, Adams KF Jr, Hill JA, Aranda JM Jr, Johnson JA.: Synergistic polymorphisms of beta1 and alpha2C-adrenergic receptors and the influence on left ventricular ejection fraction response to beta-blocker therapy in heart failure. Pharmacogenet Genomics. 2007, 17:277-82.

58. Liu J, Liu ZQ, Yu BN, Xu FH, Mo W, Zhou G, Liu YZ, Li Q, Zhou HH.: beta1-Adrenergic receptor polymorphisms influence the response to metoprolol monotherapy in patients with essential hypertension. Clin Pharmacol Ther. 2006, 80:23-32.

59. Beitelshees AL, Zineh I, Yarandi HN, Pauly DF, Johnson JA.: Influence of phenotype and pharmacokinetics on beta-blocker drug target pharmacogenetics. Pharmacogenomics J. 2006, 6:174-8.

60. Terra SG, Hamilton KK, Pauly DF, Lee CR, Patterson JH, Adams KF, Schofield RS, Belgado BS, Hill JA, Aranda JM, Yarandi HN, Johnson JA.: Beta1-adrenergic receptor polymorphisms and left ventricular remodeling changes in response to beta-blocker therapy. Pharmacogenet Genomics. 2005, 15:227-34.

61. Liu J, Liu ZQ, Tan ZR, Chen XP, Wang LS, Zhou G, Zhou HH.: Gly389Arg polymorphism of beta1-adrenergic receptor is associated with the cardiovascular response to metoprolol. Clin Pharmacol Ther. 2003, 74:372-9.

62. White HL, de Boer RA, Maqbool A, Greenwood D, van Veldhuisen DJ, Cuthbert R, Ball SG, Hall AS, Balmforth AJ; MERIT-HF Study Group.: An evaluation of the beta-1 adrenergic receptor Arg389Gly polymorphism in individuals with heart failure: a MERIT-HF sub-study. Eur J Heart Fail. 2003, 5:463-8.

63. Johnson JA, Zineh I, Puckett BJ, McGorray SP, Yarandi HN, Pauly DF.: Beta 1-adrenergic receptor polymorphisms and antihypertensive response to metoprolol. Clin Pharmacol Ther. 2003, 74:44-52.

64. Yang P, Kanki H, Drolet B, Yang T, Wei J, Viswanathan PC, Hohnloser SH, Shimizu W, Schwartz PJ, Stanton M, Murray KT, Norris K, George AL Jr, Roden DM.: Allelic variants in long-QT disease genes in patients with drug-associated torsades de pointes. Circulation. 2002, 105:1943-8.

65. Sun Z, Milos PM, Thompson JF, Lloyd DB, Mank-Seymour A, Richmond J, Cordes JS, Zhou J.: Role of a KCNH2 polymorphism (R1047 L) in dofetilide-induced Torsades de Pointes. J Mol Cell Cardiol. 2004, 37:1031-9.

66. Niu Y, Gong Y, Langaee TY, Davis HM, Elewa H, Beitelshees AL, Moss JI, Cooper-Dehoff RM, Pepine CJ, Johnson JA.: Genetic variation in the beta2 subunit of the voltage-gated calcium channel and pharmacogenetic association with adverse cardiovascular outcomes in the INternational VErapamil SR-Trandolapril STudy GENEtic Substudy (INVEST-GENES). Circ Cardiovasc Genet. 2010, 3:548-55.

67. van Noord C, Aarnoudse AJ, Eijgelsheim M, Sturkenboom MC, Straus SM, Hofman A, Kors JA, Newton-Cheh C, Witteman JC, Stricker BH.: Calcium channel blockers, NOS1AP, and heart-rate-corrected QT prolongation. Pharmacogenet Genomics. 2009, 19:260-6.

68. Beitelshees AL, Gong Y, Wang D, Schork NJ, Cooper-Dehoff RM, Langaee TY, Shriver MD, Sadee W, Knot HJ, Pepine CJ, Johnson JA; INVEST Investigators.: KCNMB1 genotype influences response to verapamil SR and adverse outcomes in the INternational VErapamil SR/Trandolapril STudy (INVEST). Pharmacogenet Genomics. 2007, 17:719-29.

69. Duan JJ, Ma JH, Zhang PH, Wang XP, Zou AR, Tu DN.: Verapamil blocks HERG channel by the helix residue Y652 and F656 in the S6 transmembrane domain. Acta Pharmacol Sin. 2007, 28:959-67.

70. Bartnicka L, Kurzawski M, Drozdzik A, Plonska-Gosciniak E, Górnik W, Drozdzik M.: Effect of ABCB1 (MDR1) 3435C >T and 2677G >A,T polymorphisms and P-glycoprotein inhibitors on salivary digoxin secretion in congestive heart failure patients. Pharmacol Rep. 2007, 59:323-9.

71. Chowbay B, Li H, David M, Cheung YB, Lee EJ.: Meta-analysis of the influence of MDR1 C3435T polymorphism on digoxin pharmacokinetics and MDR1 gene expression. Br J Clin Pharmacol. 2005, 60:159-71.

72. Morita N, Yasumori T, Nakayama K.: Human MDR1 polymorphism: G2677T/A and C3435T have no effect on MDR1 transport activities. Biochem Pharmacol. 2003, 65:1843-52.

73. Morita Y, Sakaeda T, Horinouchi M, Nakamura T, Kuroda K, Miki I, Yoshimura K, Sakai T, Shirasaka D, Tamura T, Aoyama N, Kasuga M, Okumura K.: MDR1 genotype-related duodenal absorption rate of digoxin in healthy Japanese subjects. Pharm Res. 2003, 20:552-6.

74. Verstuyft C, Schwab M, Schaeffeler E, Kerb R, Brinkmann U, Jaillon P, Funck-Brentano C, Becquemont L.: Digoxin pharmacokinetics and MDR1 genetic polymorphisms. Eur J Clin Pharmacol. 2003, 58:809-12.

75. Gerloff T, Schaefer M, Johne A, Oselin K, Meisel C, Cascorbi I, Roots I.: MDR1 genotypes do not influence the absorption of a single oral dose of 1 mg digoxin in healthy white males. Br J Clin Pharmacol. 2002, 54:610-6.

76. Kim RB, Leake BF, Choo EF, Dresser GK, Kubba SV, Schwarz UI, Taylor A, Xie HG, McKinsey J, Zhou S, Lan LB, Schuetz JD, Schuetz EG, Wilkinson GR.: Identification of functionally variant MDR1 alleles among European Americans and African Americans. Clin Pharmacol Ther. 2001, 70:189-99.

77. Hoffmeyer S, Burk O, von Richter O, Arnold HP, Brockmöller J, Johne A, Cascorbi I, Gerloff T, Roots I, Eichelbaum M, Brinkmann U.: Functional polymorphisms of the human multidrug-resistance gene: multiple sequence variations and correlation of one allele with P-glycoprotein expression and activity in vivo. Proc Natl Acad Sci U S A 2000, 97:3473-8.

A New Method for Identification of Partially Similar Indian Scripts

Rajiv Kapoor *rajivkapoor@dce.edu*
Department of Electronics and Communication Engg.
Delhi Technological University
Delhi, India

Amit Dhamija *dhamija.amit@hotmail.com*
Department of Electrical Engg.
YMCA University of Science and Technology
Faridabad, Haryana, India

Abstract

In this paper, the texture symmetry/non-symmetry factor has been exploited to identify the Indian scripts. Biwavelants have been proposed to obtain the script texture using third order cumulant and bispectra. As the Indian scripts are partially similar to each other, in order to identify them, the samples must include more number of dissimilar characters. The features of individual lines are added repeatedly to enhance the dissimilarity until it reaches to a saturation level which in turn is used to compute a confidence factor i.e. amount of confidence attained in identifying a particular script sample. This variation in confidence factor also gives an estimate of the optimum sample size (number of lines) required for expected results. Cumulants are sensitive to the script curvatures and therefore are most suitable for the partially similar Indian scripts. The double discrete Fourier transform of third order cumulant gives bispectra which estimates the factor of symmetry/non-symmetry in terms of the quadratically coupled frequencies. The envelope of bispectra (biwavelant) obtained using wavelet (db8) provides an accurate behavior of the script texture; which along with Newton-Raphson technique is used to classify the Indian scripts. Various classifiers have been tested for script identification and out of them SVM gives the best results. The method successfully identified the 8 Indian scripts like Devanagari, Urdu, Gujarati, Telugu, Assamese, Gurmukhi, Kannada, and Bangla with desired accuracy.

Keywords: Indian Scripts, Cumulant, Bispectra and Support Vector Machine (SVM)

1. INTRODUCTION

Script identification is a key part of automatic processing of document images. A document script must be known in order to choose an appropriate OCR algorithm. Further processing like indexing or translation of scripts depends on identifying the language used in a document and here again script identification is crucial. Now-a-days documents are stored digitally so as to have quicker access and to save them from any kind of environmental effect. Most of the states in India have their own language of communication and independent scripts. Thus, many official documents are written in regional scripts. Identification of these regional scripts is one of the challenging tasks faced by the designer of an OCR system. Script identification makes the task of analysis and recognition of the text easier by suitably selecting the modalities of OCR. What makes recognition of Indian scripts daunting is their undistinguishable closeness. A number of attempts have already been made to isolate and identify the scripts of the texts in the case of multi-script Indian documents. Patil and Subbareddy [1] developed a system having a feature extractor and a modular neural network. They dilated the documents using 3 x 3 masks in horizontal, vertical, right diagonal, and left diagonal directions. Average pixel distribution was found in these resulting images. A combination of separately trained feed forward neural network was utilized as classifiers for each script. Hochberg [2] approach was to discover frequent character shapes in each script and then look for same instances in new documents. Some

identification techniques have also used the directional features, however to a meager amount. Dhanaya, Ramakrishnan and Pati [3] used basically two features of the scripts like Roman and Tamil. First was Spatial Spread Features like Zonal pixel concentration and character density. Directional Features were detected by using Gabor filter responses. It was concluded that Tamil script has more horizontal lines and strokes while English has more slant strokes. They used Gabor filters to effectively capture the concentration of energies in various directions. Chaudhuri and Pal [4] used skew angle detection for scanned documents containing popular Indian scripts (Devanagari and Bangla). Most characters in these scripts have horizontal line at the top called headlines (Shirorekha). Chaudhuri and Sheth [5] proposed a Gabor filter-based feature extraction scheme for the connected components. Pal and Chaudhuri [6] proposed an automatic technique of separating the text lines using script characteristics and shape-features. Spitz [7] developed techniques for distinguishing the script into two broad classes: Han-based and Latin-based. This classification was based on the spatial relationships of features related to the upward concavities in character structures. Language identification within the Han script class (Chinese, Japanese, and Korean) was performed by analysis of the distribution of optical density in the text images. Tan [8] extracted rotation invariant texture features and then used such features in script identification from document images. Rotation invariant texture features are computed based on the popular multi-channel Gabor filtering technique. Hochberg [9] used features of connected components to classify six different scripts (Arabic, Chinese, Cyrillic, Devanagari, Japanese, and Roman). Srinivasan, Ramakrishnan and Budhlakoti [10] proposed the spatial entropy obtained after decomposing the characters from the document image. The method is not adaptive to the writing styles and moreover after decomposing the characters, the spatial entropy will be definable under so many constraints which have not been discussed. Veena and Sinha [11] proposed a technique using smallest segments of the Devanagari structures to define the Devanagari characters. The method is very time consuming and detection is an issue. Sameer and Lalitha [12] suggested a preliminary technique based upon multiple classifiers like k-means classifier and Minimum Hamming Distance classifier. Anup and Anil [13] could extract temporal information due to online detection recognition and a set of features like Horizontal Inter-stroke Direction for capturing the writing direction like in the case of Arabic which is written from left to right, detection of Shirorekha for Devanagari, average stroke length, number of strokes per unit length, aspect ratio and few more like VD and VID. In these scripts, specific features could work because the scripts chosen for analysis are not related to each other and therefore the task is easier. Second kind of feature is heuristic and depends highly upon the writing style and hence will not work for all Indian scripts because they are highly related. Andrew, Wageeh and Sridharan [14] considered all scripts as texture of their own kind. Yes, this is true but the use of clustering techniques and the wavelet decomposition helps more in case of grey level images as compared to binary. Scripts which are closely related will have similar structures and texture. Texture of the scripts is formed by symmetrical spread of the structural features like horizontal lines, vertical lines and curves. This texture is of binary levels and not like grey ones as in wooden texture. Therefore the kind of features considered by Andrew, Wageeh and Sridhar do not give the high identification accuracy in case of scripts having structural and textural similarity. Morphological reconstruction [15] based upon the continuous erosion and opening was carried out in 4 directions and the average pixel distribution was found as the feature point. MLP [16] has also been used as classifier with the fuzzy-features from the Hough transform. In [17], support vector machine (SVM) based hierarchical classification scheme has been used for the recognition of handwritten Bangla characters. SVM classifier is found to outperform the other classifiers like multilayer perceptron and radial basis function network. [18] elaborates various noises that affect the performance of a script recognition system and the techniques to counter them.

What makes recognition of Indian scripts difficult is their similarity. But, since they are partially similar, their inherent dissimilarity should be enhanced in order to make them completely distinguishable. The features of individual lines are added repeatedly to enhance the dissimilarity until it reaches to a saturation level. As cumulants are sensitive to the script curvatures, they are completely suitable for identifying the Indian Scripts. This paper discusses the use of symmetry/non-symmetry factor of the script texture for identifying the partially similar Indian scripts. Biwavelants have been proposed to obtain the script texture using the third order

cumulant and the bispectra. The double discrete Fourier transform of third order cumulant gives bispectra which estimates the factor of symmetry/non-symmetry in terms of the quadratically coupled frequencies. The envelope of bispectra (biwavelant) provides an accurate behavior of the script texture which along with Newton-Raphson technique is used to classify the Indian scripts. The paper shows that for the proposed feature extraction technique, SVM gives the best classification results and can successfully identify 8 Indian scripts like Devanagari, Urdu, Gujarati, Telugu, Assamese, Gurmukhi, Kannada and Bangla.

The paper is organized as following: Section 2 describes the sample collection and pre-processing of scripts. Section 3 defines the higher order cumulants and the corresponding poly-spectra estimation. It also shows the results obtained by computing the 3rd order cumulant for different script samples. Section 4 describes the optimum parameter selection for the estimation of bispectra. Section 5 introduces biwavelants and shows the corresponding results obtained for the different Indian scripts. Section 6 describes the pre-classification stage using Newton-Raphson Technique. Section 7 elaborates different classifiers used for the proposed feature extraction technique and section 8 gives a comparison of the results obtained with different classifiers. Section 9 concludes the paper.

2. SAMPLE COLLECTION & PRE-PROCESSING

One third of the training and test data set used in this paper was collected from the news papers (*) available online, an equal amount of data was obtained by preparing the documents using different Indian fonts (#) and the last type of data comprised of the handwritten documents (^). The handwritten data was collected on a normal white paper. The documents were written using a blue ball pen. The documents were scanned offline on a canon scanner with 600 dpi resolution. The contents were not fixed and the choice was left to the writer. The total statistics of the sample collected has been mentioned in table (1) below.

Sr. No.	Script	Number of Pages	Number of Lines	Number of Words	Number of Writers
1	Devanagari	5*+10#+5^	210*+351#+100^	7462	5
2	Gujarati	5*+10#+4^	203*+336#+80^	6979	4
3	Gurmukhi	5*+10#+5^	200*+325#+90^	7000	5
4	Telugu	5*+10#+4^	215*+356#+85^	7475	4
5	Kannada	5*+10#+3^	215*+356#+60^	7225	3
6	Bangla	5*+10#+5^	198*+320#+95^	6920	5
7	Assamese	5*+10#+3^	187*+300#+60^	6305	3
8	Urdu	5*+10#+4^	180*+280#+80^	6300	4

Total number of words = 55666

TABLE 1: Number of pages, lines and words collected for each script

The handwritten samples were not just straight lines but had lines and words written irregularly and spread over the whole document. The variety of documents made the task of pre-processing very complex and therefore, the next section is dedicated to the pre-processing.

2.1 Skew Correction

When a document is fed to the optical sensor either mechanically or manually, a few degrees of skew (tilt) is unavoidable. Person scanning the printed data document can also add skew to the text. Hand-written documents written irregularly also contain heavy skew. The lines in sample documents have been written even vertically to each other. To detect the skew angle in the printed documents, we took Radon transform of the whole document image. For an ideal skew free document, peaks corresponding to the horizontal text lines should occur at 90° in Radon image. However the scanned document will actually have peaks at an angle (Ø) different from 90° due to the presence of skew. Thus the document is rotated by 90°- Ø for skew correction. In figure (1), the Radon transform image of the scanned document showed peaks at Ø=80°, thus

document was rotated by 10° anticlockwise to remove the skew error. [19] discusses the method in detail.

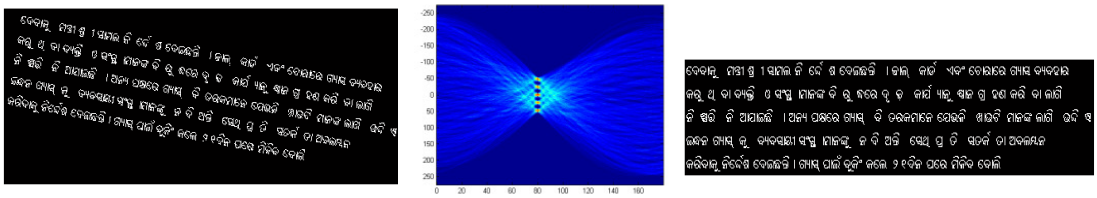

(a) (b) (c)

FIGURE 1: (a) The original scanned document image, (b) Radon transform of the document showing peaks at Ø=80° and (c) The document image after skew correction

2.2 Segmentation

Case 1: In figure (2), the lines were separated using horizontal projection and similarly the words were separated using the vertical projection. The printed documents after skew correction could be segmented completely with 100% accuracy. Separated words were concatenated to each other to remove any space in-between them and finally, the words were joined together to make a bigger line. The length of the line was approximately 14 words. These lines were used as input to the next stage of script recognition process. Space between the words was removed to avoid its effect on the result of the cumulant.

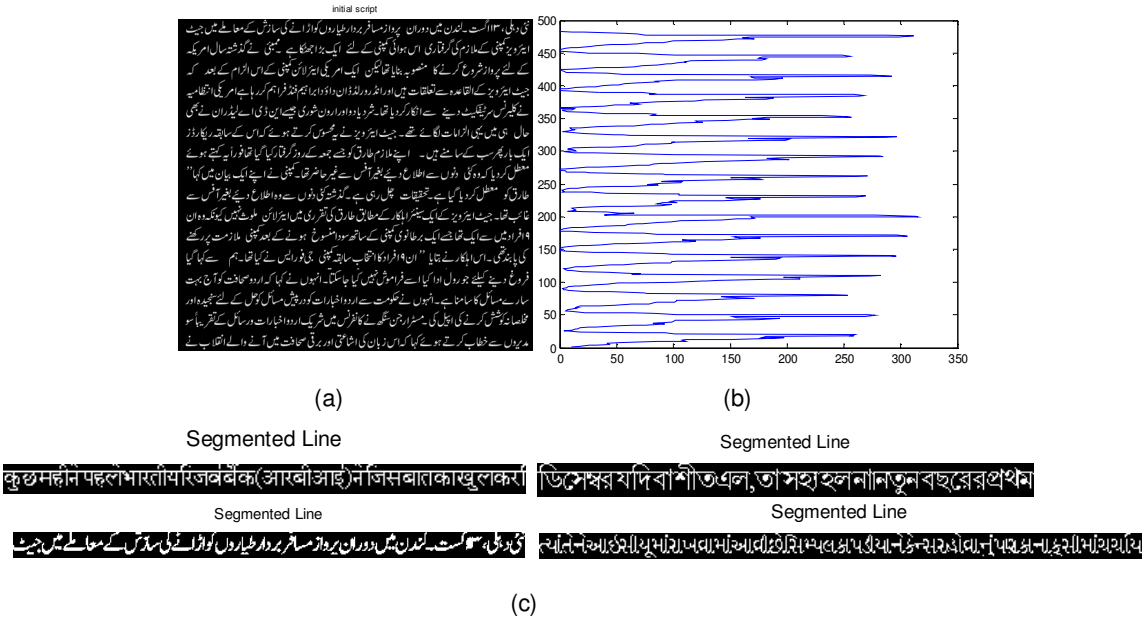

(a) (b)

(c)

FIGURE 2: First technique - line segmentation
(a) Original script, (b) Horizontal projection and (c) Segmented lines

Case 2: In some of the hand-written documents, words could not be separated using the projection technique and hence the morphologically conditioned k-means was used to separate them. The structuring element used was a line of three pixel length at an angle of 90°. Size of the structuring element was decided to make the word look like a cluster. When analyzed, the three pixel length was an optimum choice to make the word of any font and size separable. The documents were initially eroded and then k-means clustering method was applied to get the cluster centroids. The major limitation of using k-means is that it requires the optimal number of

clusters as input i.e. the total number of words in the sample document should be known very precisely before applying the unsupervised clustering techniques. MDL (minimum description length) criteria was used [20] to determine the optimum number of clusters (words) for the individual document. k-NN was used to isolate the words of the hand-written document. This method also works perfectly for the documents having words with some ligature connecting them. Figure (3) shows the document and the segmentation results.

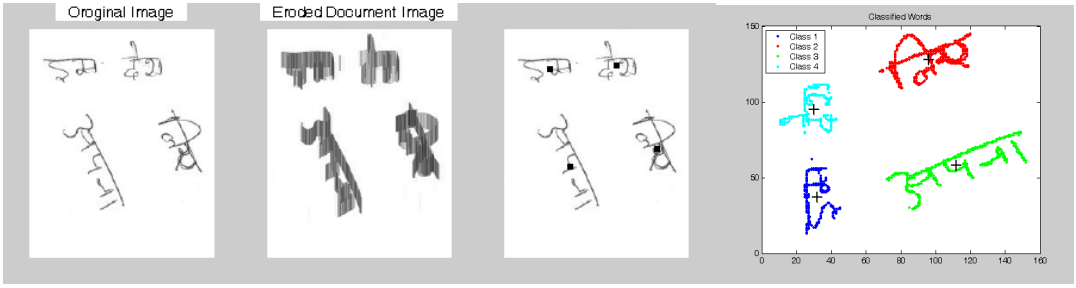

FIGURE 3: Second technique – word segmentation

Space was never allowed to be considered as part of the text for analysis. The script identification is a process which does not consider the space and the carriage return as a part of the text for getting the script features.

3. CUMULANTS

Cumulants are used to extract the inherent features of Indian scripts which are otherwise extremely difficult to extract. Higher order cumulant helps in understanding the multi-dimensional information. Structures are generally specific to the scripts, very complex and some times vary slightly from one script to the other. The paper has successfully attempted to distinguish the Indian Scripts. The first-order cumulant of a stationary process is the mean, $C_{1x} = E\{x(t)\}$. The higher-order cumulants represent central moments and therefore are invariant to the mean shift. Hence, it is convenient to define them under the assumption of zero mean. If the process has a nonzero mean, we subtract the mean and then apply the following definitions to the resulting process. The second, third and fourth-order cumulants of a zero-mean stationary process are defined by equations (1, 2 and 3).

$$C_{2x}(k) = \mathrm{E}\{x^*(n)x(n+k)\} \tag{1}$$

$$C_{3x}(k,l) = \mathrm{E}\{x^*(n)x(n+k)x(n+l)\} \tag{2}$$

$$C_{4x}(k,l,m) = \mathrm{E}\{x^*(n)x(n+k)x(n+l)x^*(n+m)\} - C_{2x}(k)C_{2x}(l-m) - C_{2x}(l)C_{2x}(k-m) - M^*_{2x}(m)M_{2x}(k-l) \tag{3}$$

where $M_{2x}(m) = E\{x(n)x(n+m)\}$ and equals $C_{2x}(m)$ for a real valued process. The zero-lag cumulants have special names like $C_{2x}(0)$ is the variance and $\sigma_x^2 : C_{2x}(0,0)$ and $C_{4x}(0,0,0)$ are usually denoted by γ_{3x} and γ_{4x}. We will refer to the normalized quantities $\gamma_{3x}/\sigma_{2x}^3$ as the skewness and γ^4/σ_{2x}^4 as the kurtosis. These normalized quantities are both shift and scale invariant. If $x(n)$ is symmetrically distributed, its skewness is necessarily zero (but not vice versa); if $x(n)$ is Gaussian distributed, its kurtosis is necessarily zero (but not vice versa). Often the terms skewness and kurtosis are used to refer to the un-normalized quantities, γ_{3x}andγ_{4x}. Equation (4) shows that the cumulants of a stationary real-valued process are symmetric in their arguments.

$$C_{2x}(k) = C_{2x}(-k)$$

$$C_{3x}(k,l) = C_{3x}(l,k) = C_{3x}(-k,l-k)$$
$$C_{4x}(k,l,m) = C_{4x}(l,k,m) = C_{4x}(k,m,l) = C_{4x}(-k,l-k,m-k) \quad (4)$$

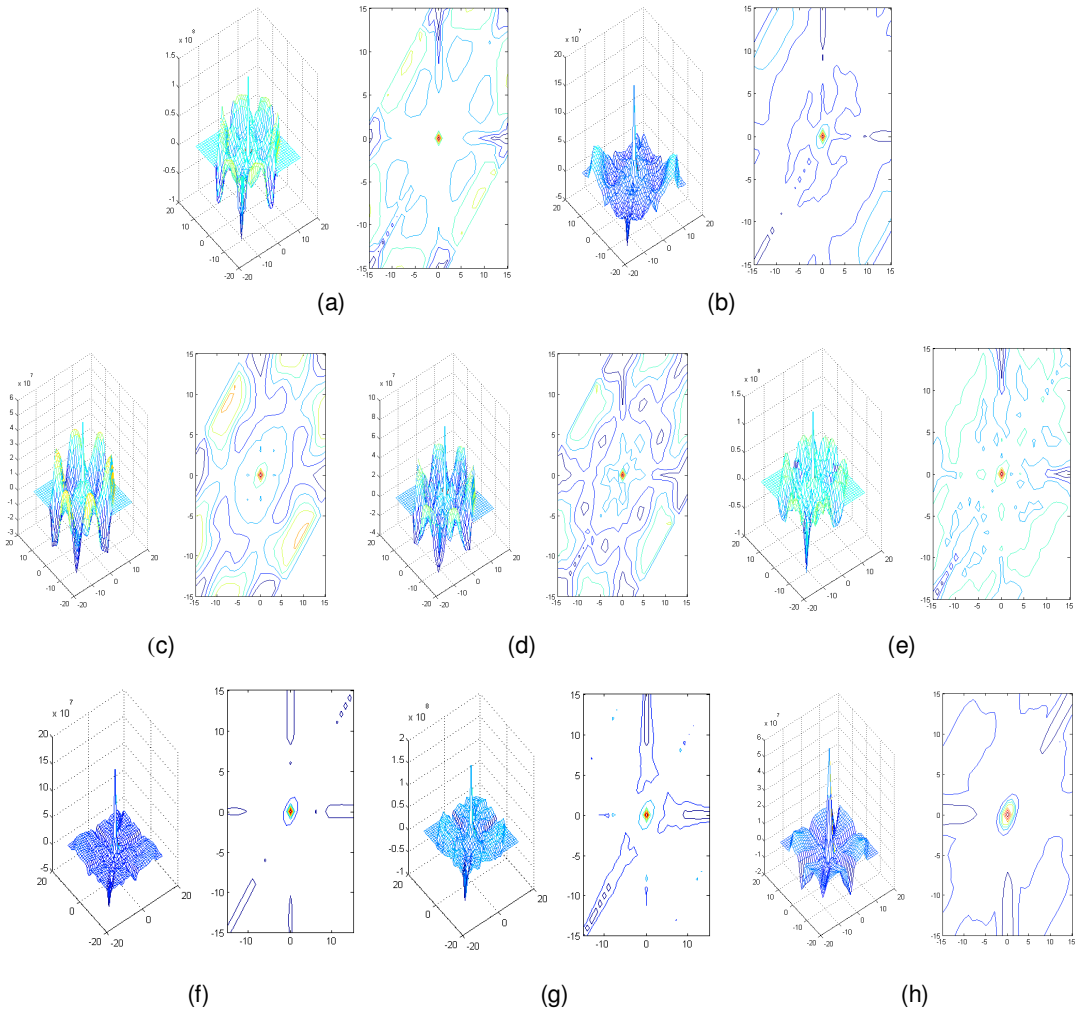

FIGURE 4: 3rd order cumulant computed for different script samples

Figure 4 (a-b) shows the 3rd order cumulant taken for the closely related scripts like Assamese and Bangla. The results demonstrate efficiency of the cumulants to distinguish among the said scripts. Similarly, figure 4(c-h) shows the 3rd order cumulant of the Gujarati, Devanagari, Gurumukhi, Telugu, Kannada and Urdu scripts, respectively. Spectrum of higher order cumulants provides features that are inherent to the script. The k^{th}order poly-spectrum is defined as the FTs of the corresponding cumulant sequence:

$$S_{2x}(f) = \sum_{k=-\infty}^{\infty} C_{2x}(k)\, e^{-j2\pi fk} \quad (5)$$

$$S_{3x}(f_1,f_2) = \sum_{k=-\infty}^{\infty}\sum_{l=-\infty}^{\infty} C_{3x}(k,l)\, e^{-j2\pi f_1 k} e^{-j2\pi f_2 l} \quad (6)$$

$$S_{4x}(f_1,f_2,f_3) = \sum_{k,l,m=-\infty}^{\infty} C_{4x}(k,l,m)\ e^{-j2\ \pi\ (\ f_1 k + f_2 l + f_3 m)} \quad (7)$$

which are the power spectrum, bi-spectrum and tri-spectrum, respectively. In contrast with the power spectrum which is real-valued, bispectra and tri-spectra are complex valued. For a real-valued process, symmetry properties of cumulants are carried forward to the symmetry properties of corresponding poly-spectra. The power spectrum is symmetric: $S_{2x}(f) = S_{2x}(-f)$.

Equation (8) shows the symmetry properties of the bi-spectrum:

$$S_{3x}(f_1,f_2) = S_{3x}(f_2,f_1) = S_{3x}(f_{1,} - f_1 - f_2) = S_{3x}(-f_1,-f_2,f_2) = S^*_{3x}(-f_1,-f_2). \quad (8)$$

Equation (9) shows the symmetry properties of the tri-spectrum:

$$S_{4x}(f_1,f_2,f_3) = S_{4x}(f_1,f_3,f_2) = S_{4x}(f_2,f_1,f_3) = S_{4x}(-f_1,f_2-f_1,f_3-f_1) = S^*_{4x}(-f_1,-f_2-f_3) \quad (9)$$

Equation (10) defines the cross-cumulants which are similar to the cross-correlations:

$$C_{xyz}(k,l) = \mathrm{E}\{x^*(n)\,y(n+k)\,z(n+l)\} \quad (10)$$

And equation (11) defined the cross-bi-spectrum:

$$S_{xyz}(f_1,f_2) = \sum_{\kappa=-\infty}^{\infty}\sum_{l=-\infty}^{\infty} C_{xyz}(\kappa,l)\ e^{-j2\pi f_1 \kappa}\ e^{-j2\pi f_2 l} \quad (11)$$

Note that the bi-spectrum $S_{2x}(f_1,f_2)$ is a special case of the cross-bi-spectrum obtained when $x = y = z$. The cross-bi-coherence is another useful statistic which is defined in equation (12):

$$bic_{xyz}(f_1,f_2) = \frac{S_{xyz}(f_1,f_2)}{\sqrt{S_{2x}(f_1+f_2)S_{2y}(f_1)S_{2z}(f_2)}} \quad (12)$$

And the cross-bi-spectrum of three processes is defined in equation (13).

$$b_{xyz}(m,n) = \int\int ln\,(S_{xyz}(f_1,f_2))\ e^{j2\pi f_1 m}\ e^{j2\pi f_2 n}\ df_1\ df_2 \quad (13)$$

This equation is well-defined only if $S_{xyz}(f_1,f_2)$ is nonzero everywhere. The 3rd order cumulant and its bispectra effectively measure the symmetry/non-symmetry of the structures belonging to different scripts. The results shown in the next section demonstrate that bispectra can effectively differentiate various Indian scripts.

4. BISPECTRA ESTIMATION

The cross-bispectra is estimated as the FT of third-order cross-cumulant of a sequence given by equation (14):

$$I^N_{xyz}(f) = \sum_{k=-N+1}^{N-1}\sum_{l=-N+1}^{N-1} \bar{C}_{xyz}(k,l)e^{-j2\pi f_1 k}e^{-j2\pi f_2 l} = \frac{1}{N^2}X^*_N(f_1+f_2)Y_N(f_1)Z_N(f_2) \quad (14)$$

Where $X_N(f)$ is the FT of $\{x(n)\}_{n=0}^{N-1}$. This estimate is known as the cross-biperiodogram but it is not a consistent estimate. As in the case of the power spectrum, the estimate can be made consistent by suitable smoothing. The bi-spectrum and the bi-periodogram are special cases obtained when $x = y = z$. Smoothing can be accomplished by multiplying the third-order cumulant estimates by a lag window function. Let $w(t,s)$ be a 2-D window function whose 2-D FT is bounded and nonnegative with the following assumptions given in equation (15):

$$w(0,0) = 1;$$

$$\iint w^2(t,s)dtds < \infty;$$
$$\iint f_i^2 W(f_1,f_2)df_1df_2 < \infty;$$
$$\iint f_i W(f_1,f_2)df_1df_2 = 0; \quad (15)$$

The window function $w(t,s)$ should also satisfy the symmetry properties of the third-order cumulant. Equation (16) can be used to derive the 2-D lag windows from 1-D lag windows.

$$w(t,s) = w(t)w(s)w(t-s) \quad (16)$$

This satisfies the symmetry conditions of $C_{3x}(m,n)$. Consider the scaled-parameter window $w_M(t,s) = w(t/M, s/M)$ and the smoothed frequency response, given in equation (17).

$$\hat{S}_{xyz}(f_1,f_2) = \sum_{k=-N-1}^{N-1} \sum_{l=-N-1}^{N-1} \hat{C}_{xyz}(k,l)\, w_M(k,l)\, e^{-j2\pi f_1 k} e^{-j2\pi f_2 l} \quad (17)$$

Under the assumption that the cross-bispectrum $\hat{S}_{xyz}(f_1,f_2)$ is sufficiently smooth, the smoothed estimate is known to be consistent with variance given by equation (18).

$$\mathrm{var}(\hat{S}_{xyz}(f_1,f_2)) = \frac{M^2}{N} S_{2x}(f_1+f_2) S_{2y}(f_1) S_{2z}(f_2) \iint w^2(t,s)dtds \quad (18)$$

for $0 < f_1 < f_2 < \pi$. Note that the implied consistency condition is $M \to \infty$ and $M^2/N \to \infty$ as $N \to \infty$ and $\iint w^2(t,s)dtds < \infty$. Equation (17) is used to estimate the bispectra for $x = y = z$. An alternative approach is to perform the smoothing in the frequency domain. As in the case of power spectra, it is possible to segment the data into K records of length $L = N/K$, compute and average the biperiodogram, and then perform the frequency smoothing using the frequency-domain filter $W_M(f_1,f_2)$ estimated by taking the FT of $w_M(t,s)$. In this case,

$$var\left(\hat{S}_{xyz}(f_1,f_2)\right) = M^2/LK\, S_{2x}(f_1+f_2) S_{2y}(f_1) S_{2z}(f_2) \iint w^2(t,s)dtds \quad (19)$$

for $0 < f_1 < f_2 < \pi$. Windowing is not required in case K is very large. The following sub-section describes the parameter selection and optimization for the estimation of bispectra.

4.1. Parameters Selection and Optimization

The following table comprises various parameters and their corresponding optimized values required to compute the bispectra of collected script samples. Larger MaxLag gives more number of coupled frequencies and the value lesser than this will make the process of script identification difficult. The value of the MaxLag also depends upon the data size. Here data size means size of the character of a particular script. Maximum value of the MaxLag can be the no. of pixels which describe the height of the character therefore the MaxLag value is proportional to the data size (Height of the character). Hamming window was utilized. The parameters have been optimized for the targeted scripts.

Name of the Parameter	MaxLag	Sample Rate	Window	Scale
Optimized Value	15	5	Hamming	Unbiased

TABLE 2: Optimized parameters for the bispectra estimation of collected samples

The parameters given in table (2) were utilized for the computation of bispectra of various script samples and the results are given below.

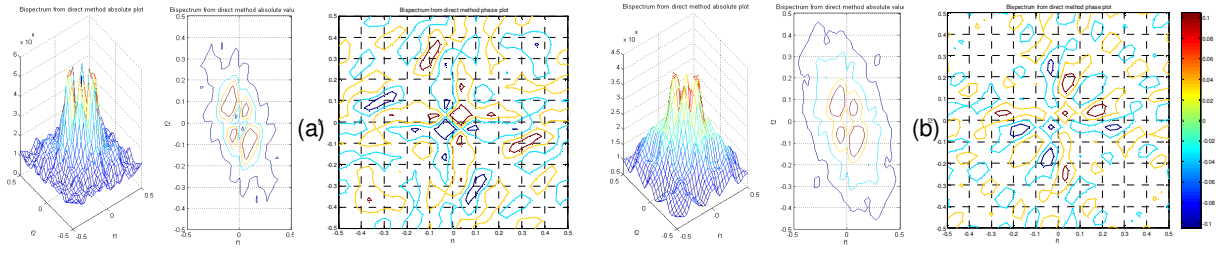

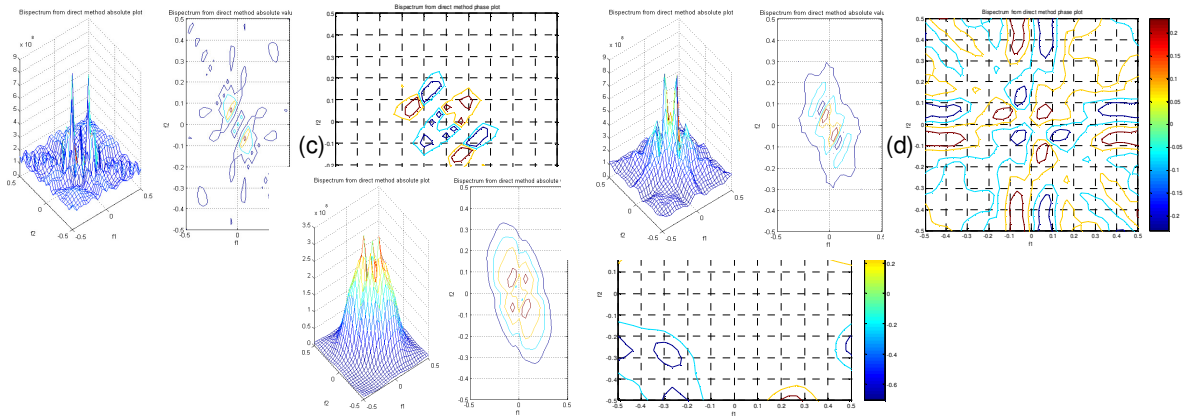

(e)

FIGURE 5: (a-e) Bispectra results (magnitude and phase) obtained for Kannada, Telugu, Assamese, Bangla and Urdu scripts, respectively

Figure (5) shows that bispectra can completely distinguish the partially similar Indian scripts.

5. BIWAVELANT

As the Indian scripts are partially similar to each other, in order to identify them, the samples must include more number of dissimilar characters. The features of individual lines are added repeatedly to enhance the dissimilarity until it reaches to a saturation level. The experimental results provided in figure (4) and (5) show that a sample size of 100 lines is sufficient to get the expected results. In order to use bispectra for script identification, the redundant information (high frequency components) is removed keeping only the prominent features (low pass information) which is described further.

5.1 Smoothing Filter vs. Wavelet

Both smoothing filter and wavelet transform can be used to remove the high frequency components from bispectra. But a smoothing filter can't protect the precious details while removing the high pass information, therefore wavelet transform is used. The wavelet transform was introduced in [21], [22], [23] and defined as

$$W_{xy}(b,a) = \frac{1}{\sqrt{a}} \int x(t)\, y(\frac{t-b}{a}) dt \qquad (20)$$

where $x(t)$ is the signal being transformed and $y(t)$ is the 'analyzing wavelet'. $y(t)$ satisfies the admissibility condition $\int |Y(\omega)|^2 \frac{d\omega}{\omega} < \infty$ which is equivalent to $\int Y(t) dt = 0$ i.e. a wavelet has zero mean. The use of the wavelet transform as a multi-resolution analysis tool has been widespread involving many applications such as fractal signal analysis, pitch detection and image compression. However, Frisch [24] and Messer [25] took a different interpretation of the continuous wavelet transform and considered it as a two parameter correlation operation where time and dilation are the correlation parameters i.e. $x(t)$is considered as a received noisy signal with known amplitude, delay and dilated factor. $y(t)$ is the template of the known shape. Therefore using the continuous wavelet transform and an appropriate decision statistic, the detection can be made for a signal buried in Gaussian noise. This interpretation will be later used in the use of wavelants. Two important properties of the cumulants are:

1. The third order cumulant for a Gaussian (or any symmetrically distributed) random process is zero.
2. If a subset of k random variables $\{x_i\}$ is independent of the rest, then the third-order cumulant is zero.

The above formulation exhibits properties closely related to those of cumulants. The higher order wavelant can also be expressed using the Fourier representations of the signals given by equations (21) and (22):

$$W^3_{XYZ}(b_1,a_1;b_2,a_2) = 1/\sqrt[3]{a_1 a_2}\iint S_{3X}(f_1,f_2)Y(a_1 f_1)Z(a_2 f_2)e^{-j(w_1 b_1+w_2 b_2)}dw_1 dw_2 \quad (21)$$

$$W^3_{XXX}(b_1,a_1;b_2,a_2) = 1/\sqrt[3]{a_1 a_2}\iint S_{3X}(f_1,f_2)X(a_1 f_1)X(a_2 f_2)e^{-j(w_1 b_1+w_2 b_2)}dw_1 dw_2 \quad (22)$$

The 2-D cross-wavelant for an image can be expressed as:

$$W^3_{xyz}(b_{X1},b_{Y1},a_{X1},a_{Y1};b_{X2},b_{Y2},a_{X2},a_{Y2}) = \cdots \frac{1}{\sqrt[3]{a_{X1}a_{X2}a_{Y1}a_{Y2}}}\iint X(t_X,t_Y)Y\left(\frac{t_X-b_{X1}}{a_{X1}},\frac{t_Y-b_{Y1}}{a_{Y1}}\right)Z\left(\frac{t_X-b_{X2}}{a_{X2}},\frac{t_Y-b_{Y2}}{a_{Y2}}\right)dt_X dt_Y \quad (23)$$

The equations (21) and (22) define the third-order cross and auto wavelants and equation (23) defines the cross-wavelant for 2D images.

5.2 Properties

When the input used for computing the wavelant is translated and/or followed by dilation then the following properties result

If	$x(t),y(t),z(t)$	maps to	$W^3_{XYZ}(b_1,a_1;b_2,a_2)$	
Then	$x\left(\frac{t-\tau}{A}\right),y(t),z(t)$	maps to	$W^3_{XYZ}\left(\frac{b_1-\tau}{A},\frac{a_1}{A};\frac{b_2-\tau}{A},\frac{a_2}{A}\right)$	
and	$x(t),\frac{1}{\sqrt{A}}y\left(\frac{t-\tau}{A}\right),z(t)$	maps to	$W^3_{XYZ}(b_1+a_1\tau,a_1A;b_2,a_2)$	
and	$x(t),y(t),\frac{1}{\sqrt{A}}z\left(\frac{t-\tau}{A}\right)$	maps to	$W^3_{XYZ}(b_1,a_1;b_2+a_2\tau,a_2A)$	(24)

However, if the input is first dilated and then translated, then the results are given by

If	$x(t),y(t),z(t)$	maps to	$W^3_{XYZ}(b_1,a_1;b_2,a_2)$	
then	$x(At-\tau),y(t),z(t)$	maps to	$W^3_{XYZ}(Ab_1-\tau,a_1A;Ab_2-\tau,a_2A)$	
and	$x(t),\sqrt{A}y(At-\tau),z(t)$	maps to	$W^3_{XYZ}\left(\frac{b1+\tau}{A},\frac{a_1}{A};b_2,a_2\right)$	
and	$x(t),y(t),\sqrt{A}z(At-\tau)$	maps to	$W^3_{XYZ}\left(b_1,a_1;\frac{b_2+\tau}{A},\frac{a_2}{A}\right)$	(25)

Before applying the wavelet transform, the 2D bispectra is first converted to a 1D frequency response. The following figure shows a comparison of the results obtained at different levels of approximations (low pass filtering) by applying wavelet transform (db8) on the bispectra results.

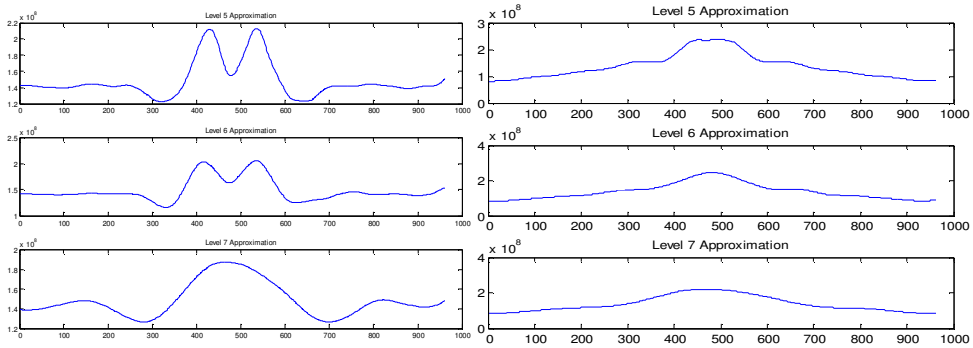

FIGURE 6: Approximation (low pass filtering) results at levels 5, 6 and 7 for (a) Assamese and (b) Bangla scripts

Figure (6) shows that after the 5th level approximation, we start loosing the precious details and therefore, before using bispectra results for identification/classification, they are approximated only up-to the 5th level. Following figure shows the results obtained for various Indian scripts.

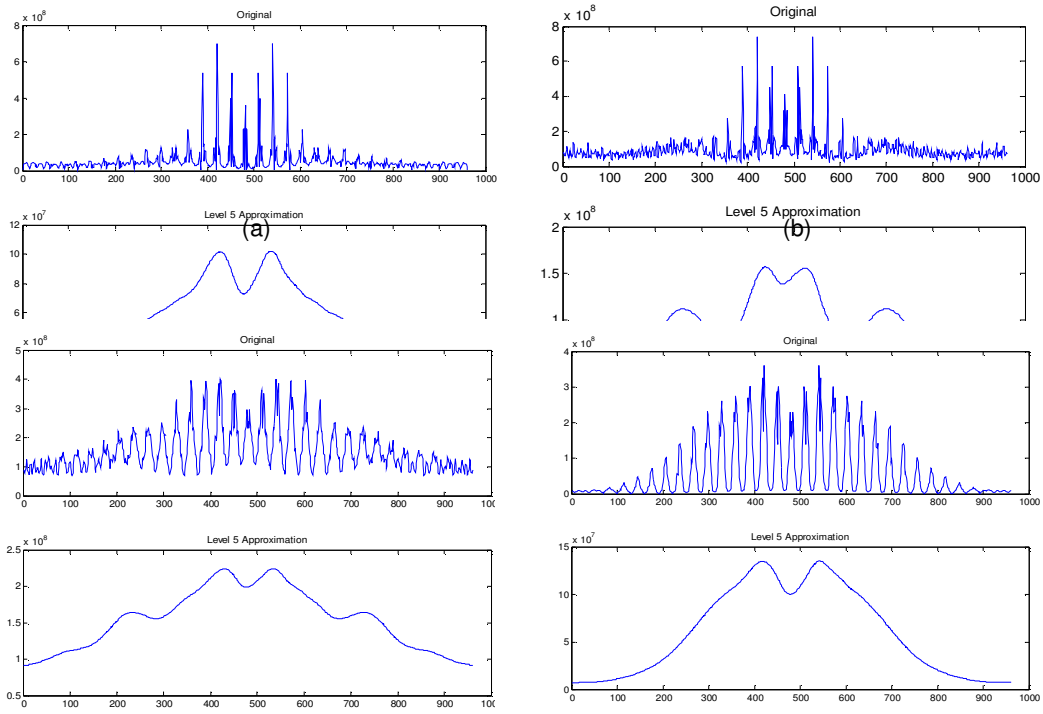

FIGURE 7: Approximated bispectra results for (a) Gujarati, (b) Bangla, (c) Telugu and (d) Urdu scripts

The following figure shows that in addition to the dissimilar results obtained for different scripts, the method gives fairly similar results for same script with different font types and sizes.

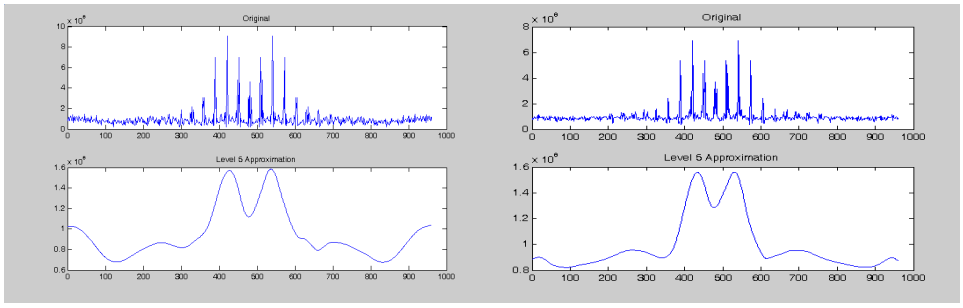

FIGURE 8: Biwavelant results obtained for font size (a) 14 and (b) 16

Figure (8) shows the biwavelant results obtained for Devanagari script for two different font sizes. Figures (7) and (8) illustrate that biwavelant (bispectra + wavelet) gives an envelope of the bispectra which proves to be a convincing feature for script identification.

6. PRE-CLASSIFICATION

6.1. Newton-Raphson Technique

The above results show that a biwavelant envelope can clearly distinguish/identify an Indian script; but using it directly for the classification/identification of a script sample is not suitable because of its high dimensionality. Therefore, Newton-Raphson technique is used to obtain the roots of a biwavelant envelop for each script sample in order to reduce the dimensionality of the feature space. The following table shows that the obtained roots clearly distinguish the Indian scripts.

ROOTS TABLE		
Script	**Root 1**	**Root 2**
Urdu	1.36E+16	2.51E+15
Urdu	1.41E+16	2.45E+15
Urdu	1.39E+16	2.47E+15
Telugu	6.11E+15	1.68E+15
Telugu	6.39E+15	1.66E+15
Telugu	6.35E+15	1.68E+15
Bangla	1.74E+16	1.23E+15
Bangla	1.86E+16	1.26E+15
Bangla	1.62E+16	1.10E+15
Kannada	3.44E+13	1.95E+15
Kannada	3.75E+13	2.12E+15
Kannada	3.94E+13	2.11E+15
Guajarati	4.22E+15	5.10E+14
Guajarati	4.16E+15	5.27E+14
Guajarati	4.18E+15	5.16E+14
Gurmukhi	6.73E+15	9.70E+14
Gurmukhi	5.22E+15	6.60E+14
Gurmukhi	8.86E+15	10.3E+14
Assamese	2.03E+16	4.75E+14
Assamese	2.13E+16	4.78E+14
Assamese	1.97E+16	4.84E+14
Devanagari	1.05E+16	5.93E+14
Devanagari	1.06E+16	6.22E+14
Devanagari	1.06E+16	6.02E+14

TABLE 3: Roots obtained for Indian scripts using the Newton-Raphson technique

Script	No. of Lines Used	Root-1	Root-2
Assamese	110	1.70E+16	3.99E+14
Assamese	105	1.55E+16	3.64E+14
Assamese	100	1.42E+16	3.29E+14
Assamese	90	1.14E+16	2.67E+14
Assamese	80	8.97E+15	2.11E+14
Assamese	70	6.75E+15	1.63E+14
Assamese	60	4.85E+15	1.23E+14
Assamese	50	3.37E+15	8.56E+13
Assamese	40	2.07E+15	5.62E+13
Assamese	30	1.14E+15	3.23E+13
Assamese	20	5.16E+14	1.43E+13
Assamese	11	1.58E+14	4.35E+12
Assamese	6	4.69E+13	1.30E+12
Assamese	3	1.22E+13	3.14E+11

TABLE 4: Variation of the roots for Assamese script with the number of lines used in the paragraph of a script sample

This variation of roots is plotted and shown in the following figure (9).

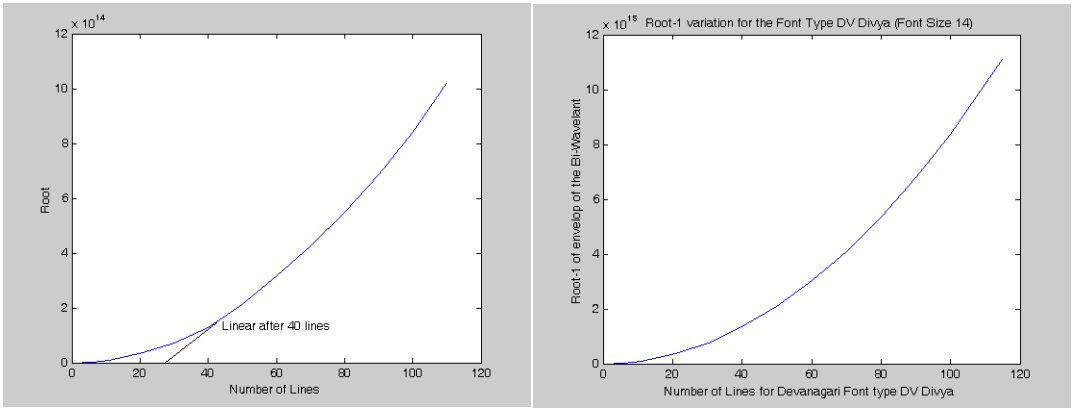

(a) (b)

FIGURE 9: Variation of the roots with number of lines used in the paragraph of a script sample for (a) Guajarati, (b) Devanagari scripts

Figure (9) shows that the variation of roots is linear to the sample size (no. of lines) and it holds for all Indian scripts. The small non-linear portion is common to all scripts and hence, the deferential effect gets cancelled. In order to estimate the level of confidence attained in identifying a script sample and the possibility of making an erroneous decision, two parameters, $ConfidenceLevel$ and $ErrorPossibility$ are defined in equation (26) as a function of the number of lines constituting the test sample:

$$ConfidenceLevel = \frac{\sum_{k=1}^{L-1} Cum(k) - Cum(L)}{\sum_{k=1}^{L-1} Cum(k)}$$

$$ErrorPossibility = 1 - ConfidenceLevel \quad (26)$$

where $Cum(k)$ represent the third order cumulant of the k^{th} line and L is number of lines in the script sample. For a particular script sample $4 \leq L \leq 120$. The following figure shows the variation of $ConfidenceLevel$ and $ErrorPossibility$ with the number of lines in the script sample.

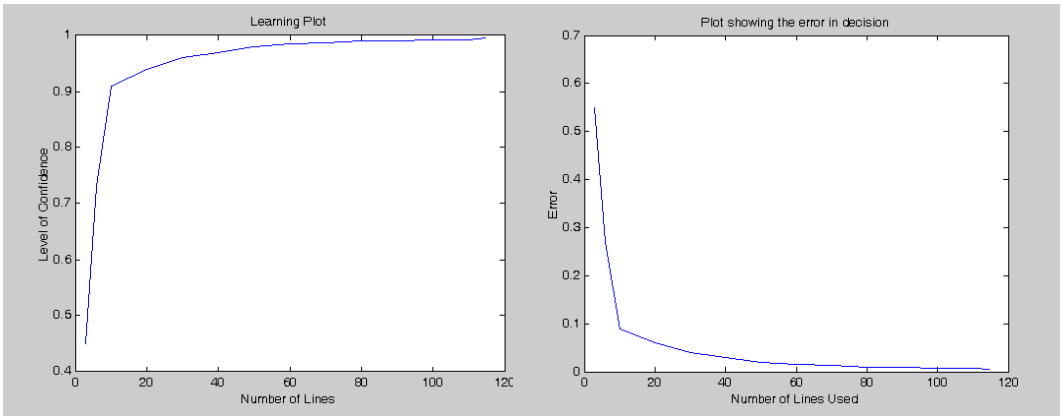

(a) (b)

FIGURE 10: Variation of (a) $ConfidenceLevel$ and (b) $ErrorPossibility$ with the number of lines used by the algorithm to identify the script sample

Figure (10) shows that the motive behind using more number of lines for feature extraction is to have a higher confidence level in identifying a script sample.

7. CLASSIFICATION

7.1. k-Nearest Neighbor Classification

The k-means clustering algorithm is a fast, unsupervised, nondeterministic and iterative method for generating a fixed number of disjoint clusters. Each data point is randomly assigned to one of k-initial clusters, such that each cluster has approximately the same number of points. In the subsequent iterations, distance of each point to each of the clusters is calculated using some metric and subsequently moved into the cluster corresponding to the minimum distance. Commonly used metrics are Euclidian distance to the centroid of the clusters or a weighted distance which considers only the closest n-points. The algorithm terminates when no points are moved in a single iteration. As the final result is highly dependent on the initialization of the clusters, the algorithm is often repeated a number of times, with each solution scored according to some evaluation function. The following figure shows the classification results obtained for various Indian scripts using the nearest neighbor classifier.

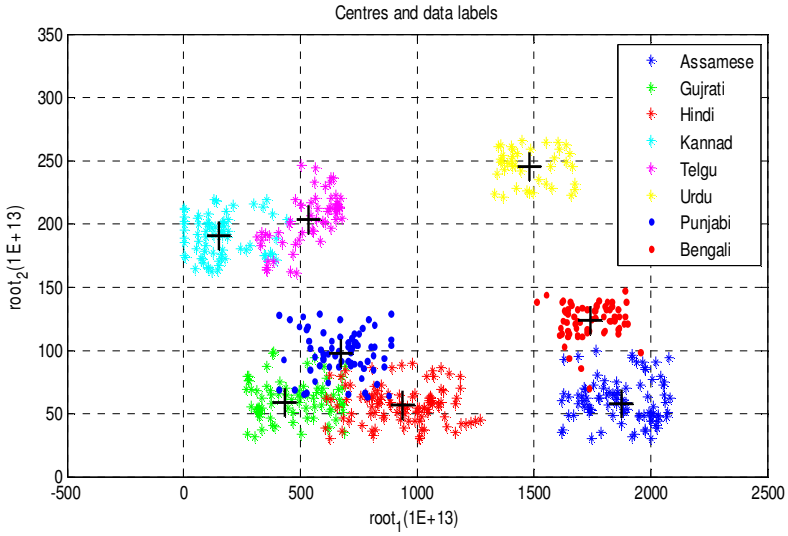

FIGURE 11: Classification results obtained for the Indian scripts

Each point in figure (11) represents the feature vector (root1, root2) corresponding to a script sample. Each sample is classified and associated to one of the eight clusters (scripts) i.e. to a particular script. The clusters are shown with different colors and markers for easy understanding. Centroid of each cluster, represented with + in figure (11), is computed using unsupervised k-means clustering and given in the following table.

CENTROIDS		
Script	**Root 1**	**Root 2**
Urdu	1.48E+16	2.45E+15
Telugu	5.36E+15	2.03E+15
Gujarati	4.31E+15	5.90E+14
Bangla	1.74E+16	1.23E+15
Kannada	1.53E+15	1.90E+15
Assamese	1.87E+16	5.70E+14
Gurmukhi	6.73E+15	9.70E+14
Devanagari	9.39E+15	5.60E+14

TABLE 5: Centroids of the clusters representing individual scripts

7.2. Multi-Layer Perceptron

The designed MLP network with logistic outputs has been trained with a quasi-Newton optimization algorithm and various other optimized parameters given below in table (6). The multilayer perceptron network takes two dimensional feature vectors as input.

MULTI-LAYER PERCEPTRON NETWORK		
Sr. No.	**Parameter Name**	**Parameter Value**
1	Algorithm Used	quasi-Newton optimization algorithm
2	No. of input neurons	2
3	No. of hidden layer neurons	6
4	No. of output layer neurons	1
5	Rate of weight decay	0.2
6	No. of training cycles	100
7	Activation function for hidden neurons	tanh

TABLE 6: Characteristic parameters of the multilayer network used for the training and classification

The classification results obtained using the above MLP network are shown in the following figure.

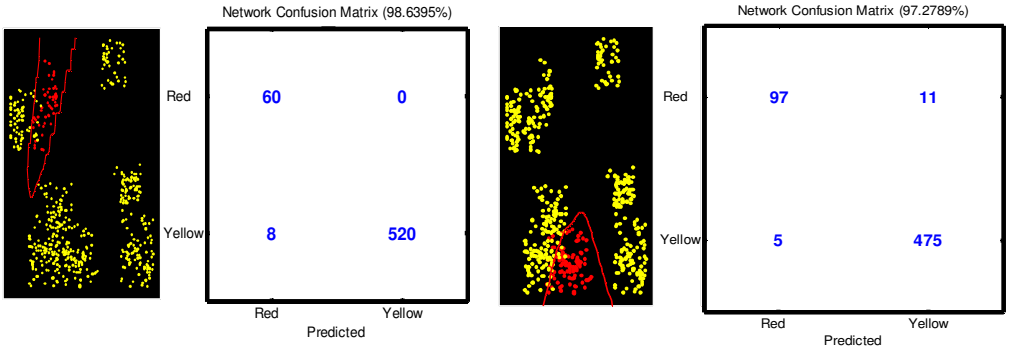

(a) (b)

FIGURE 12: Classification results and the corresponding confusion matrix for (a) Telugu, (b) Devanagari scripts

7.3. Support Vector Machine

Finally, the one vs. rest support vector machine was used to classify the partially similar Indian scripts. Various optimized parameters used to design the support vector machine are given below.

Sr. No.	Parameter Name	Parameter Value
1	Classifier Type	One vs. Rest
2	Kernel	Radial Basis Function
3	Scale	0.2
4	C	1000
5	Optimizer	libsvm

TABLE 7: Various parameters used to design the support vector machine

The classification results obtained using the proposed support vector machine is given below in the form of a confusion matrix.

Scripts	Assamese	Bangla	Gujarati	Devanagari	Kannada	Gurmukhi	Telugu	Urdu
Assamese	0.9826	0.0174	0	0	0	0	0	0
Bangla	0.0199	0.9801	0	0	0	0	0	0
Gujarati	0	0	0.9442	0.0421	0	0.0137	0	0
Devanagari	0	0	0.0540	0.9172	0	0.0288	0	0
Kannada	0	0	0	0	0.9899	0	0.0101	0
Gurmukhi	0	0	0.0521	0.0464	0	0.9015	0	0
Telugu	0	0	0	0	0.0118	0	0.9882	0
Urdu	0	0	0	0	0	0	0	1.0000

TABLE 8: Classification results obtained for various scripts and the corresponding confusion matrix

8. SCRIPT SAMPLES & CLASSIFICATION RESULTS

The proposed system was tested for eight Indian scripts using both printed and hand written samples as shown in the following figure.

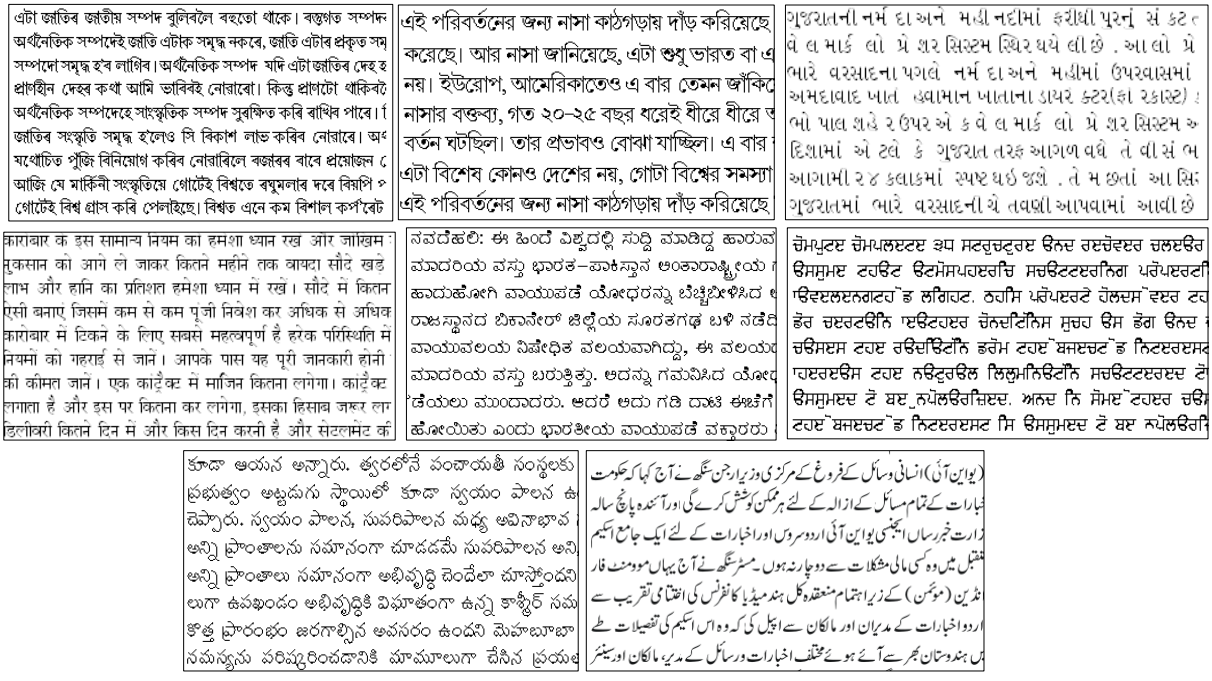

FIGURE 13: Samples of eight Indian scripts used for training and testing of the proposed algorithm

In addition to the above, the proposed system was also tested on same script samples with different font types and sizes as shown in figure (14).

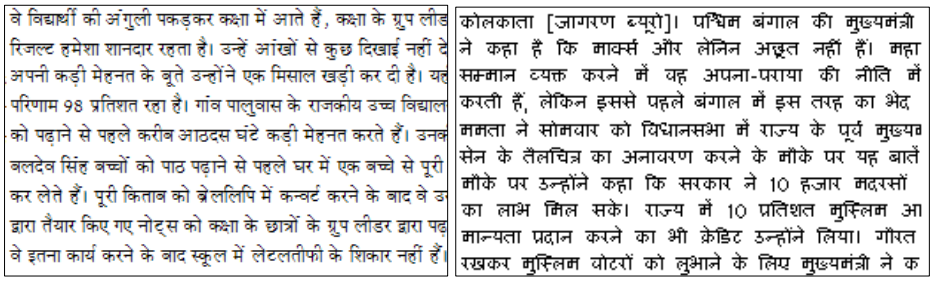

FIGURE 14: Samples of Devanagari script with different font types and sizes

The comparison of identification results obtained with various classifiers mentioned in the previous section is given in table (9).

Sr. No.	Classifier Type	Classification Accuracy (%)
1	Bayes Quadratic	90
2	Decision Layer	91
3	Nearest Neighbour Classifier	87
4	Multi Layer Perceptron	94
5	Support Vector Machine	95

TABLE 9: Classification accuracy with various classifiers

9. CONCLUSION

The method has successfully identified eight Indian scripts and is expected to work for scripts from other nations also. Indian scripts are closely related to each other and as the proposed technique is sensitive to the structural changes in the script, it is able to distinguish them successfully. But, the same sensitivity makes the method vulnerable to noise in the samples, so the document has to be noise free for expected results. However, the pre-processing becomes very complex for the removal of noise from the samples. The features of individual lines were added until they reach to a saturation level. This saturation level in turn helped in determining the confidence level for indentifying a sample. The variation in confidence level with the number of lines in the sample was used to determine an optimum number of lines required in identifying a script. A sample size of 100 lines gives the best result as it considers most of the features in the script. The method works well for both the printed and hand written samples of the scripts, independently. However, it does not work for the sample with a mixture of printed and hand-written lines of a script. Pre-processing of hand-written scripts also adds to the complexity of the method. In such a case of mixed characters, cumulants are not useful as being very sensitive to the curvatures. Indian scripts are partially similar to each other. Because of the partial similarity, we first consolidated on the number of words which enhances the partial dissimilarity and makes it look significant. Then we used the method which is very sensitive to the curvatures and the results were as expected.

REFERENCES

[1] S. B. Patil and N. V. Subbareddy, “Neural network based system for script identification in Indian documents”, *SADHNA,* vol. 27, pp. 82-97, Feb. 2002.

[2] J. Hochberg, P. Kelly, T. Thomas and L. Kerns, “Automatic script identification from document images using cluster-based templates”, *IEEE Transactions on Pattern Analysis and Machine Intelligence,* vol. 19 (2), pp.176-181, Feb. 1997.

[3] D. Dhanaya, A. G. Ramakrishnan and P. B. Pati, “Script identification in printed bilingual documents”, *SADHNA,* vol. 27, pp. 73-82, Feb. 2002.

[4] B. B. Chaudhuri and U. Pal, "Skew angle detection of digitized Indian script documents", *IEEE Transactions on Pattern Analysis and Machine Intelligence,* vol. 19 (2), pp.182-186, Feb. 1997.

[5] S. Chaudhuri and R. Sheth, "Trainable script identification strategies for Indian languages", *International Conference on Document Analysis and Recognition*, pp. 657-660, Sep. 1999.

[6] U. Pal and B. B. Chaudhuri, "Script line separation from Indian multi-script documents", *International Conference on Document Analysis and Recognition*, pp. 406-409, Sep. 1999.

[7] A. Spitz, "Determination of the script and language content of document images", *IEEE Transactions on Pattern Analysis and Machine Intelligence*, vol.19 (3), pp. 235-245, 1997.

[8] T. N. Tan, "Rotation invariant texture features and their use in automatic script identification", *IEEE Transactions on Pattern Analysis and Machine Intelligence*, vol. 20 (7), pp. 751-756, Jul. 1998.

[9] J. Hochberg, K. Bowers, M. Cannon and P. Kelly, "Script and language identification for handwritten document images", *International Journal on Document Analysis and Recognition*, vol. 2, pp. 45-52, Feb. 1999.

[10] S. H. Srinivasan, K. R. Ramakrishnan and S. Budhlakoti, "Character decomposition", *Indian Conference on Vision Graphics and Image Processing* at ISRO Ahmedabad, 2002.

[11] V. Bansal and R. M. K. Sinha, "On how to describe shapes of Devanagari characters and use them for recognition", *International Conference on Document Analysis and Recognition*, pp. 410-413, Sep. 1999.

[12] S. Antani and L. Agnihotri, "Gujarati character recognition", *International Conference on Document Analysis and Recognition*, pp. 418-421, Sep. 1999.

[13] A. M. Namboodiri and A. K. Jain, "Online handwritten script recognition", *IEEE Transactions on Pattern Analysis and Machine Intelligence*, vol. 26 (1), pp. 124-130, Jan. 2004.

[14] A. Busch, W. W. Boles and S. Sridharan, "Texture for script identification", *IEEE Transactions on Pattern Analysis and Machine Intelligence*, vol. 27 (11), pp. 1720-1732, Nov. 2005.

[15] B. V. Dhandhra, P. Nagabhushan, M. Hangarge, R. Hegadi and V. S. Malemath, "Script identification based on morphological reconstruction in document images", *International Conference on Pattern Recognition*, vol. 2, pp. 950-953, 2006.

[16] S. Sural and P. K. Das, "Recognition of an Indian script using MLP and Fuzzy features", *International Journal on Document Analysis and Recognition,* pp. 1120-1124, 2001.

[17] T. K. Bhowmik, P. Ghanty, A. Roy and S. K. Parui, "SVM based hierarchical architectures for handwritten Bangla character recognition", *International Journal on Document Analysis and Recognition*, vol. 12(2), pp. 97-108, July, 2009.

[18] D. Lopresti, S. Roy, K. Schulz and L. V. Subramaniam, "Special issue on noisy text analytics", *International Journal on Document Analysis and Recognition*, vol. 12(3), Sept. 2009.

[19] R. Kapoor, D. Bagai and T. S. Kamal, "A new technique for skew detection", *Pattern Recognition Letters, Elsevier Science Direct*, vol. 25(11), pp. 1215-1229, 2004.

[20] I. O. Kyrgyzov, H. Maitre and M. Campedel, "Kernel mdl to determine the number of clusters", *International Conference on Machine Learning and Data Mining,* Jul. 2007.

[21] J. M. Combes, A. Grossman and P. Tchamitchan, "Wavelets, time-frequency methods and phase space", Springer-Verlag, 1989.

[22] A. Grossman and R. Kronland-Martinet, "Time and scale representation obtained through

[23] continuous wavelet transform", Signal Processing IV, Theories and Applications, vol. Elsevier Science Pub. B. V. 1988, pp. 475-482.

[24] S. G. Mallat, "A theory for multiresolution signal decomposition", *IEEE Transactions on Pattern Analysis and Machine Intelligence*, vol. 11 (7), Jul. 1989.

[25] M. Frisch and H. Messer, "The use of the wavelet transform in the detection of an unknown transient signal", *IEEE Transaction on Information Theory*, *Special Issue on Wavelet Transforms and Multiresolution Signal Analysis*, vol. 38(2), pp. 892-897, Mar. 1992.

[26] M. Frisch and H. Messer, "Detection of a transient signal of unknown scaling and arrival time using the discrete wavelet transform", *International Conference on Acoustics, Speech and Signal Processing,* vol. 2, pp. 1313-1316, Apr. 1991.

A Step towards Method Configuration From Situational Method Engineering

Daya Gupta and Rinky Dwivedi

Computer Engineering Department, Delhi Technological University

Bawana, New Delhi, INDIA

Daya_gupta2005@yahoo.co.in, rinkydwivedi@gmail.com

Abstract-**We define a two part SME process having a configuration part and an assembly part. The former is to obtain methods that are configurable and individually meet partial requirements of the desired method. The assembly process then puts these methods together to form a coherent situated method. Thus, the SME process relies on the configuration sub process to provide a degree of assurance that the required situated method shall indeed be produced. We show how configurable methods can be produced and how these can be configured. The point when assembly is to be done is identified. An outline of the method base to support the SME process is presented.**

Keywords-**Configuration process, Situational method engineering, Variant.**

1. INTRODUCTION

Situational method engineering (SME) is the technique for constructing Information System Development Methods that address specific project needs. It relies on a method base that is the repository of method components. These components can be retrieved and assembled together to form the desired method. A number of approaches exist for component retrieval. These rely on notions of descriptors [1], project contingency factors [2] or method contexts [3]. Components are defined in compliance with Meta models and may be fragments [4], contexts [5], decisions [6] etc. The assembly technique itself has been illustrated in [9] for putting together state chart and object model.

A number of issues arise in these approaches to SME. The first issue is that of the appropriateness of the components retrieved. The retrieved component may or may not be found suitable to form the desired method during the assembly process. The second issue is of ensuring coherence of an assembly of components. Evidently, to get a coherent method, it is not enough to assemble only coarse grained components but the assembly process must go down to the finest grained components. Since assembly is to be done for all levels of granularity, it becomes a detailed tedious task.

Recently there are proposals to provide a rich set of guidelines and structured approaches [8, 10] to form a coherent method. These proposals are analogous to software engineering domain and are two staged first architecture of situated method is formed and then method is organized from this architecture. Thus method construction task is performed in a more disciplined and cohesive way. Still the issues of appropriateness of the method component being selected remain unanswered.

In recent times, the SME has moved to method configuration to construct a project specific method [20, 21]. They rely on base method/method components which can be transformed into a situation specific method through process of tailoring, extension or assembly. Recently configurability is gaining importance in industrial domain, two important case studies that reflect the practical application of this approach Case study of IBM global services on configurability of Work Products [12] and Case Study of Intel Shannon configuring agile methods [13]. We now shall extent the notion of configurability to situation method engineering.

We draw an analogy between method configuration and system configuration. The system configuration is based on the construction of a 'configurable system model' that represents the essential system concepts and inter-relationship between these. The configuration process then considers these to form the new system. It is assumed that the configurable system model is sufficiently generic to be specialized into a range of systems.

A number of issues need to be addressed for method configuration. The first is of a Meta model to be used to model the concepts of configured method. The second issue is what 'good component' is and what the 'right

granularity' is. The third is regarding the Selection of a method component and lastly the process of configuration to reach coherent desired method.

We approach the first issue by modifying the decisional Meta model of Prakash [6] to reach configurable Meta model capable enough to model the concepts of our configurable method. The proposed configurable method can be atomic, compound, transformational or constructional and it exhibits characteristic which can either be *common* or *variable*. Commonality in our view is the characteristic of a method which if configured, the method will lose its identity and Variability is the characteristic of a method which can be configured.

Secondly we define method component are entire methods, whether atomic or compound. From forgoing these method models are configurable and will have characteristics of commonality and variability. This is also the right granularity because such methods provide to us the most basic, coherent assembly of method components. Coming to the third issue, that of ensuring appropriateness of the retrieved component. As the method base now contains methods, we propose to do retrieval based on global properties of methods like stage of the life cycle for which the method is applicable and method concepts used. Since the retrieved components shall satisfy global method properties, the chance of retrieving relevant components becomes high.

Finally after retrieving the configurable component we configure them as per requirements. Now with configured method, any assembly with other components can be carried out. This reduces the assembly process to manageable proportions: there is some assurance that the components being assembled have a reasonable chance of producing the desired method and the detailed work of assembling components is limited to such components. Thus our proposal is to make a two stage SME process. The first stage is the configuration of retrieved methods and the second is to assemble the configured methods to form the situated method.

In the next section we review the related research and formulate our proposal for method configurability by analogy with system configurability. In section 3, we build a Meta model for method configurability by introducing notions of commonality and variability in the basic Meta model of [6]. In section 4 we apply the process of defining configurable methods to UML and represent it as a configurable model. Section 5 contains our configuration process. This process takes a configurable method as input and produces a configured method. We consider our two stage SME process in section 6. Here we consider the method base of configurable components, retrieval from it, and application of the configuration process. Finally, an identification of where assembly is needed. Section 7 contains a discussion of related work.

2. Method configuration

In this section we illustrate method configurability. We first review work on configurability, commonality and variability in systems development, situational method engineering and then present our view for method engineering. We will see that the configuration process concentrates on variable aspects of a method to yield the method required for a specific situation.

Configurability has been defined in many ways. The IEEE glossary considers it to be "The arrangement of a computer system or component, defined by the number, nature, and interconnections of its constituent parts". In the context of business process models, it has been treated as dealing with the question "How to model business processes that are similar to one another in many ways, yet differ in some other ways from one organization, project or industry to another?"[14].

The task of configurability is to first create a new model called a configurable model followed by selecting those parts of the configurable model that are relevant to the user's requirement. Configurable models use notions of commonality and variability. Coplien et al [15] define **commonality** as an assumption held uniformly across a given set of objects whereas **variability** is an assumption that is true for only some elements of the set. In [16] we have the definition of **variability** as "an assumption about how members of a family may differ from one another". A configurable model identifies commonality and variability that can be exploited in developing a new system from the configurable model.

Davenport [17] describes the process of configuration as a methodology performed to allow a business to balance their IT functionality with the requirements of their business. Soffer et al. [18] consider configuration as an alignment process of adapting the enterprise system to the needs of the enterprise. [19] Proposes a method that systematically develops requirements using commonality and variability in product line approaches.

Recently configurability is gaining importance in industrial domain, two important case studies that reflect the practical application of this approach Case study of IBM global services on configurability of Work Products

[12] and Case Study of Intel Shannon configuring agile methods [13].

Configurability based SME process relies on a Base Method. [20, 21] this is in contrast to earlier approaches for situation method engineering that relies on a method base. Formal definition of base method is given in [20] as "A base Method is the systems engineering method chosen as the starting point for the configuration work". The essential activity of configurability based SME approach is method tailoring, here the base or candidate method is tailored as per the situational need. The notion of method tailoring can be in any form whether reduction [22] or extension [22]. Karlsson [20] has presented a frame work for configuring methods called MMC (Method for Method Component). Here project specific method is configured from base method by administrating configuration packages. However, Wistrand [21] has defined a conceptual construct named as 'Method Component' which aims to transfer a base method for given goals in form of required artifacts. These proposals are in the infant stage.

We extend the notion of commonality and variability to method engineering. We assume that a configurable model of a method is an association of commonality and variability with method concepts. Table 1 states that ER has method components that can be qualified as common and variable, a method derived from ER must have the notions of *entity* and *relationship sets, attributes, primary key, role* and *cardinality*. However, notions of *weak entity set, arity of relationships* and *multiplicity of attributes* are variable.

TABLE 1
A CONFIGURABLE MODEL OF ER

Method concepts	Essentiality
Entity set	Common
Relationship set	Common
Weak Entity set	Variable
Attribute	Common
Primary Key	Common
Role	Common
Cardinality	Common
N-ary relationship	Variable
Multiplicity of attribute	Variable

By analogy with the process of configuration [18], we define the method configuration process as an alignment of a method to the needs of the situated method. Now just as the system configuration process yields a configured system belonging to the family so also the method configuration process produces a family of methods. A few members of the family of Table 1 are shown in Table 2. The configuration process includes all common concepts of ER in a method family member but selects variable ones based on the need of the specific project being handled. Table 2 shows three ER family members obtained through three instances of the configuration process.

TABLE 2
SOME FAMILY MEMBERS OF ER

Family Member	Concepts
1	No weak entity set, all others as in ER
2	All ER concepts but only single valued attributes
3	All ER concepts but binary relationships only

3. A META MODEL FOR METHOD CONFIGURABILITY

In this section we develop a Meta model for configurable method models. The decisional Meta model of [6] has a generic model part that treats a method as a triple < MB, Dep, E> where MB is a set of method blocks, Dep is a set of dependencies between these, and E is the enactment algorithm. Our generic configurability model introduces commonality and variability concepts in this basic generic model as shown in Fig. 1. The generic configurability model is centered round MB and Dep. E is the procedure that exploits the given set of MB and Dep to produce the product. It cannot be configured but comes as a given with the Meta model. The set Dep establishes dependencies between instances of method blocks. Thus, if a method block is common then all dependencies in which it participates are relevant to the configured method. However, if a method block is a variant and not included in the configured method then all dependencies in which these variants participate are meaningless. Since Dep is configured by the very act of inclusion/exclusion of method blocks, it is not to be directly configured by the method engineer. We treat it as not configurable in our Meta model.

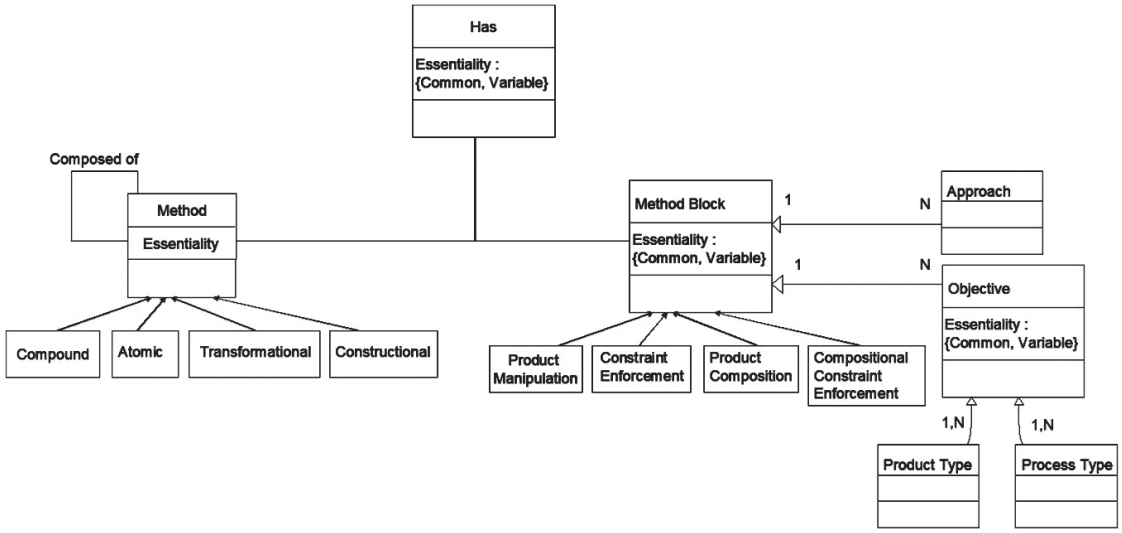

FIG. 1: THE CONFIGURABLE META MODEL

Fig. 1 shows the presence of an attribute called essentiality. Essentiality=common specifies commonality whereas Essentiality=variable specifies a variant. This figure shows that a method can be common or variable. This has particular relevance for compound configurable methods for example, UML which is compound method consisting is a unification of atomic methods:

< Use Case Diagram, Activity Diagram, Class Diagram, Sequence Diagram, Collaboration Diagram, State Chart Diagram, Deployment Diagram, Component Diagram>.

It is possible to declare Use Case Diagram [UCD] and Class Diagram as common and other component as variable. Any method configured from this shall necessarily have a Use Case Diagram and Class Diagram components whereas the others are optional. In contrast, an atomic configurable method can only be common.

Within a method, it is possible for method blocks to be either common or variable. This is shown in the Fig. 1 by the essentiality attribute of the concept method block. Thus in the foregoing example, the common class diagram can have its individual concepts as common or variable. For example, we may define an *object class* as common but an *operation* of the class as variable. Similarly in UCD we can define *actor, use case, communication* as essential whereas *generalization* can be variable.

Our basic process of defining configurable methods is as follows:

- Define the scope of the configurable method by identifying the family members.
- If the method is compound then define the essentiality property of each component method else define its essentiality as common.
- For every concept of the method, define the essentiality property.

This process is top down in the sense that we first establish essentiality for the global method and then proceed down to determine essentiality of coarse grained concepts and eventually to the finest grained ones.

As mentioned earlier, the decisional Meta model is an instantiation of the generic model. Correspondingly the configurable decisional method model is an instantiation of the generic configurable model. The instantiation relevant to our purposes is shown in Table 3.

TABLE 3
THE DECISIONAL META MODEL

Generic Model Concept	Decisional Meta Model Concept
Method block	Decision
Objective	Purpose
Product type	Structure
Process type	Operation

A method block is an aggregate of approach and purpose. For simplicity, let us ignore the notion of an approach. Thus a method block reduces to a purpose. Now, in a purpose, there is a structure part and an operation part. As we will see, the set of operations are a given in the Meta model. Thus, they are not configurable. The only

configurability is of the concept structure. This results in the purpose and consequently, the decision to be configurable. Again, however, this configurability can be algorithmically determined, only that subset of purposes/ decisions is included in the situated method which is built on the included concept structures. Thus, there is no need for the method engineer to explicitly do this configuration.

In the rest of this section, we consider configurable structures and outline the set of non-configurable operations of the configurable decision Meta model.

3.1 Structure

There are two kinds of structures, those whose instances can be created and destroyed by application engineers and those whose instances are pre-defined. The former are called conceptual structures and the latter are called fixed structures. Conceptual structures constitute the set of concepts in terms of which a product is expressed. Fixed structures are those that are defined once and all for by a method engineer. An example of fixed structure is a method constraint such as completeness and conformity which cannot be created or destroyed by the application engineer.

Conceptual Structures

As shown in Fig. 2, conceptual structures are partitioned into two dimensions. The first dimension classifies them as either simple or compound. The second dimension represents conceptual structures into disjoint classes of structures called constraint, definitional, constructional, link, and collection of concepts respectively.

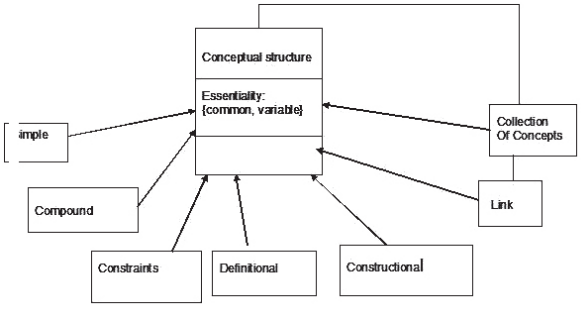

FIG. 2: THE CONFIGURABLE CONCEPTUAL STRUCTURE

Simple *constructional* structures cannot be decomposed into other components. *Links* are conceptual structures that are used to build collections of concepts from given concepts. For example ISA and aggregation are links, as they build abstraction hierarchies. *Collections of concepts* are constructed whenever constructional structures are connected by links. Aggregations, specialization hierarchies, and subtype hierarchies are examples of collection of concepts. A collection of concept is complex if it is defined out of other collections. *Definitional* structures define the properties of conceptual structures.

Constraints impose application-related constraints on conceptual structures. For example, such a constraint could say that the ages of employees should be less than 65 years.

The presence of the attribute, essentiality, in Fig. 2 shows that conceptual structures are configurable. We will illustrate this configurability in section 4 with an example.

Fixed Structures

Fixed structures deal with the restrictions that are used to enforce quality of conceptual structures. They are defined by the method engineer to help the application engineer in creating well defined and well formed conceptual structures. In their simplest form, they are the method constraints of completeness, consistency, conformity and fidelity.

Similarly there are compositional constraints which are specified between conceptual structures of the different simple component methods of a compound method. A structure of one of these cannot compose any arbitrary structure of the other. Such composition is governed by constraints that control the product resulting from the use of compound methods. The method engineer defines these constraints at the time the compound method is defined. For example in UML, *operation* in Class Diagram must be a use case in Use Case Diagram.

Fixed structures are shown in Fig. 3. Notice that they are configurable due to the presence of the essentiality attribute.

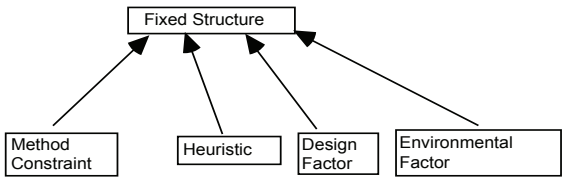

FIG. 3: CONFIGURABLE FIXED STRUCTURES

3.2 The Operation

Operations identify the set of process types that operate upon product types to provide product manipulation and verification capability to application engineers. Operations are classified into two four classes as follows:

- *Basic Life Cycle:* For each conceptual structure there are operations to *create,* and *delete* it. Create and delete are not defined for the fixed structures.

- *Relational:* These allow different structures to be related to one another. *These are attach, join,* couple, *associate,* relate*, apply* and their inverses.
- *Integration* This class of operations is defined for compound methods. These operations are, *export*, *import*, *correspond*, *convert* and their inverse operations.
- *Constraint Enforcement:* For each conceptual structure of a method and the method constraint applicable to it, a *method constraint enforcement* operation is defined.

4. UML AS A CONFIGURABLE METHOD

We apply the process of constructing a method described in section 3 to Unified Modeling Language which is composed of nine component methods such as Class Diagram, Sequence Diagram, Collaboration Diagram, State Chart Diagram, Component Diagram etc. We are assuming following qualification for these components< common, variable> as given below

TABLE 4
ESSENTIALITY OF UML METHOD COMPONENTS

Method component	Essentiality
Use Case Diagram	Variable
Activity Diagram	Variable
Class Diagram	Common
Sequence Diagram	Variable
Collaboration Diagram	Variable
State Chart Diagram	Variable
Component Diagram	Variable
Deployment Diagram	Variable
Object Diagram	Common

This table shows that the Class Diagram and Object Diagram are considered as essential to any method configured from UML. This means that UML can yield a family of methods that may be object oriented or data oriented [23] in nature. The assumptions about commonality and variability for each method concept of Class Diagram are shown in Table 5.

TABLE 5
CLASS DIAGRAM AS A CONFIGURABLE MODEL

Method concepts	Essentiality
Class	Common
Data_type	Common
Association	Common
Aggregation	Variable
Operation	Variable
Generalization	Variable
Generalization-link	Variable
Aggregation-link	Variable
Cardinality	Common
Degree of association	Variable
Multiplicity	Variable
Degree of association	Variable

The Class Diagram configurable model has *class, Data_ type, association and cardinality* as common to its family. The rest of the Class Diagram concepts are variants.

5. THE CONFIGURATION PROCESS

The configuration process assumes the existence of a configurable method. In producing a method, the process first considers the essentiality property of the global method. If the method is atomic then it is accepted as such and renamed. If it is a compound method then all components that have Essentiality=common are accepted in the method To-Be. Similarly, all method concepts of selected methods having Essentiality=common are accepted in the new method.

The focus of the configuration process now shifts to variants. These are to be examined by the method engineer for appropriateness for the new method. If relevant then they are included else they are excluded. Thus, the intellectual task of the method engineer is centered on variants.

It may happen that the new method needs concepts that are not present in the configuration produced. In such a case we propose to do method assembly by looking at other methods that may have these concepts.

As an example, let us configure Class Diagram to yield the ER model. As mentioned above, Class diagram has Essentiality = common. It is therefore renamed as ER and is now configured: all common concepts are present in ER (with *entity set* as alias for *class* and *relationship* set as alias for *association*). Out of the variants only *multiplicity* of *attributes* is taken. However, some concepts of ER, like *primary* key are not configurable from Class Diagram.

6. THE SME PROCESS

Our SME process consists of two sub processes, the configuration sub process and the assembly sub process. We propose that the configuration process is basic to the SME process and that assembly should be attempted only

when configurability fails to deliver the desired method. This failure can happen in two ways:

- An entire method of a compound method is missing in the configurable method.
- Method concepts are missing.

Our SME process relies on the existence of a method base of configurable methods. Configurable methods can be retrieved based on global properties. These properties provide a broad indication of the family of methods that can be produced. We propose properties as follows:

(i) The part of the systems development life cycle catered to, requirements engineering, system design, complete life cycle etc.

(ii) The nature of the configurable method. This can be atomic or compound. These methods are further classified as proposed by [23] as data, process, or behavior oriented. Additionally, methods can be object oriented. Requirements engineering methods can be model driven or not, goal oriented, scenario oriented, and so on.

(iii) The application area of the method, whether constructional or transformational [24].

(iv) Component methods of compound methods having essentiality=common.

Additionally, for each method in the base, the method concepts that have essentiality = common can be used to retrieve these concepts.

This yields a method base structure (only relevant part shown. Details can be obtained from the authors.) Consisting of relations as follows:

I. Method_base(Method_id, method_name, life_ cycle, application, method_type, method_nature). This relation keeps global method information: life_cycle identifies the stage of the life cycle addressed; application takes on values from {constructional, transformational}; method_ type tells us whether the method is atomic or compound; method_nature is the method class like data oriented, process oriented.

II. Compound_Method(method_id, component_id, essentiality). This relation keeps track of the component methods of a compound method.

III. Configurable method (method_id, method _concept, essentiality). Commonality and variablility information about the concepts of a method are maintained.

Retrieval from the method base starts off by first retrieving configurable methods of interest. For example,

Select method_id, method_name, method_type
From method_base
Where life_cycle = system design application = constructional
And method_nature = data- oriented.

Evidently, the intention is to build a data oriented method for constructing system designs.

Individual methods from the list obtained can then be examined. Assume that a compound method is retrieved. Now, the method engineer obtains its component methods along with their essentiality in the compound method. For example, if a method named UML is having method_ id=27 had been retrieved then the following query is made

Select component_ id, essentiality
From Compound_Method
Where method _id = 27

At this moment the method engineer knows which component methods are common and which are variants. The method engineer can now decide about the appropriateness of the configurable method for the situated method.

Once the configurable method is selected based on global properties, a detailed examination at the method concept level is performed. For example, if a component id=35, say Activity Diagram, is a potential candidate for inclusion in the situated method then a query to examine it can be formulated:

Select method concept
From configurable _method
Where method_ id = 35 and essentiality = common

As a result, all the retrieved common method concepts are examined for their appropriateness for the situated method. If these are acceptable then the variants can be obtained and their suitability assessed.

A list of missing methods/concepts is now made. The method base is searched again for methods that may contain these concepts. Thus a collection of configured methods is obtained that need to be assembled together to form the situated method.

To sum up, three cases arise:

1. A configurable method retrieved from the method base cannot be configured to yield the situated method. It is discarded and another one is considered.
2. The configured method is the method To-Be. In this case no assembly is required.

3. The configured method only partially meets the requirements of the method To-Be. Evidently, assembly with other configured methods is now to be done.

7. Related work

A body of knowledge exists for configuring information/ software systems from a configurable model. Such a system is viewed as a monolithic whole and the entire system is configured. However, in method engineering, we are dealing with relatively diverse phenomena: atomic/ compound methods, constructional/transformational methods, different methods for different stages of the life cycle [7]. It is not necessary that even after configuration is done, a full acceptable situated method is produced. Therefore, in contrast to system configuration, assembly plays an important role in situational method engineering. The basic techniques for building configurable methods and the basic configuration process can however be adopted from system engineering. According to [25] there are five main steps (a) establish scope (b) identify commonalities and variability (c) bind the variability by placing appropriate limits (d) exploit commonalities and (e) accommodate variability. In this paper we have shown that these steps can be seen in configurability for methods.

Regarding determining what is common [19] introduces a threshold. If the percentage of family members showing the feature is above this threshold then the feature is considered to be common. However, [25] is silent on how commonalities are determined. At this stage in our work, we have left this decision to the experience of the configurable method engineer. However, we intend to explore a mechanism for determining commonality in the future.

8. Conclusion

In this paper we extend the notion of configurability to method engineering. The approach adopted in this paper is shown in Fig. 4

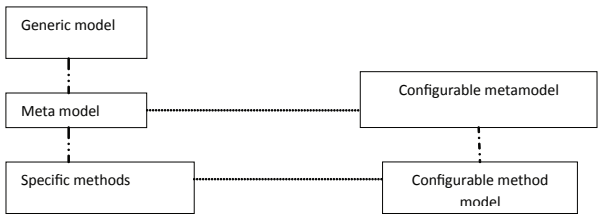

FIG. 4: INSTANTIATION OF CONFIGURABILITY USING GENERIC META MODEL

On the left hand side of the figure is the view of traditional method engineering [26]: a meta-model is an instantiation of a generic model and methods are instantiations of the meta-model. In order to facilitate configurability, we introduce configurability in the Meta model and consequently in the configurable method. The latter is an instantiation of the former.

We propose a two-part SME process of configuration and assembly. The former ensures that the methods being assembled are 'good' methods in the sense that individually they meet a part of the requirements of the situated method. The collection of methods to be assembled therefore provides a degree of assurance of yielding the situated method.

The main advantage of our approach is significant reduction in efforts to be put in by Method Engineers. Firstly, with the introduction of common and variable concepts, the method engineer has to focus only on the variable concepts as per situational requirements. Secondly, assembly process is mitigated until new concepts other than common and variable are required. This remarkably reduces the method engineer's efforts.

In future, we expect to lay down a criterion for defining commonality. This will be based on hierarchy of conceptual structures which can be instantiated by the CAME tool MERU [11] and then method knowledge will decide common and variable. An implementation of the configurability proposals made here is under way and we expect to verify it for configurability against a number of methods. Subsequently, we shall implement the full SME process as proposed here. Lastly we are extending MERU to support method configuration and assembly.

References

[1] C. Rolland, N. Prakash, "A proposal for Context-specific Method Engineering, Method Engineering Principles of Method Construction and Tool Support," *Brinkkemper S., Lyytenin K., and Welke R.J., (eds.), Chapman & Hall*, pp. 191-208, 1996.

[2] K. van Slooten, B. Hodes, "Characterizing IS Development Projects, Method Engineering Principles of Method Construction and Tool Support," *Brinkkemper S., Lyytenin K., and Welke R.J., (eds.), Chapman & Hall*, pp. 29-44, 1996.

[3] R. Deneckere, E. Kornyshova, B. Claudepierre, "Contextualization of Method Components," *Proc. RCIS*, pp. 235-246, 2010.

[4] F. Harmsen, S. Brinkkemper, J.L. Han Oei, "Situational method engineering for informational system project approaches," *Methods and Associated Tools for the Information Systems Life Cycle,* pp. 169-194, 1994.

[5] G. Grosz, C. Rolland, S. Schwer, C. Souveyet, V. Plihon, S. Si-Said, C. Ben Achour, C. Gnaho, "Modelling and Engineering the Requirements Engineering Process: An Overview of the NATURE Approach," *Requirements Engineering Journal*, Vol. 2, No. 3, pp. 115-131, 1997.

[6] N. Prakash, "On Method Statics and Dynamics, Information Systems," *Pergammon press,* Vol. 24, No. 8, pp. 613-637, 1999.

[7] N. Prakash, Goyal S.B. "Towards a Life Cycle for Method Engineering," *In Proceedings Eleventh International Workshop on Exploring Modeling Methods in Systems Analysis and Design (EMMSAD'07)*, pp. 27-36, 2007.

[8] Prakash, N. and S.B. Goyal, "Method architecture for situational method engineering," *In RCIS*, pp. 325-336, 2008.

[9] S. Brinkkemper, "Method Engineering-Engineering of Information Systems Development Methods and Tools," *in Information and software technology,* Vol. 38, pp. 275-280, 1996.

[10] S. Moaven et.al. "Towards an Architectural-Centric Approach for Method Engineering," *In IASTED conference on Software Engineering, Austria* pp. 74-79, 2008.

[11] D. Gupta and N. Prakash, "Engineering Methods from their Requirements Specification," *in Requirements Engineering Journal* , Vol. 3, pp. 133-160, 2001.

[12] J. Cameron, "Configurable development processes," *Communications of the ACM*, Vol. 45, No. 3, pp. 72-77, 2002.

[13] B. Fitzgerald, G. Hartnett and K. Conboy, "Customizing agile methods to software practices at Intel Shannon," *in European Journal of Information Systems*, Vol. 15, No. 2, pp. 197-210, 2006.

[14] M.L. Rosa, "Managing Variability in Process-Aware Information Systems", *Doctor of Philosophy, Faculty of Science and Technology Queensland University of Technology, Brisbane, Australia, 2009.*

[15] J. Coplien, D. Hoffman, D. Weiss, "Commonality and Variability in Software Engineering," *IEEE Software*, pp. 37-45, 1998.

[16] D.M. Weiss, C.T.R. Lai, "Software Product-line engineering: A Family based Sofwtare development Process," *Addison Wesley, 1999.*

[17] T.H. Davenport, "Putting the enterprise into the enterprise system," *Harvard Business Review* Vol. 76, No. 4, 1998.

[18] P. Soffer, B. Golany, D. Dori, "ERP modeling: a comprehensive approach," *Information Systems* Vol. 28, No. 6, 2003.

[19] M. Moon, K. Yeom, "An Approach to developing Domain Requirements as a Core Asset based on Commonality and Variability Analysis in a Product Line," *IEEE TSE,* Vol. 31, No. 7, pp. 551- 569, 2005.

[20] F. Karlsson, P.J. Ågerfalk, "Method Configuration: Adapting to Situational Characteristics While Creating Reusable Assets," *In Information and Software Technology* Vol. 46, pp. 619-633, 2004.

[21] K. Wistrand, F. Karlsson, "Method Components – Rationale Revealed," *In Advanced Information Systems Engineering 16th International Conference, CAiSE 2004, Riga, Latvia, June 7-11, 2004, Proceedings, A. Persson, J. Stirna, Eds. Springer-Verlag, LNCS 3084, Berlin,* pp. 189-201, 2004.

[22] J. Ralyté, C. Rolland, "An Assembly Process Model for Method Engineering," *In Advanced Information Systems Engineering, K.R. Dittrich, A. Geppert, M.C. Norrie, Eds. Springer, LNCS2068, Berlin,* pp. 267-283, 2001.

[23] T.W. Olle, J. Hagelstein, I.G Nacdonald, C. Rolland, H.G. Sol, F.J.M van Assche, A.A. Verrijn-Stuart, "Information Systems Methodologies A Framework for Understanding," *Addison Wesley, 1991.*

[24] N. Prakash, "Towards a Formal Definition of Methods," *Requirements Engineering Journal, Springer, Vol. 2, No. 1, pp. 23-50, 1997.*

[25] J. Coplien, D. Hoffman, D. Weiss, "Commonality and Variability in Software Engineering," *IEEE Software,* pp. 37-45, 1998.

[26] N. Prakash, "On generic method models," *Requirement engineering Journal11 (4), Springer,* **pp. 221-237, 2006.**

ABOUT THE AUTHORS

Prof. Daya Gupta is Professor in the Department of Computer Engineering, Delhi Technological University New Delhi, India and is currently the Head of the Department there. She has done M.Sc. Post M.Sc. (Computers Sc.) from IIT, Delhi, and PhD from Delhi University. She is a senior member of IEEE and a life member of CSI. Her research interests are in the field of requirement engineering, method engineering, information security, image characterization and software estimation. She has published several research papers in international journals and conferences and has chaired sessions and delivered invited talks at many national and international conferences.

Ms. Rinky Dwivedi has received the B.Tech. degree in Computer Science from Guru Gobind Singh Indraprastha University, Delhi, India and M.E. degree from Delhi College of Engineering, Delhi, India. She is now pursuing PhD from Delhi Technological University, Delhi India. Her areas of interests include Method Engineering, Software Methodologies and Agile Techniques .Rinky can be contacted by e-mail at rinkydwivedi@gmail.com.

Aptamer based electrochemical sensor for detection of human lung adenocarcinoma A549 cells

2012 J. Phys.: Conf. Ser. 358 012001

(http://iopscience.iop.org/1742-6596/358/1/012001)

Aptamer based electrochemical sensor for detection of human lung adenocarcinoma A549 cells

Rachna Sharma[1, 3], Ved Varun Agrawal[1], Pradeep Sharma[2], R Varshney[2], R K Sinha[3] and B D Malhotra[4]

[1]Biomedical Instrumentation Section, National Physical Laboratory, Dr. K.S. Krishnan Marg, New Delhi 110012, India

[2]Institute of Nuclear Medicine & Allied Sciences, Lucknow Road, Timarpur, Delhi 110 054, India

[3]Department of Applied Physics, Delhi Technological University, Main Bawana Road, Delhi 110042, India

[4]Department of Biotechnology, Delhi Technological University, Main Bawana Road, Delhi 110042, India

E-mail: bansi.malhotra@gmail.com or bansi.malhotra@dce.ac.in

Abstract. We report results of the studies relating to development of an aptamer-based electrochemical biosensor for detection of human lung adenocarcinoma A549 cells. The aminated 85-mer DNA aptamer probe specific for the A549 cells has been covalently immobilized onto silane self assembled monolayer (SAM) onto ITO surface using glutaraldehyde as the crosslinker. The results of cyclic voltammetry and differential pulse voltammetry studies reveal that the aptamer functionalized bioelectrode can specifically detect lung cancer cells in the concentration range of 10^3 to 10^7 cells/ml with detection limit of 10^3 cells/ml within 60 s. The specificity studies of the bioelectrode have been carried out with control KB cells. No significant change in response is observed for control KB cells as compared to that of the A549 target cells.

1. Introduction

Lung cancer is currently a major cause of cancer related deaths both in the developed and developing nations[1-3]. To reduce high mortality rate arising due to lung cancer, an early diagnosis of the disease is essential. Most of the existing methods presently being used for cancer detection are X-ray, spiral computed tomography[4], sputum cytology[5], positron emission tomography[6], virtual bronchoscopy[7] etc .These methods are based on morphological criteria that cannot be used for early detection of this important disease. Besides this, these are known to be non-specific for cancer classification. Since cancer results from the accumulation of a variety of genetic events (e.g., mutations, rearrangements, and deletions)[8-12] controlling cell growth and differentiation, the studies on these changes may perhaps serve as diagnostically useful molecular markers[13-15]. Development of molecular probes that

4 To whom any correspondence should be addressed.

can recognize molecular abnormalities during the lung carcinogenesis process is likely to enable clinicians for diagnosis of cancer at early stage and identify its subtypes.

Development of noninvasive tests has been the focus of cancer research that may facilitate earlier diagnosis and treatment of lung cancer. Several studies on variation of the surface specific antigens to differentiate between normal and cancer cells have been performed using antibodies[16]. These surface [1]

specific antigens cannot be exclusively expressed for any single type of cells and may result in false-positivity. To address to this problem, aptamers have emerged as attractive alternatives to antibodies[17,18]. Aptamers, single-stranded oligonucleotides, have been identified for specific cancer cell recognition by applying a cell-SELEX (cell-based systematic evolution of ligands by exponential enrichment) method[19]. Besides this, these biomolecules can fold into unique three dimensional conformations to bind to selected molecules ranging in size from small organic molecules to whole cells with high affinity and selectivity[20].

Aptamers are known to possess several advantages over other recognition molecules like ease of synthesis and modification, long term stability, high specificity etc which making these biomolecules as potential candidates for development of desired analytical devices[21]. Several studies relating to the fabrication of aptamer based biosensors for the detection of proteins[22], molecules[23], cancer cells[24-27] etc have been performed indicating high affinity and specificity of the aptamer probes towards their respective targets. And the electrochemical method of detection is being preferred over other methods of detection since this technique exhibits high signal to noise ratio resulting in high sensitivity, rapid response and reproducibility of the biosensor[28]. Pan et al have fabricated an aptamer based electrochemical sensor for label-free recognition and detection of leukemia cells[26]. Rodriguez et al have reported an aptamer based biosensor for lysozyme detection using electrochemical impedance spectroscopy[29].

In the present manuscript, we report results of studies relating to fabrication of an electrochemical biosensor for detection of lung cancer cells using aptamers. The aptamer functionalized bioelectrode has been prepared by covalent immobilization of the aptamer probe on self assembled monolayer of silane onto the ITO surface using glutaraldehyde as the crosslinker. The response of the bioelectrode towards the target cancer cells has been investigated using cyclic voltammetry and differential pulse voltammetry.

2. Materials and methods

3-(2-aminoethylamino) propyl trimethoxysilane (AEAPTS), glutaraldehyde and amine-terminated aptamer sequence have been purchased from Sigma-Aldrich. All the reagents are of analytical grade and have been used without further purification. De-ionized water (Milli Q 10 TS) with resistivity >18.2 MΩ-cm has been used for preparing all aqueous solutions. Indium-tin-oxide (ITO) coated glass plates have been obtained from Balzers, UK, (Baltracom 247 ITO, 1.1 mm thick) with sheet resistance and transmittance 25 Ωsq^{-1} and 90%, respectively.

Aptamer probe: NH_2 - 5'- ACG CTC GGA TGC CAC TAC AGG GTT GCA TGC CGT GGG GAG GGG GGT GGG TTT TAT AGC GTA CTC AGC TC ATG GAC GTG CTG GTG AC -3'[30]

Target cells: A549 cells

Control cells: KB cells

2.1. Culture medium for cells

A549 cells derived from human lung adenocarcinoma and KB (control) cells derived from head and neck squamous carcinoma are maintained as monolayer cultures at 37 ºC in a humidified CO_2 incubator (5% CO_2, 95% air). A549 and KB cells are maintained in high glucose DMEM supplemented with 10% fetal bovine serum (FBS), HEPES (10 mM) and antibiotics (30 μgml^{-1} penicillin G, 50 μgml^{-1} streptomycin and 2 μgml^{-1} nystatin). All the cell lines are routinely sub-cultured (twice a week) using 0.05 % trypsin in 0.02 % EDTA and reseeded in fresh medium. FBS and DMEM (both low and high glucose) were purchased from SIGMA chemicals.

2.2. Fabrication of Aptamer-functionalized bioelectrode

ITO coated glass plates are washed with acetone, ethanol and copious amount of deionized water followed by hydrolyzation in $NH_4OH:H_2O_2:H_2O$ (1:1:5) solution at 80°C for 45 min. Hydrolyzed ITO plates are dipped in 1% ethanolic solution of AEAPTS for 2 h for formation of self-assembled monolayer (SAM) and then washed with ethanol followed by deionized water. Silanized ITO surfaces are then soaked in 0.5% aqueous solution of glutaraldehyde for 6 h for SAM formation. Glutaraldehyde acts as a crosslinker between the amine group at the silanized ITO surface and the amine-terminated aptamer sequence. 20 µL of 1 µM aptamer solution is then dispensed onto the silanized ITO surface for about 2 h for covalent immobilization resulting in the fabrication of aptamer functionalized bioelectrode.

2.3. Characterization

The morphology of the aptamer functionalized bioelectrode and morphological changes on incubation of the bioelectrode with target cells have been studied using SEM, LEO 440 scanning electron microscope. The transmission studies of the silanized ITO surface and the aptamer functionalized bioelectrode in the infrared region have been carried out on Perkin Elmer, Spectrum BX II spectrophotometer in the wavenumber range of 4000-450 cm^{-1}.

The electrochemical experiments have been conducted on Autolab PGSTAT 302N System (Ecochemie, The Netherlands) in a three electrode system. All electrochemical experiments have been carried out in a cell containing 15 ml of 100 mM Phosphate Buffer Solution (PBS, pH 7.4) containing 0.9% NaCl and 5 mM $K_3/K_4[Fe(CN)_6]$ as a redox probe and using a platinum wire as auxiliary, a Ag/AgCl wire as reference, and the modified ITO as the working electrode.

3. Results and discussion

3.1. SEM studies

Figure 1 shows the morphology obtained for the apt-glu-silane-ITO bioelectrode before and after cell binding. The observed granular structure on immobilization of single-stranded DNA aptamer indicates covalent binding of aminated aptamer probe onto silanized ITO surface (figure 1(a)). The uniform spindle like structure appears on incubation of the apt-glu-silane-ITO bioelectrode with A549 cells (figure 1(b)) revealing the affinity of aptamers with target cells.

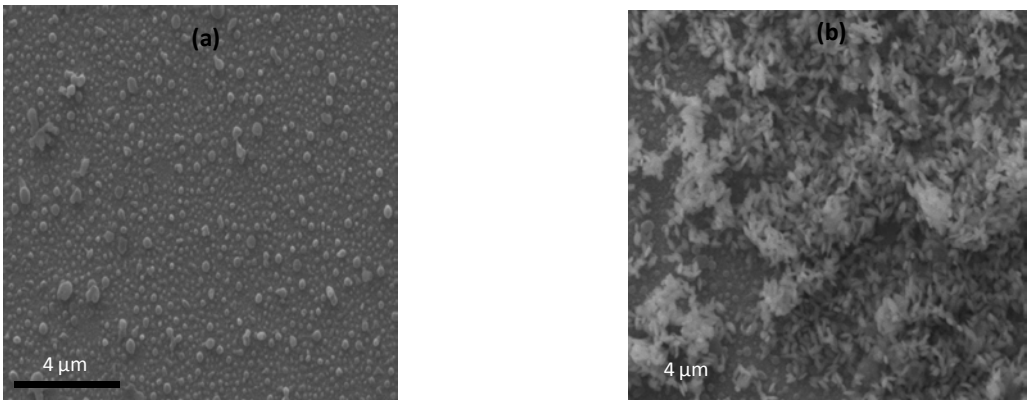

Figure 1. SEM micrographs of apt-glu-silane-ITO bioelectrode before (a) and after (b) cell binding.

3.2. FTIR studies

Figure 2 shows the transmittance spectra observed for the silanized ITO electrode and aptamer functionalized bioelectrode. The peaks seen at 679 cm^{-1} and 1113 cm^{-1} corresponding to $Si\text{-}CH_3$ stretch and Si-O-Si antisymmetric stretch respectively, indicate the formation of siloxane bond between the

silane and the ITO surface[31] [figure 2(a)]. Peaks found at 1415 cm^{-1}, 2808 cm^{-1} and 3265 cm^{-1} correspond to C-N, C-H and N-H stretch in the AEAPTS, respectively. Further, the peak at 1585 cm^{-1} corresponding to NH_2 deformation reveals the presence of amine groups at the silanized ITO surface.

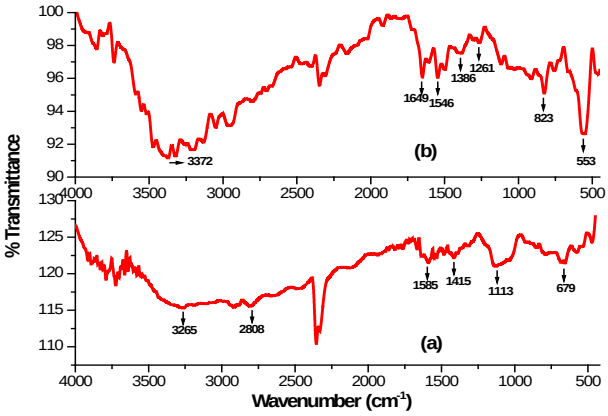

Figure 2. FTIR spectra of (a) AEAPTS/ITO surface and; (b) Apt/Glu/AEAPTS/ITO surface.

In figure 2(b), peaks at 553 cm^{-1} and 823 cm^{-1} correspond to C-O and N-H bending vibrations in amino acids, respectively. Peaks seen at 3372 cm^{-1} and 1386 cm^{-1} correspond to N-H stretch and C-N stretch, respectively. Further, the peak at 1261 cm^{-1} corresponds to P-O stretch of the phosphate backbone of DNA, peaks at 1546 cm^{-1} and 1649 cm^{-1} pertain to the C-O stretch of the purine and pyrimidine rings of DNA[32]. All these peaks reveal the immobilization of the amine-terminated aptamer probe onto the silanized ITO electrode.

3.3. Electrochemical characterization

Figure 3a shows the cyclic voltammograms obtained for the ITO electrode, silane-ITO electrode, glu-silane-ITO electrode and apt-glu-silane-ITO bioelectrode in the potential range of -0.7V to +0.7V at scan rate of 50 mV/s. The 0.4V peak corresponds to the oxidation peak of the redox couple, K_3/K_4 $[Fe(CN)_6]$ present in the buffer. It can be seen that there is a significant increase in the anodic peak current for the silane-ITO electrode (figure 3a (ii)) compared to that of the ITO electrode (figure 3a (i)). The NH_2-terminal of the silane acquires positive charge in the buffer and thus attracts the negatively charged cyanide ions present in the buffer. The electrostatic attraction between the positively charged silanized ITO surface and the negatively charged redox species present in the buffer facilitates electron transfer across the electrode-electrolyte interface leading to increased oxidation current[33]. Futher, decrease in oxidation current may perhaps be attributed to the formation of an insulating layer of glutaraldehyde on the silanized ITO surface (figure 3a (iii)). Again, the increase in the oxidation current on immobilization of the amine-terminated aptamer probe (figure 3a (iv)) can perhaps be asisgned to the electrostatic attraction between the positively charged surface of apt-glu-silane-ITO bioelectrode and the negatively charged redox species present in the buffer resulting in facile transfer of electrons.

Figure 3b shows the differential pulse voltammograms obtained for the ITO electrode, silane-ITO electrode, glu-silane-ITO electrode and apt-glu-silane-ITO bioelectrode in the potential range of -0.7V to +0.7V. The increase in the peak current for silane-ITO electrode (figure 3b (ii)) compared to that of the ITO electrode (figure 3b (i)) is attributed to the facile electron transfer aided by the opposite charges on electrode and the electrolyte. The decrease in the peak current for glu-silane-ITO electrode (figure 3b (iii)) reveals the formation of an insulating layer of glutaraldehyde. Further, increase in the current on immobilization of the amine-terminated aptamer sequence (figure 3b (iv)) is ascribed to the

transfer of electrons facilitated due to the electrostatic attraction between positive electrode surface and negative redox species in the buffer.

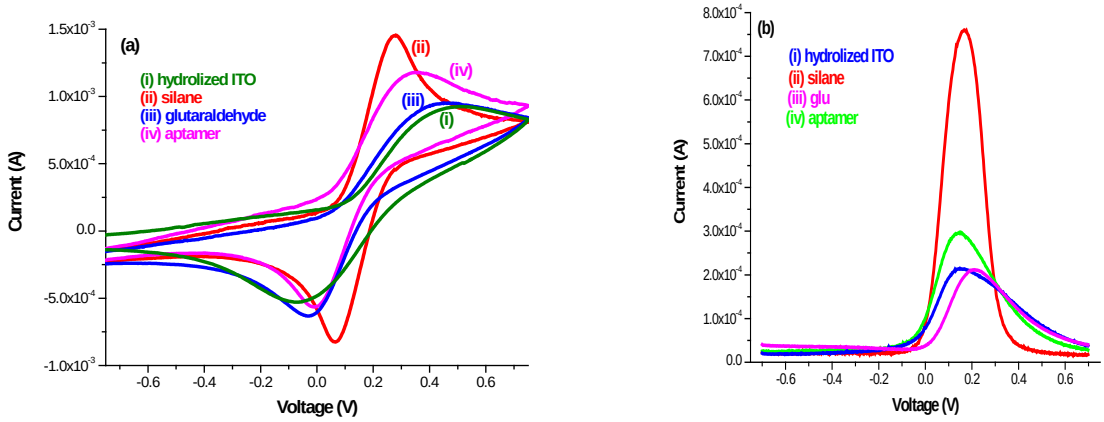

Figure 3. Stepwise characterization of aptamer functionalized bioelectrode using CV (a) and DPV (b).

3.4. Surface coverage of aptamer

The cyclic voltammteric investigations of apt-glu-silane-ITO bioelectrode have been conducted as a function of scan rate (ν) (10–100 mV/s) to determine the surface coverage of aptamer probe. The anodic peak potential (E_{pa}) is found to vary linearly with logarithm of scan rate and follows Eq.1:

$E_{pa} = 0.2051 \log \nu - 0.0433$; R = 0.9949; SD = 0.0046 Eq.1

According to Laviron's theory, the slope of the linear curve between the anodic peak potential and the logarithm of scan rate represents RT/αnF (α- transfer coefficient). This can be used to calculate the surface concentration of the aptamer using the following equation:

$i_p = n^2F^2\nu CA\,(4RT)^{-1}$ Eq.2

where, i_p/ν can be calculated from the i_p Vs. ν plot (i_p- anodic peak current; ν- scan rate)[34].

The total surface concentration of the aptamer probe has been found to be 1.627×10^{-10} mol cm^{-2} (using $i_p/\nu = 9.754 \times 10^{-6}$).

3.5. Response studies of aptamer functionalized bioelectrode

The response of the aptamer functionalized bioelectrode towards target cell (A549) binding has been investigated using cyclic voltammetry in PBS buffer containing $K_3/K_4[Fe(CN)_6]$ as a redox couple in the voltage range of -0.7 V to +0.7 V at scan rate of 50 mV/s. The decrease in the oxidation current is observed due to binding of the A549 cells (figure 4a). This is because the biological cells on attachment to the substrate form an insulating layer that perhaps provides barrier to the flow of electrons through the electrode surface resulting in the decrease of the current[26]. The resistance to the flow of electrons increases with increasing concentration of A549 cells and thereby results in the decrease of current with rising concentration of target cells.

The calibration curve for the apt-glu-silane-ITO bioelectrode can be obtained by plotting the anodic peak current for logarithmic values of the different concentrations of cholesterol (figure 5(a)). Linear relation is obtained between the anodic peak current and logarithmic value of cell concentration over the range of 10^3-10^7 cells/ml with standard deviation and correlation coefficient of 62.91 µA and 0.9831, respectively.

The binding of target cells to the apt-glu-silane-ITO bioelectrode has been studied using differential pulse voltammetry. The decrease in current is observed with the increasing concentrations of target cells (figure 4b) due to formation of the insulating layer which impedes the flow of electrons through the electrode surface indicating binding of the cells to the aptamer. The calibration curve

obtained by plotting the DPV peak current for the logarithmic values of cholesterol concentrations (figure 5(b)) reveals the linearity over the concentration range of 10^3-10^7 cells/ml with standard deviation and correlation coefficient of 13.38 µA and 0.9863, respectively.

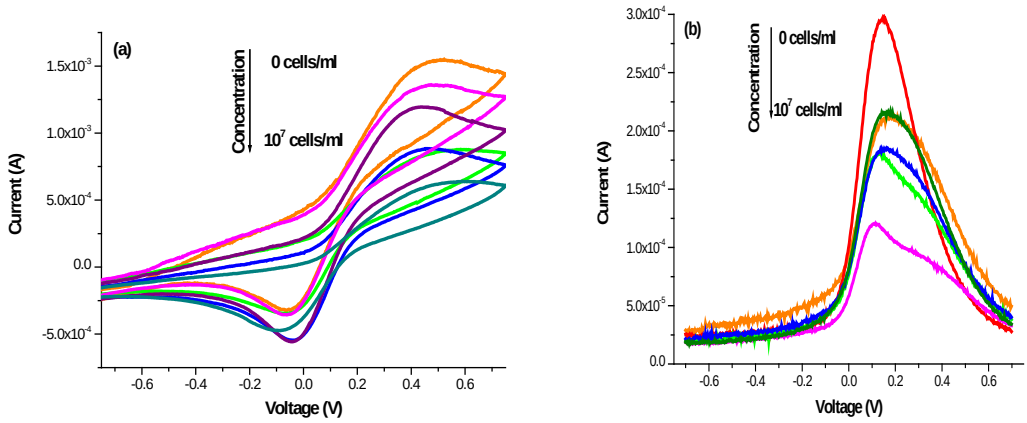

Figure 4. Response Studies of the aptamer functionalized bioelectrode using CV (a) and DPV (b) with target A549 cell concentrations of (i) 0; (ii) 10^3; (iii) 10^4 ; (iv) 10^5 ; (v) 10^6 and; (vi) 10^7 cells/ml.

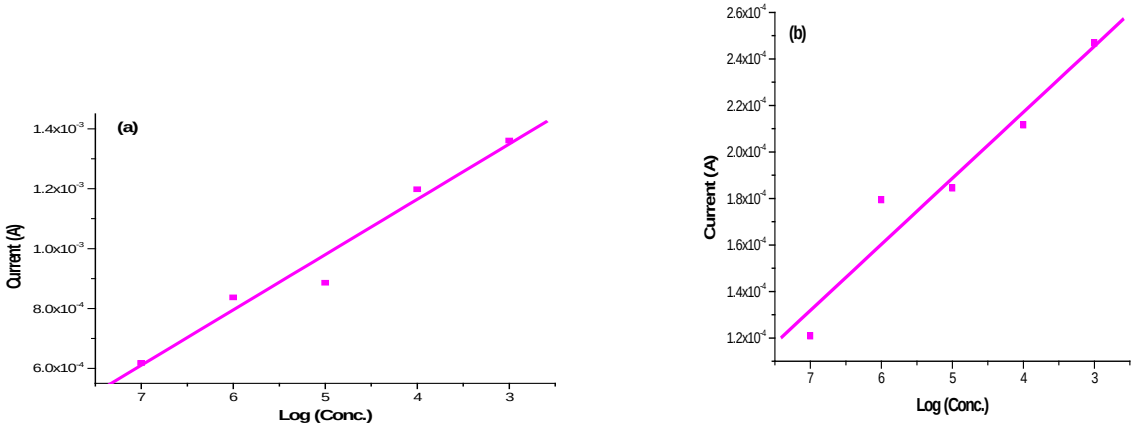

Figure 5. Calibration plot for CV response (a) and DPV response (b) of the aptamer functionalized bioelectrode towards different concentrations of A549 cells.

3.6. Response studies of aptamer functionalized bioelectrode

The specificity of the apt-glu-silane-ITO bioelectrode towards detection of A549 cells has been investigated using cyclic voltammetry (figure 6a). In the control experiments, the response of the bioelectrode towards culture medium and the control KB cells has been studied. The observed decrease in the current observed on incubation of the bioelectrode with culture medium without cells may be attributed to the physical adsorption of the species from the environment. The decrease in the current on incubation of the bioelectrode with KB cells is approximately half of that in case of A549 cells for the same concentration. Thus, the binding of the A549 cells to the bioelectrode surface perhaps dominates the CV response.

The selective response of the apt-glu-silane-ITO bioelectrode towards the A549 cells has been further confirmed by differential pulse voltammetry (figure 6b). The decrease in signal observed with the target A549 cells is much higher as compared to that obtained with culture medium and the control

KB cells. This further reveals the selectivity of the aptamer functionalized bioelectrode towards human lung adenocarcinoma A549 cells.

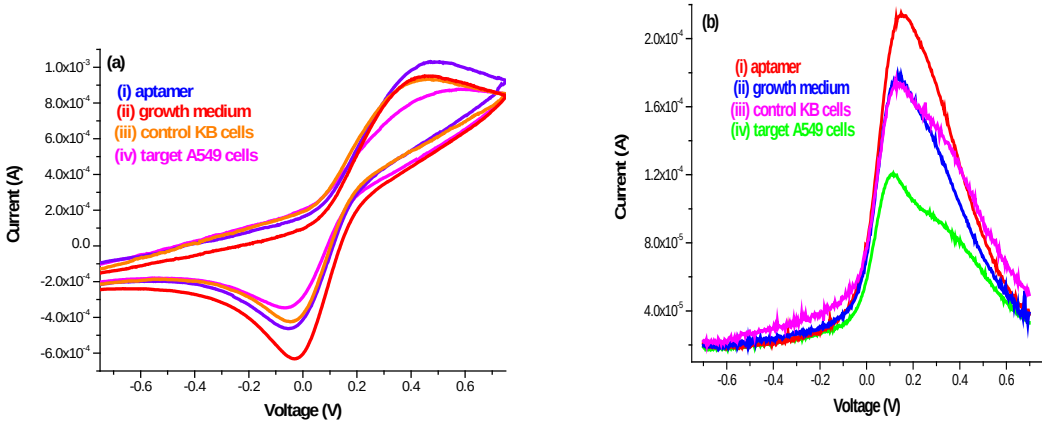

Figure 6. Specificity studies of the aptamer functionalized bioelectrode with control KB cells using CV (a) and DPV (b).

4. Conclusions

An aptamer based biosensor has been fabricated for detection of human lung adenocarcinoma A549 cells using aminosilane as the platform. The amine-terminated aptamer probe has been covalently bonded to the amine functionalized silane surface onto ITO using glutaraldehyde as the crosslinker. The surface coverage of the aptamer probe onto the silanized ITO electrode is found to be 1.627×10^{-10} mol cm^{-2}. This electrochemical aptamer sensor exhibits detection limit of 10^3 cells/ml with response time of 60 s for the target A549 cells. Aptamers show selectivity towards their target cells as the electrochemical signal response for control KB cells is about 50% as compared to that of the target cells. Thus aptamers can be utilized for the detection of the lung cancer cells. It should be interesting to utilize conducting polymers and nanomaterials including nanostructured metal oxides etc [35,36] to obtain increased sensitivity of this aptasensor.

References

[1] Kumar M, Agarwal S K and Goel S K 2009 *Mol. Cell Biochem.* **322** 73
[2] Pathak A K, Bhutani M, Mohan A, Guleria R, Bal S and Kochupillai V 2004 *Indian J. Chest Dis. Allied Sci.* **46** 191
[3] Behera D and Balamugesh T 2004 *Indian J. Chest Dis. Allied Sci.* **46** 269
[4] Sutedja G 2003 *Eur. Respir. J.* **21** 57s
[5] Mao L, Hruban R H, Boyle J O, Tockman M and Sidransky D 1994 *Cancer Res* **54** 1634
[6] Weder W, MD, Schmid R A, Bruchhaus H, Hillinger S, Schulthess G K and Steinert H C 1998 *Ann. Thorac Surg.* **66** 886
[7] Schmiemann V, Bocking A, Kazimirek M, Onofre A S C,Gabbert H E, Kappes R, Gerharz C D and Grote H J 2005 *Clin Cancer Res* **11** 7728
[8] Zhu H, Smith C, Ansah C and Gooderham N J 2005 *Cancer Cell International* **5** 28
[9] Mitsudomi T, Steinberg S M, Oie H K, Mulshine J L, Phelps R, Viallet J, Pass H, Minna J D and Gazdar A F 1991 *Cancer Res.* **51** 4999
[10] Wu W, Fan Y H, Kemp B L, Walsh G and Mao L 1998 *Cancer Res.* **58** 4082
[11] Lynch T J,Bell D W,Sordella R, Gurubhagavatula S, Okimoto R A, Haluska F G, Louis D N, Christiani D C, Settleman J and Haber D A 2004 *N. Engl. J. Med.* **350** 21
[12] Croce C M 2008 *N. Engl. J. Med.* **358** 502
[13] Li Y, Lee H J and Corn R M 2007 *Anal. Chem.* **79** 1082

[14] Li Z, Wang Y, Wang J, Tang Z, Pounds J G and Lin Y 2010 *Anal. Chem.* **82** 7008
[15] Wang H, Cao C, Li B, Chen S, Yin J, Shi J, Ye D, Tao Q, Hu P, Epstein A and Ju D 2008 *Cancer Immunol Immunother* 57 677
[16] Lee T Y and Song J T 2010 *Thin Solid Films* **518** 6630
[17] Syed M A and Pervaiz S 2010 *Oligonucleotides* **20** 215
[18] Cho E J, Lee J W and Ellington A D 2009 *Annu. Rev. Anal. Chem.* **2** 241
[19] Guo K T, Paul A, Schichor C, Ziemer G and Wendel H P 2008 *Int. J. Mol. Sci.* **9** 668
[20] Mok Wand Li Y 2008 *Sensors* **8** 7050
[21] Proske D, Blank M, Buhmann R and Resch A 2005 *Appl. Microbiol. Biotechnol.* **69** 367
[22] Ishii Y, Tajima S and Kawarada H 2011 *App. Phys. Exp.* **4** 027001
[23] Prabhakar N, Matharu Z, Malhotra B D 2011 *Biosensors and Bioelectronics* **26** 4006
[24] Liu G, Mao X, Phillips J A, Xu H, Tan W and Zeng L 2009 *Anal. Chem*. **81** 10013
[25] Jie G, Wang L, Yuan J and Zhang S 2011 *Anal. Chem*. **83** 3873
[26] Pan C, Guo M, Nie Z, Xiao X, Yao S 2009 *Electroanalysis* **21** 1321
[27] Pan Y, Guo M, Nie Z, Huang Y, Pan C, Zeng K, Zhang Y and Yao S 2010 *Biosensors and Bioelectronics* **25** 1609
[28] Willner I and Zayats M 2007 *Angew. Chem. Int. Ed.* **46** 6408
[29] Rodriguez M C, Kawde A N and Wang J 2005 *Chem. Commun.* 4267
[30] Zhao Z, Xu L, Shi X, Tan W, Fang X and Shangguan D 2009 *Analyst* **134** 1808
[31] Das M, Sumana G, Pandey M K, Nagarajan R and Malhotra B D 2011 *Sensor Letters* **9** 499
[32] Das M, Dhand C, Sumana G, Srivastava A K, Nagarajan R, Nain L, Iwamoto M, Manaka T and Malhotra B D 2011 *Biomacromolecules* **12** 540
[33] Arya S K, Prusty A K, Singh S P, Solanki P R, Pandey M K, Datta M, Malhotra B D 2007 *Anal. Biochem.* doi:10.1016/ j.ab.2007.01.029
[34] Singh R, Dhand C, Sumana G, Verma R, Sood S, Gupta R K and Malhotra B D 2010 *J. Mol. Recognit.* DOI:10.1002/jmr.1014
[35] Huang Y F, Lin Y W and Lin Z H 2009 *Nanopart. Res.* **11** 775
[36] Lin M M, Kim D K, Haj A J and Dobson J 2008 *IEEE Trans. Nanobiosci.* **7** 298

Biodiesel production of non-edible oils through ultrasound energy

Amit Pal, *S. S. Kachhwaha

Department of Mechanical Engineering, Delhi Technological University, Bawana Road, Delhi 110042, India

*Department of Mechanical Engineering, Pandit Deendayal Upadhayaya University, Gandhinagar India

Abstract-- **This paper presents the comparative details of biodiesel production process using low frequency ultrasound energy (28.5 kHz) and conventional mechanical stirrer method. For this purpose a non-edible oil Thumba (Citrullus colocyntis) is used as the biodiesel feedstock. The experiments have been performed for molar ratio (alcohol/oil) 6:1 and 4.5:1, with three different catalyst percentages (0.5%, 0.75% and 1%) of Potassium Hydroxide. The present study concludes that biodiesel production through ultrasound energy seem to be a relatively simple, efficient, time saving, eco-friendly and industrially viable process.**

Key words-- Biodiesel; Ultrasound energy; Transesterification, Non-edible oils;

I. INTRODUCTION

Presently majority of the world's energy needs are supplied through petrochemical sources, coal and natural gases, all these sources are finite and at current usage rates will be consumed shortly [1]. Also, petroleum fuels are currently the dominant global source of CO_2 emissions and their combustion is posing a severe threat to the clean environment. This has stimulated the recent interest in alternative sources for petroleum-based fuels [2]. Vegetable oils are good alternative source in Indian context because of its agriculture based economy. Keeping in its vast demand of edible oils, biodiesel production through only non-edible oil is feasible in India.

Vegetable oils have good heating power and provide exhaust gas with negligible sulphur and aromatic polycyclic compounds. It possesses high biodegradability and lubricating property which makes it even better fuel. As vegetable oils are produced from plants, their burning is completely recyclable as it produces carbon dioxide (CO_2), which is consumed by the plants in photosynthesis [3]. Vegetable oils can be directly used as fuels for diesel engines, but their viscosities are much higher (10 to 20 times) than usual diesel fuel and require modifications in the engines [4]. The glycerides present in the oils restrict its use in the I.C. engines but it can can also be separated in the transesterification reaction and used as a by-product [5]. Bio-diesel production is a very modern and technological area for researchers because of its relevance due to increase in the petroleum price and the environmental advantages [6].

Biodiesel can be produced by various conventional methods such as: alkali catalysis, acid catalysis, lipase catalysis etc. Non-edible oil and alcohols are immiscible, so that their reaction takes place at the interface in a very slow process. Considering these limitations, there is a strong quest to develop an efficient, time-saving, economically functional and environmental friendly biodiesel production process at industrial scale having superiority over the classical procedure. Keeping this aspect into consideration, some of the recently developed biodiesel production technologies are supercritical methanol processes, hydrodynamic cavitation and power ultrasound.

Among recently developed techniques, hydrodynamic cavitation is a potential method for biodiesel production at industrial scale due to its easy scale-up property [7]. In the last decade due to its unique chemical and physical effects that arise from the collapse of the cavitation bubbles. Ultrasound mixing efficiency was stated as one of the most important factors affecting the yield of the transesterification[8]. Thus using ultrasounds the problems of efficient mixing could be overcome. During the collapse of cavitational bubbles of methanol supersonic jets are created generating nano sized drops that are efficiently mixed thus abundantly enhancing the reaction surface. Biodiesel production from canola oil with methanol was performed by Thanh et al. [10] in the presence of a base-catalyst by a circulation process at room temperature.

In India mainly Jatropha is identified as the potential feedstock for biodiesel production. The *Citrullus colocyntis* (Thumba) oil is also a non-edible vegetable oil which can be a potential alternative fuel for CI engines. Present study explores its possibility for use as fuel oil. It is a native of Turkey and found in Asia and Africa. In India it mainly grows in rain fed parts of Rajasthan and Gujarat states. The plant is in the form of creeper and grows well in sandy soil. The plant has annular and rough stems, rough leaves which are 3 to 7 lobed, 5-10 cm long in middle. The multifold objectives of the present research study is the production of biodiesel from Thumba using alkaline catalysis by ultrasound assisted transesterification, and compare the completion, product quality and time of the reaction with the conventional procedure.

II. Experimental Work

2.1 Test rig for ultrasound cavitation technique

The transesterification reactions were carried out in a horn type ultrasound reactor (shown in Figure 1) in which horn is attached with the transducer which produces ultrasound irradiation in the mixture. This type of configuration is suitable for laboratory-scale characterization/ feasible experiments, because intense but local cavitation is generated. The horn operates at a frequency of 28.5 kHz with a rated power dissipation of 50W and time limit is ranging between 3 min to 30 min. The submerged irradiating surface area of the horn is 25 cm^2. The operating intensity of irradiation is (defined as power dissipated per unit area of the horn) 2 W/cm^2. The transesterification reaction is carried out by ultrasound irradiation from the acoustic rod horn incorporated with the transducer. Conventional mechanical transesterification was conducted in reactor equipped with a 100 ml glass vessel and magnetic stirrer.

2.2 Fuel properties

The important chemical and physical properties of Thumba biodiesel were determined and compared with diesel in Table 1. Kinematic viscosity of Thumba biodiesel is slightly higher than diesel. Flash point of Thumba biodiesel is significantly higher as compared to petroleum diesel. Therefore, based on the property data, the Thumba biodiesel is considered to be suitable for blending and can be used in CI engines.

III. Results and Discussion

As shown in Table 2, for prescribed non-edible oil, transesterification reaction is performed for molar ratios 6:1 and 4.5:1 respectively. Further for each molar ratio, catalyst quantity has been taken as 0.5%, 0.75% and 1.0% (by weight of oil) respectively. Methyl alcohol and potassium hydroxide are mixed and stirred till potassium hydroxide is dissolved in alcohol. The ultrasound horn is dipped into the prepared liquid mixture. During the reaction the generation, subsequent growth and collapse of bubble cavities result in very high irradiation densities. The temperature of mixture is kept between 50-60 ^{0}C.

Tables 3 and 4 represent the data for biodiesel production time and yield (%) using conventional mechanical stirring and ultrasound energy respectively for parameters such as molar ratio and catalyst percentage. Further graphical comparisons are given in Figure 2. For mechanical stirring method, yield (%) varies as 79 to 90%, whereas for ultrasound method yield (%) values are 81 to 95% respectively. From the experimental data it is clear that there is a significant reduction in time for biodiesel production and an increase in yield (%) in ultrasound technique as compared to mechanical stirring method. It can be concluded from Table 4 that ultrasound cavitation can be successfully applied to transesterification reactions with more than 90% yield of the product and significant reduction in time for molar ratio 4.5:1 and minimum catalyst percentage of 0.5. Therefore, the ultrasound energy technique appears to be a rapid and effective technique compared to the conventional approach, for preparing alkyl esters from triglycerides at laboratory scale of operation.

Irrespective of the molar ratio the percentage of yield is higher in the ultrasound energy method for all the observations of catalyst percentage. Another signifiacant result is that even at 0.5% catalyst and molar ratio 4.5:1, the yield quantity is above 90%. Therefore, the requirement of catalyst as well as excess alchohol is significantly reduced. It can be seen that using ultrasound method reaction time is almost half compare to conventional method which is beneficial for industrial point of view. The effect of molar ratio is trivial on the yield percentage. For a given molar ratio, the yield initially increases and then decreases with increase in catalyst percentage(varied from 0.5% to .75% and then 1% . The yield data for ultrasound method is 2 to 5 % higher as compared to conventional mechanical stirring method.

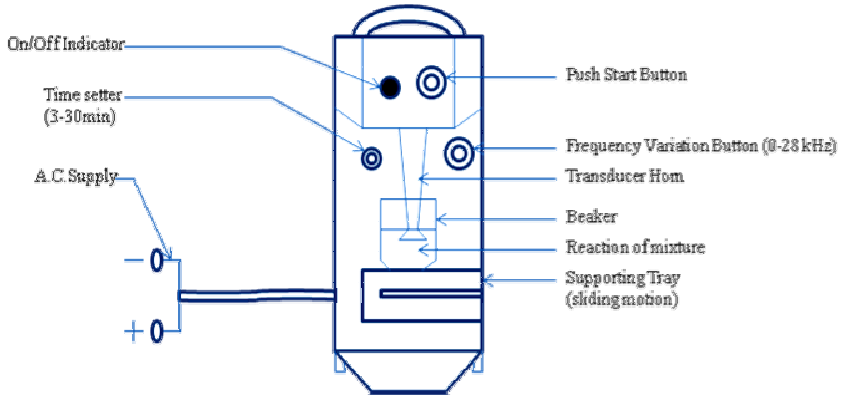

Figure 1: Schematic diagram of ultrasonic horn type reactor

Table 1: Comparison of biodiesel properties with diesel

Property	**Biodiesel from Thumba**	**Unit**	**Limit**	**Diesel ASTM D 975**
Appearance	clear	----	----	clear
Color	Brownish	----	----	----
Density at 15 ^{0}C	890	kg/m^3	860-900	830
Kinematic viscosity at 40 ^{0}C	5.86 x 10^{-6}	m^2/s	3.5-5 x 10^{-6}	(2.5-6)x 10^{-6}
Flash point	>66	^{0}C	Min 100	51
Sulphur contents	<100	ppm	Max 350	500
Water content	0.05	w/w%	0.02-0.05	0.005
Calorific Value	38.24	MJ/kg	---	42.0

Table 2: Quantities of non-edible oil, alcohol and catalyst

Molar ratio (alcohol/oil)	**Quantity of non-edible oil (g)**	**Quantity of methanol (g)**	**Catalyst (KOH)**		
			0.5%	**0.75%**	**1.0%**
6:1	100 g	22 g	0.5 g	0.75 g	1 g
4.5:1	100 g	16.56 g	0.5 g	0.75 g	1 g

Table 3: Conventional mechanical stirring/ Ultrasonic horn method (molar ratio 4.5:1)

KOH used	**Yield obtained in %-** Ultrasonic horn			**Yield obtained in %-** mechanical stirring		
	20min	**30 min**	**40 min**	**30 min**	**45 min**	**60 min**
0.5%	81	85	85.60	68	71.26	84.62
0.75%	86.42	89.48	92	77.41	77.44	87.2
1%	84.88	86.10	90.22	76.06	76.74	84.32

Table 4: Conventional mechanical stirring/ Ultrasonic horn method (molar ratio 6:1)

KOH used	**Yield obtained in %-** Ultrasonic horn			**Yield obtained in % -** mechanical stirring		
	20min	**30 min**	**40 min**	**30 min**	**45 min**	**60 min**
0.5%	87.72	90	96	76.4	82.22	90.90
0.75%	89.36	92	95.82	89	90.1	93.42
1%	86.58	88.74	90.60	84.6	87.24	90.04

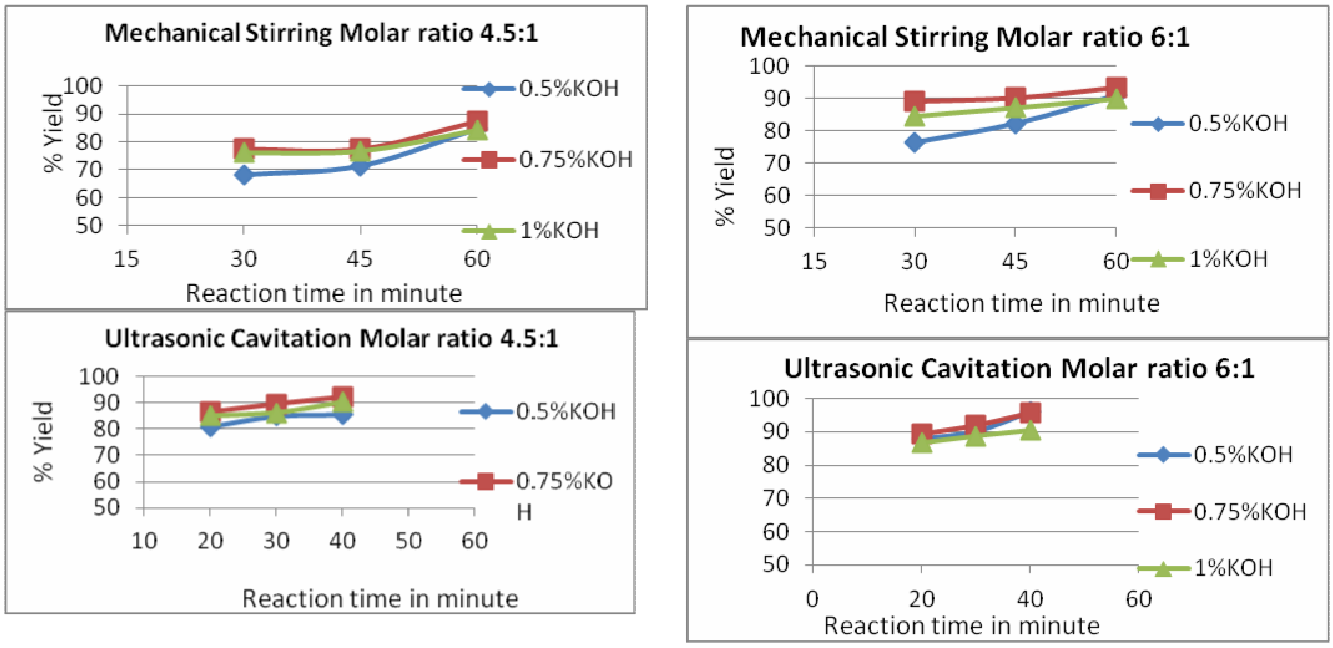

Figure 2: Comparisons for the Thumba biodiesel % yield from different methods and molar ratios

IV. CONCLUSIONS

The present study demonstrates that the reaction time for methyl ester formation using non-edible oils is significantly shorter for ultrasound cavitation method as compare to conventional mechanical stirring method. The percentage yield obtained using ultrasound method is relatively higher. Thus low frequency ultrasound is an efficient, time saving and economically functional, offering a lot of advantages over the classical methods. The engine performance test shows that opacity reduces whereas brake power and brake thermal thermal efficiency improves significantly for blending of B-30 which encourages the possibility of further investigations using higher blending.

V. REFERENCES

1. Srivastava, A., Prasad, R., 2000. Triglycerides based diesel fuels. Renew Sustain Energy Rev, 4, 111–133.
2. Agarwal, A. K., 2007. Biofuels (alcohols and biodiesel) applications as fuels for internal combustion engines. Progress in Energy and Combustion Science, 33, 233-271.
3. Marchetti, J. M., Miguel, V. U., Errazu, A. F., 2005. Possible methods for biodiesel production. Renew Sustain Energy Rev., 11, 1300–1311.
4. Stavarache, C., Vinatoru, M., Nishimura, R., Maeda, Y., 2005. Fatty acids methyl esters from vegetable oil by means of ultrasound energy. Ultrason Sonochem, 12, 367–72.
5. Wang, Y. D., Al-Shemmeri, T., Eames, P., McMullan, J., Hewit,t N., Huang, Y. 2006. An experimental investigation of the performance and gaseous exhaust emissions of a diesel engine using blends of a vegetable oil. Appl. Thermal Eng, 26, 1684–91.
6. Dmytryshyn, S. L, Dalai, A.K., Chaudhari, S. T., Mishra, H. K., Reaney, M. J., 2004. Synthesis and characterization of vegetable oil derived esters: evaluation for their diesel additive properties. Bioresource Technology. 92, 55–64.
7. Pal, A., Verma, A., Kachhwaha, S. S., Maji, S., 2010. Biodiesel production through hydrodynamic cavitation and performance testing. Renewable Energy, 35(3), 619–624.
8. Hoang Duc Hanh, Nguyen The Dong, Kenji Okitsu, Rokuro Nishimura, Yasuaki Maeda, 2009. Biodiesel production through transesterification of triolein with various alcohols in an ultrasound field. Renewable Energy, 34, 766–768.
9. Stavarache, C., Vinatoru, M., Nishimura, R., Maeda, Y., 2005. Fatty acids methyl esters from vegetable oil by means of ultrasound energy. Ultrasound Sonochemistry, 12, 367–372.
10. Thanh, L. T., Okitsu, K., Sadanaga, Y., Takenaka, N., Maeda, Y., and Bandow, H., 2010. Ultasound assisted production of biodiesel fuel from vegetable oils in a small scale circulation process. Bioresource Technology, 101, 639-645.

Electrochemical Urea Biosensor Based on Sol-gel Derived Nanostructured Cerium Oxide

2012 J. Phys.: Conf. Ser. 358 012006

(http://iopscience.iop.org/1742-6596/358/1/012006)

Electrochemical Urea Biosensor Based on Sol-gel Derived Nanostructured Cerium Oxide

Anees A Ansari[1]*, Md. Azahar[2] and B. D. Malhotra[3*]
[1]King Abdullah Institute for Nanotechnology, King Saud University, Riyadh, 11451 Kingdom of Saudi Arabia
[2]Department of Science & Technology Centre on Biomolecular Electronics,National Physical Laboratory, Dr. K S Krishnan Marg, New Delhi-110012, India
[3]Department of Biotechnology, Delhi Technological University,Shabad Daulatpur, Main Bawana Road, Delhi 11042,India

E-mail: aneesaansari@gmail.com ; bansi.malhotra@gmail.com

Abstract. Urease (Urs) and glutamate dehydrogenase (GLDH) have been co-immobilized onto a nanostructured–cerium oxide (Nano-CeO_2) film deposited onto a indium-tin-oxide (ITO) coated glass substrate by dip-coating via sol-gel process for urea detection. This nanostructured film has characterized using X-ray diffraction (XRD), Fourier transform infrared (FTIR), Scanning electron microscope (SEM) and electrochemical techniques, respectively. The particle size of the Nano–CeO_2 film has been found to be 23 nm. Electrochemcial response (CV) studies show that Ur-GLDH/Nano-CeO_2/ITO bioelectrode is found to be sensitive in the 10–80 mg/dL urea concentration range and can detect urea concentration upto 0.1 mg/dL level. The value of Michaelis–Menten constant (K_m) estimated using Lineweaver–Burke plot found as 6.09 mg/dL indicates enhancement in the affinity and/or activity of enzyme attached to their nanobiocomposite. This bioelectrode retained 95% of enzyme activity after 6 months at 4^{o}C.

1. Introduction

Novel analytical devices based on nanostructured metal oxides are known to be cost-effective and highly sensitive due to the large surface-to-volume ratio, show excellent selectivity and their optical and electrical properties arising from electron and phonon confinement. These nanostructured materials can be used as sensing biomolecules[1-18]. Besides these nanostructured metal oxides have unique properties such as non-toxicity, biocompatiblity, high chemical and thermal stability, high isoelectric point (IEP ~9.2) and negligible swelling in both aqueous and non-aqueous solvents[1-6]. A large number of nanomaterials such as carbon nanotubes[7], conducting polymers[8], grapheme[9], nanowires[10], zinc oxide nanoparticles and chitosan composite[11] film and nanoporous materials have been used for fabrication of various biosensors. Many nanostructured metal oxide such as zirconium oxide (ZrO_2), tin oxide (SnO_2), cerium oxide (CeO_2) and zinc oxide (ZnO) have been utilized for immobilization of proteins, enzymes and antigens for accelerated electron transfer between active sites of protein and electrode[12-13]. On the other hand, MnO_2 and TiO_2 having low IEP values are suitable for the immobilization of high IEP proteins.

* To whom any correspondence should be addressed.

Recent times have been significant advances towards the production of nanocrystalline metal oxides using a variety of physical and chemical processes, such as sputtering, sol–gel, hydrothermal, spray pyrolysis etc. Among the various methods sol-gel technique has been considered as very attractive for the preparation of metal oxide particles due to easy preparation under ambient conditions, tunable porosity, high thermal stability, chemical inertness and negligible swelling in aqueous and non-aqueous solutions[14-15]. Besides this, due to inherent low temperature process, the sol-gel technology provides an attractive method for the immobilization of heat-sensitive biomolecules such as enzymes, proteins and antibodies[16]. The positively charged sol–gel cerium oxide not only provides a friendly environment for the enzyme to retain its activity but also encapsulate the negatively charged electron transfer mediator within the sol-gel film via electrostatic interaction[17]. The sensitivity and stability of the biosensors can perhaps be improved by controlling charge, porosity and electronical conductivity of a given sol-gel film. These attractive features have led to an increased research towards developing the electrochemical sensors and biosensors[18].

The estimation of urea is of clinical interest since decreased urea concentration (normal range is 15-40 mg/dl) causes hepatic failure, nephritic syndrome and cachexia and increased urea level in blood and urine causes renal failure, urinary tract obstruction, dehydration, shock, burns and gastrointestinal bleeding[19-21]. Therefore, development of rapid, cheap and reliable methods for urea determination is important. Among the numerous analytical methods reported in literature, enzymatic methods offer an improvement in terms of specificity, response time, miniature size, reproducibility and selectivity. Saha et. al. fabricated cerium oxide (CeO_2) film deposited onto platinum (Pt) electrode using pulsed laser deposition (PLD) has been utilized for immobilization of glucose oxidase (GOx)[22]. Feng *et. al.* have prepared a nanoporous CeO_2/chitosan composite matrix for the immobilization of single-stranded DNA probes for the detection of cancer genes[23]. Khan et. al. ZnO-chitosan nanocomposite has recently been used for application to urea and cholesterol biosensors[11].

We have used a facile sol-gel chemical route to prepare Nano-CeO_2 film onto indium-tin-oxide glass substrate (ITO) to immobilize a mixture of ureas and GLDH enzymes for application to urea detection using electrochemical spectroscopy technique.

2. Experimental procedure

2.1. Chemicals and reagents

Urease (Urs), glutamate dehydrogenase (GLDH), nicotinamide adenine dinucleotide (NADH) α-keto glutarate (α-KG), Na_2HPO_4 and NaH_2PO_4 were procured from Sigma Aldrich (USA). Ammonium ceric nitrate, urea, NaCl, NH_4OH and HNO_3 reagents were procured from Merck India Ltd, Mumbai, India. All these chemicals were of analytical grade and used without further purification. Indium-tin-oxide (ITO) coated glass plates were obtained from Balzers, UK. The deionized water obtained from Millipore water purification system (Milli Q 10 TS) was used for preparation of solutions and buffers.

2.2. Fabrication of sol-gel derived nano-structured CeO_2 film/electrode

1 gm of ceric ammonium nitrate [$(NH_4)_2Ce(NO_3)_6$] was dissolved in deionised water (20 ml). Then 5 ml (1 M) solution of ammonium hydroxide (NH_4OH) was added drop wise in this solution with constant stirring for 4 h at 25 ^oC to maintain pH 10. A pale yellow precipitate of $Ce(OH)_4$ thus obtained was washed several times with deionized water until a neutral pH was achieved[13]. Subsequently, dilute HNO_3 (1M) was added to the precipitate at 60 ^oC to obtain a solution of pH 1. A transparent yellow solution thus obtained was further concentrated by heating. The resulting sol was used to fabricate thin film on ITO coated glass plate via dip coating technique and was allowed to dry at 500 ^oC.

2.3. Electrode modification and immobilization Urease-GLDH

10 μL of 1:1 molar mixture of urease and GLDH (1.0 mg/mL, in PBS, 50 mM, pH 7.0) was immobilized onto sol-gel derived Nano-CeO_2 electrode by physisorption method. The biochemical reaction using mixed enzyme system is shown in Eq.1. Prior to being used, Urs-GLDH/Nano-CeO_2/ITO bioelectrode was allowed to dry overnight under desiccated conditions and then washed with phosphate buffer saline (PBS, 50 mM, pH 7.0, 0.9 % NaCl) to remove any unabsorbed enzymes (Urs-GLDH) and stored in a desiccator at 25^oC when not in use.

$$\text{Urea} \xrightarrow{\text{urease}} 2NH_4^+ + HCO_3^- \quad \text{(Eq. 1)}$$

$$2NH_4^+ + \alpha\text{- ketoglutarate} + NADH \xrightarrow{\text{GLDH}} \text{2- Glutamate} + NAD^+ \quad \text{(Eq. 2)}$$

$$NADH \longrightarrow NAD^+ + 2e^- \quad \text{(Eq. 3)}$$

2.4. Characterization of sol-gel derived Nano-CeO_2/ITO electrode and Urs-GLDH/Nano-CeO_2/ITO bioelectrode

X-ray diffraction (XRD, Cu Ka radiation (Rigaku)) study was performed to identify the crystal structure of sol-gel derived Nano-CeO_2 film. Scanning electron microscopy (SEM, LEO-440) studies were conducted to examine the surface morphology. FTIR spectra of sol-gel derived Nano-CeO_2 films were recorded using FTIR (Perkin-Elmer) spectrophotometer to investigate binding of ureas enzyme onto sol-gel derived Nano-CeO_2/ITO film. Electrochemical measurements were conducted on an Autolab Potentiostat/Galvanostat (Eco Chemie, Netherlands) using a three-electrode cell containing ITO act as a working electrode, Ag/AgCl as reference electrode and platinum (Pt) wire serve as a counter electrode in phosphate buffer saline (PBS, 50 mM, pH 7.0, 0.9% NaCl) containing 5 mM $[Fe(CN)_6]^{3-/4-}$.

3. Results and discussion

3.1. Characterization of nano- CeO_2 film

The XRD diffraction pattern (Figure 1) shows a crystallographic phase present in the sol–gel derived CeO_2 film deposited on the glass substrate via dip-coating technique. A high degree of preferential orientation is evident, giving rise to spectra resembling a single crystal diffraction pattern. XRD pattern of the deposited film reveals all reflection planes of CeO_2, corresponding to the (111), (200), (220) and (311) crystallographic plane cubic fluorite structure (space group Fm3m (225)) as identified using the standard data JCPDS Card No. 34-0394. The intensities and positions of the peaks are in perfect agreement with the literature values. No peak of any other phase is detected indicating the high purity of the material. The broadening of the reflections in the diffractogram distinctly indicates the formation of nano-dimensional crystals. The average crystallite size of CeO_2 nanoparticles was estimated by analysis of the broadening of (111) and (220) reflections via Scherrer formula found to be 10-15 nm.

3.2. Characterization of nano- CeO_2 film

The infrared absorption spectra of Nano-CeO_2/ITO (a) and Urs-GLDH/Nano-CeO_2/ITO (b) shows the characteristic absorption bands of the deposited films (Figure 2). A diffused band at 3404 cm^{-1} and two weak bands at 1414 and 1010 cm^{-1}, corresponding to the stretching and bending vibrations of the hydroxyl (O–H) groups, respectively, are observed. The appearance of these bands suggests the adsorption of moisture on the surface of nanostructured film. The FTIR spectrum shows a sharp and intense band at around 426 cm^{-1} assigned to the Ce-O stretching band and indicates the deposition of CeO_2 film on the ITO surface. These observed bands are shifted and some new bands are appearing at 1740, 1380 and 1050 cm^{-1} corresponding to the stretching and bending vibrations of the amide, the functional groups. This indicates that the Urs-GLDH mixed enzymes solution has been successfully immobilized on the Nano-CeO_2 matrix. A sharp band at 450 cm^{-1} is observed due to the electrostatic interaction and hydrogen bonding of the Nano-CeO_2 with the enzymes (Urs-GLDH).

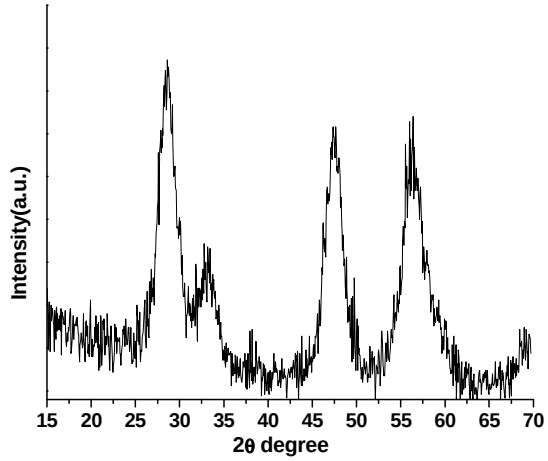

Figure 1. XRD pattern of sol-gel derived CeO_2 film

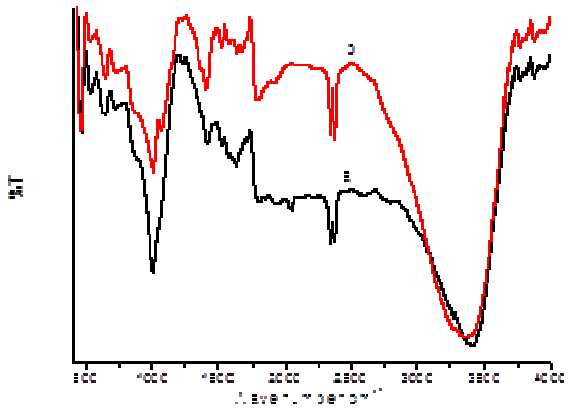

Figure 2. FTIR spectra of (a) sol-gel derived Nano-CeO_2/ITO electrode and (b) Urs-GLDH/Nano-CeO_2/ITO bioelectrode

3.3. Scanning electron microscopy studies

Figure 3 shows results of the SEM studies carried out on Nano-CeO_2/ITO film and of Urs-GLDH/Nano-CeO_2/ITO bioelectrode, respectively. The SEM micrograph shows that the film surface is free of cracks, uniform in thickness porous in nature and composed of very small fine grains that are homogenously distributed (image 3a). The adsorption or immobilization of urease enzyme onto the surface of sol-gel derived Nano-CeO_2/ITO electrode is dependent on the morphology of the substrate. It can be seen that after immobilization of Urs-GLDH onto Nano-CeO_2/ITO electrode, displays flower like structure with high porosity, inter-connectivity and significant free volume favoring the effective immobilization of a large number of enzymes (image 3b).

3.4. Rlectrochemical impedance spectroscopy

EIS measurements carried out on Nano-CeO_2/ITO electrode and Urs-GLDH/Nano–CeO_2/ITO bioelectrode at frequency range 0.0–5×10^3 Ω. It is an effective and powerful tool for characterizing the interfacial features of surface-modified electrodes. The modified electrode impedance can be presented as the sum of the real ($Z^{'}$), and imaginary ($-Z^{''}$) components that originate mainly from the resistance and capacitance of the cell, respectively. The general electronic equivalent circuit (Randles and Ershler model), includes the ohmic resistance of the electrolyte solution (R_s), the Warburg impedance (D), resulting from the diffusion of ions from the bulk electrolyte to the electrode interface. The double layer capacitance (C_{dl}) and charge-transfer resistance (R_{ct}) exists, if a redox probe is present in the electrolyte solution, where R_s and D denote bulk properties of the electrolyte solution and diffusion features of the redox probe in solution, respectively. The other two components C_{dl} and R_{ct}, depend on the dielectric and insulating features at the electrode/electrolyte interface. Figure 4 shows the Faradaic impedance spectra, presented as Nyquist plots obtained from real (Z'') and imaginary ($-Z''$) of blank ITO (curve a), Nano-CeO_2/ITO electrode (curve b) and Urs-GLDH/Nano-CeO_2/ITO (curve c) bioelectrode. The values of R_{ct} derived from the diameter of semicircle of impedance spectra are obtained as 2.3 kΩ for blank ITO electrode (curve a), 2.77 kΩ (curve b) for the Nano-CeO_2/ITO electrode and 2.92 kΩ for Urs-GLDH/Nano–CeO_2/ITO bioelectrode, respectively. The increase of R_{ct} (2.92 kΩ) value and the shift of semicircle to higher frequency after deposition of the Nano–CeO_2 layer on the ITO electrode is attributed to the low electrical conductivity of the Nano–CeO_2 particles that provides slow electron transfer between Nano-CeO_2 particles and electrode. This

result suggests that solution resistance (R_s) is slightly increased, but interfacial impedance (double layer capacitance, C_{dl} and the charge transfer resistance, R_{ct}) is greatly increased after the deposition of Nano-CeO_2 film on the ITO electrode surface. It is observed that after the immobilization of mixed Urs-GLDH enzyme on the matrix the R_{ct} value is increases dramatically due to insulating characteristics of the mixed Urs-GLDH enzyme molecules. It reveals that Warburg impedance (D), which represents the mass transfer, is enhanced after the immobilization of these enzymes (Urs-GLDH) on the Nano–CeO_2/ITO electrode surface, implying that enzyme molecules are indeed absorbed on Nano–CeO_2/ITO surfaces and induce impedance effects on the interface of the electrode surface. The double-layer capacitance (C_{dl}) is decreased, indicating that a higher enzyme (Urs-GLDH) concentration enhances the adsorption of enzyme on the Nano–CeO_2/ITO modified electrode.

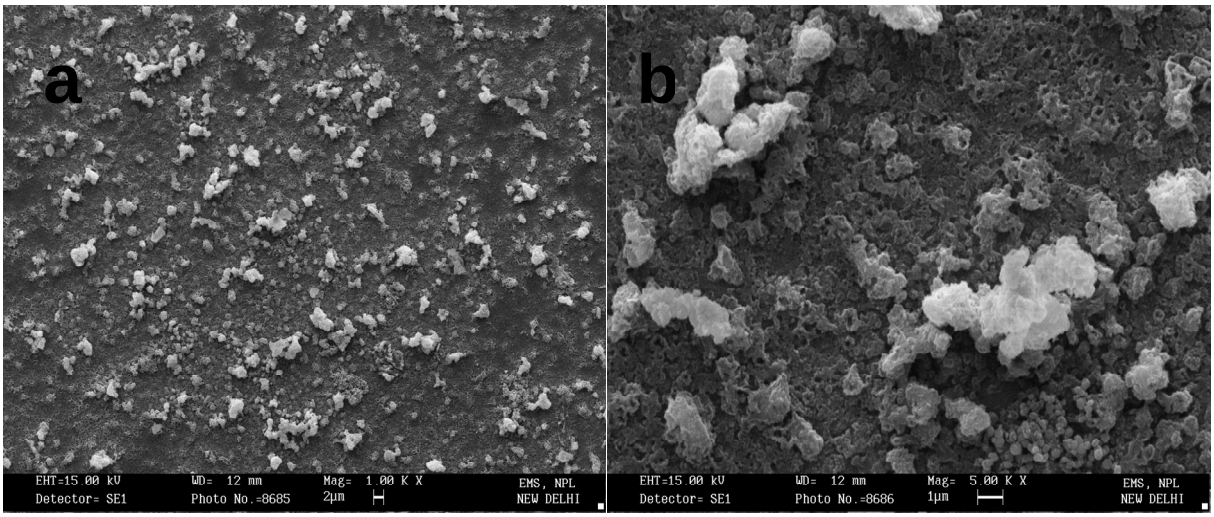

Figure 3. SEM micrographs of (a) sol-gel derived Nano-CeO_2 electrode and (b) Urs-GLDH/Nano-CeO_2/ITO bioelectrode

3.5. Rlectrochemical impedance spectroscopy

The changes of electrode behavior after surface modification with enzymes (Urs and GLDH) were studied by cyclic voltammetry (CV) in the presence of ferricyanide mediator. When the electrode surface is modified by the biocatalytic material, the change in the electron transfer kinetics of $[Fe(CN)_6]^{3-/4-}$ gives indication of the enzyme attachment. Figure 5 shows the cyclic voltammograms of blank ITO (a), Nano-CeO_2/ITO (b) and Urs-GLDH/Nano-CeO_2/ ITO bioelectrode (c) at a scan rate of 50 mVs^{-1}. As shown in Figure 5 well-defined redox couple of $[Fe(CN)_6]^{3-/4-}$ is observed on the bare ITO electrode (curve a). When the Nano–CeO_2/ITO electrode layer is deposited on the ITO electrode, the peak current gradually decreases (curve b). The decrease in the peak potential after deposition of Nano–CeO_2 may be attributed to the hindrance of the electrons flow as a result of reduction in electrical conductivity of the nanostructured Nano–CeO_2/ITO electrode. Further, redox current of Urs-GLDH/Nano–CeO_2/ITO bioelectrode is found to decrease due to insulating characteristics of Urs-GLDH indicating slow down of redox process during the biochemical reaction. The reason is that an insulating layer of non-conducting enzyme had been assembled on electrode surface, which act as a electron transfer barrier.

Figure 6 demonstrates typical CV of Urs-GLDH/Nano-CeO_2/ITO bioelectrode with scan rate varying from 10 to 100 mVs^{-1}. With increase in the scan rate, there is increase in both the cathodic and anodic peak current accompanied with small shift and increased peak-to-peak separation. The cathodic and anodic peak currents increase linearly with scan rate varying from 10 to 100mVs^{-1} indicating a surface controlled electrode process. This reveals that the electron transfer between enzyme and electrode could be easily performed and it was a surface confined electrochemical process.

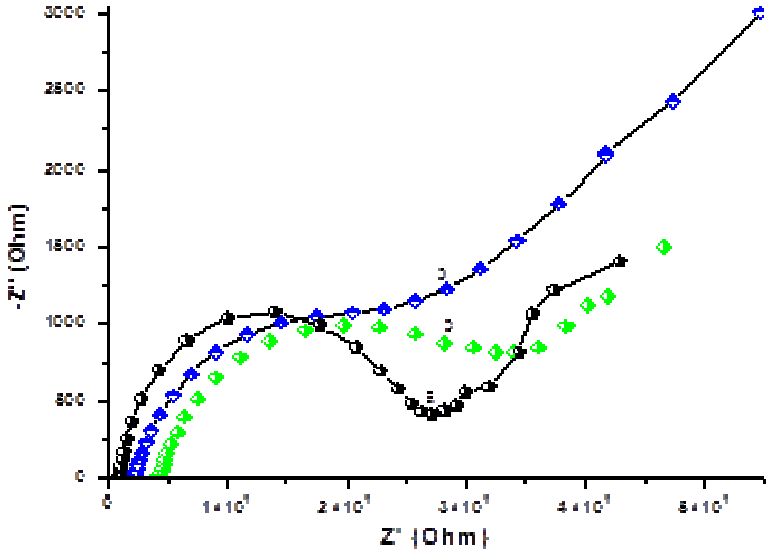

Figure 4. Electrochemical Impedance spectroscopy of (a) bare ITO electrode (b) sol-gel derived Nano-CeO_2/ITO electrode and(c) Urs-GLDH/Nano- CeO_2/ITO bioelectrode in PBS solution (50 mM, pH 7.0, 0.9% NaCl) containing 5 mM $[Fe(CN)_6]^{3-/4-}$

3.6. Rlectrochemical impedance spectroscopy

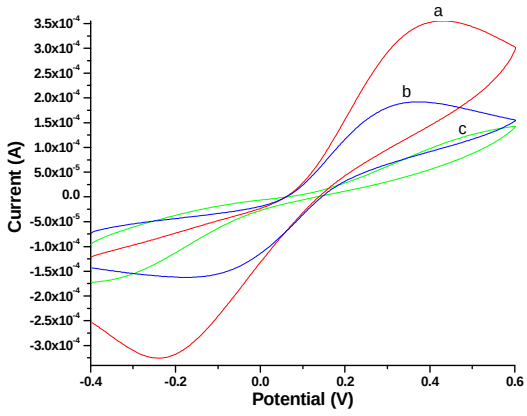

Figure 5. Cyclic voltammogram of (a) bare ITO electrode (b) sol-gel derived Nano-CeO_2/ITO electrode and(c) Urs-GLDH/Nano- CeO_2/ITO bioelectrode in PBS solution (50 mM, pH 7.0, 0.9% NaCl) containing 5 mM $[Fe(CN)_6]^{3-/4-}$

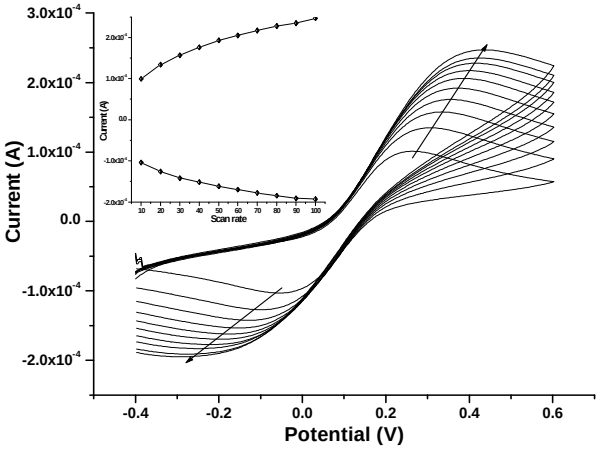

Figure 6. CV of Urs-GLDH/Nano-CeO_2/ITO bioelectrode as a function of scan rate (10-100 mV/s^{-1}) in ascending order in PBS solution containing 5 mM $[Fe(CN)_6]^{3-/4}$

Figure 7 (inset) illustrate the CV response studies of the Urs-GLDH/Nano-CeO_2/ITO bioelectrode in PBS solution {pH 7, 0.9%NaCl, containing 5mM $[Fe(CN)_6]^{3-/4-}$} in the presence of 30 µL of nicotinamide adenine dinucleotide (NADH, 3.7 mg/dL) and 70 µL of α-Keto glutamate (α-KG, 47.5

mg/dL) and a successive addition of urea at an applied 50 mV/s scan rate. The peak current rises sharply with increased concentration of urea, with the maximum response approach at the concentration of 80 mg/dL. This increase in electrochemical current response can be attributed to pH sensitive behavior of the Ur-GLDH/Nano-CeO_2/ITO bioelectrode. The sensor achieves 95% of the steady-state current in less than 5s indicating fast electron exchange between the Urs-GLDH and Nano–CeO_2/ITO electrode. Figure 7 shows the amperometric current of the fabricated biosensor increases linearly within the concentration range 10-80 mg/dL, with increasing urea concentration the correlation coefficient (*R)* as 0.991 indicating good electro-catalytic behavior of Urs-GLDH/Nano–CeO_2/ITO bioelectrode. The sensitivity of the Urs-GLDH/Nano–CeO_2/ITO bioelectrode calculated from the slope of curve was found to be 0.64 μA/mg/dL and low detection limit 0.1 mg/dL.

The value of K_m, which is a reflection of enzymatic affinity, was found to be 6.09 mg/dL. The lower K_m value with respect to glutaraldehyde-cross-linked urease-albumin gel (6.5 mM) and TMOS-based sol-gel (4.95 mM) indicates easier diffusion of substrate and product molecules into and out of the Nano–CeO_2 film and the feasible configuration of the enzyme in the nanomaterial matrix. The high affinity of Urs-GLDH to urea can be attributed to Nano–CeO_2 nanoparticles because of its biocompatibility, large surface area, and high electron communication capability. The value of ionization electron potential (IEP) of CeO_2 and urease are known to be 9.0 and 5.3, respectively. Therefore, the Nano–CeO_2 matrix is positively charged in contrast to the enzymes that are negatively charged. Thus, immobilization of Urs-GLDH on the Nano–CeO_2 nanoparticles matrix is highly favored via electrostatic interaction.

3.7. Effect of pH onto Urs-GLDH/nano-CeO_2/ITO biosensor

The influence of pH of buffer on the response of the biosensor studied over the range 6.0–8.0 indicates that the current response increases with increase of pH of the substrate solution up to 7.0, after which it decreases. In view of the prime pH of the enzyme, the neutral pH was selected throughout this work (Figure 8).

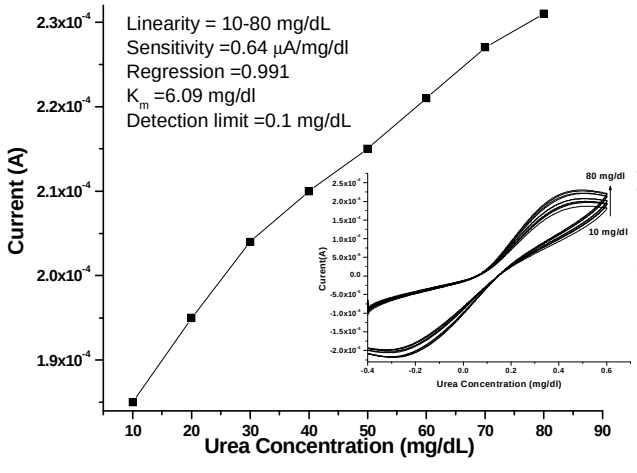

Figure 7. The calibration plot between current response and different concentration of urea in the range (10-80 mg/dl)in PBS solution containing 5 mM $[Fe(CN)_6]^{3-/4-}$; inset shows the CV response of Urs-GLDH/Nano-CeO_2/ITO bioelectrode as a function of urea concentration

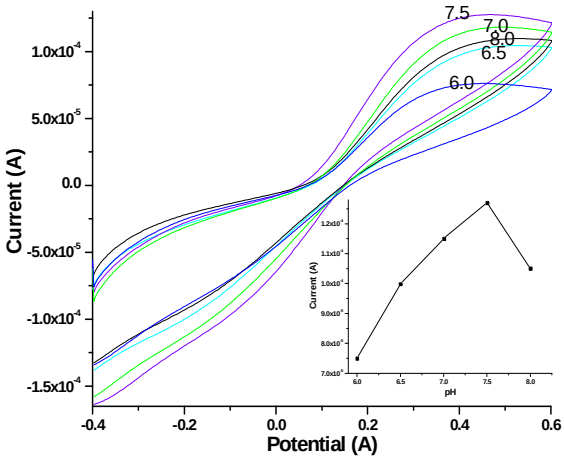

Figure 8. Effect of pH on Urs-GLDH/ Nano-CeO_2/ITO bioelectrode using CV

4. Conclusions

Nanostructured CeO_2 film was prepared by sol gel technique and used to co-immobilization of Urs and GLDH enzymes via physical adsorption for urea detection. This biosensor exhibits excellent performance characteristics, such as sensitivity (0.64μA/mg/dL) and reproducibility, wide linear range (10–80 mg/dL), low detection limit (0.10 mM), and long-term stability of about 6 months. A relatively low value of the Michaelis–Menten constant obtained as 6.09 mg/dL indicates enhanced enzyme affinity of Urs to urea. The wide range of detection and high sensitivity may be assigned to amplification of the magnitude of current due to the alignment of Nano–CeO_2 nanoparticles to the matrix. Efforts should be made to use this electrode for the detection of urea in blood serum.

References

[1] Wang J X, Sun X W, Wei A, Lei Y, Cai X P, Li C M and Dong Z L 2006 *Appl. Phys. Let*t. **88** 233106
[2] Pandey P, Datta M and Malhotra B D 2008 *Anal. Lett.* **41** 157–207
[3] Zhou H, Gan X, Wang J, Zhu X and Li G 2005 *Anal. Chem.* **77** 6102
[4] Kumar S A and Chen S M 2008 *Anal. Lett*. **41** 141
[5] Singh S P, Arya S K, Pandey M K, Malhotra B D, Saha S, Sreenivas K and Gupta V 2006 *Appl. Phys. Lett.* **91** 063901
[6] Wei A, Sun X W, Wang J X, Lei Y, Cai X P, Li C M, Dong Z L and Huang W 2006 *Appl. Phys. Lett.* **99** 123902
[7] Wang S G, Zhang Q, Wang R and Yoon S F 2003 *Biochem. Biophys. Res. Commun.* **311** 572–576
[8] Galatanu A N, Chrorrakis I S, Anghel D F and Khan A 2000 *Langmuir* **16** 4922
[9] Shao Y, Wang J, Wu H, Liu J, Aksay I A and Li Y 2010 *Electroanalysis* **22** 1027 – 103
[10] Wanekaya A K, Chen W, Myung N Vand Mulchandani A 2006, Electroanalysis **18** 533 – 55
[11] Khan R, Kaushik A, Solanki P R, Ansari A A, Pandey M K and Malhotra B D 2008 *Analytica Chimica Acta* **616** 207–213
[12] Ansari A A, Kaushik A, Solanki P R, and Malhotra B D 2008 *Electrochem. Commun.* **10** 1246
[13] Solanki P R, Kaushik A, Ansari A A, Sumana G, and Malhotra B D 2008 *Appl. Phys. Lett.* **93** 163903
[14] Suzuki T, Kosacki I and Anderson H U 2001 *J. Am. Ceram. Soc*. **84** 2007
[15] Ghodsi F E, Tepehan F Z and Tepehan G G 1999 *Electrochim. Acta* **44** 3127
[16] Jia N Q, Zhou Q, Liu L, Yan M M, and Jiang Z Y 2005 *J. Electroanal. Chem*. **580** 213
[17] Wang J 1999 *Anal. Chim. Acta* **399** 21-27
[18] Lev O, Wu Z, Bharathi S, Glezer V, Modestov A, Gun J, Rabinovich L and Sampath S 1997 *Chem. Mater*. **9** 2354-237
[19] **Ali A,** Ansari A A, Kaushik A, Solanki P R, Barik A, Pandey M K and Malhotra B D 2009 *Materials Letters* **63** 2473-2475
[20] Cho W-J and Huang H-J 1998 *Anal. Chem.* **70** 3946-395
[21] Vostiar I, Tkac J, Sturdik E and Gemeiner P 2002 *Bioelectrochemistry* **56** 113 – 115
[22] Saha S, Arya S K, Singh S P, Sreenivas K, Malhotra B D and Gupta V 2009 *Biosen. & Bioelectron.* **24** 2040-2045
[23] Feng K J, Yang Y H, Wang Z J, Jiang J H, Shen G L and Yu R Q 2006 *Talanta* **70** 561

Acknowledgements

We thank the Director, NPL, New Delhi, India for the facilities. Financial support received under the DBT project GAP-070832, DST project GAP- 070932 and in-house project OLP-070632D is gratefully acknowledged.

Estimates for the Initial Coefficients of Bi-univalent Functions

[1]S. SIVAPRASAD KUMAR, [2]VIRENDRA KUMAR AND [3]V. RAVICHANDRAN
[1,2]Department of Applied Mathematics, Delhi Technological University, Delhi—110042, India
[3]School of Mathematical Sciences, Universiti Sains Malaysia, 11800 USM, Penang, Malaysia
[3]Department of Mathematics, University of Delhi, Delhi—110007, India
[1]spkumar@dce.ac.in, [2]vktmaths@yahoo.in, [3]vravi@maths.du.ac.in

Abstract. A bi-univalent function is a univalent function defined on the unit disk with its inverse also univalent on the unit disk. Estimates for the initial coefficients are obtained for bi-univalent functions belonging to certain classes defined by subordination and relevant connections with earlier results are pointed out.

2010 Mathematics Subject Classification: 30C45, 30C80

Keywords and phrases: Univalent functions, bi-univalent functions, coefficient estimate, subordination.

1. Introduction

Let $\mathcal{A}$ be the class of analytic functions defined on the open unit disk $\mathbb{D} := \{z \in \mathbb{C} : |z| < 1\}$ and normalized by the conditions $f(0) = 0$ and $f'(0) = 1$. A function $f \in \mathcal{A}$ has Taylor's series expansion of the form

$$f(z) = z + \sum_{n=2}^{\infty} a_n z^n. \tag{1.1}$$

An analytic function is *univalent* in a domain $D \subset \mathbb{C}$ if it is one-to-one in D. The class of all univalent functions in the open unit disk $\mathbb{D}$ of the form (1.1) is denoted by $\mathcal{S}$. Determination of the bounds for the coefficients a_n is an important problem in geometric function theory as they give information about the geometric properties of these functions. For example, the bound for the second coefficient a_2 of functions in $\mathcal{S}$ gives the growth and distortion bounds as well as covering theorems. Some coefficient related problems were investigated recently in [1, 3, 8, 9, 15, 17].

Since univalent functions are one-to-one, they are invertible and the inverse functions need not be defined on the entire unit disk $\mathbb{D}$. However, the famous Koebe one-quarter theorem ensures that the image of the unit disk $\mathbb{D}$ under every function $f \in \mathcal{S}$ contains a disk of radius $1/4$. Thus, the inverse of every function $f \in \mathcal{S}$ is defined on some disk containing the disk $|z| < 1/4$. It can also be easily verified that

$$f^{-1}(w) = w - a_2 w^2 + (2a_2^2 - a_3)w^3 - (5a_2^2 - 5a_2 a_3 + a_4)w^4 + \cdots \tag{1.2}$$

in some disk of radius at least 1/4. The function $f \in \mathcal{A}$ is *bi-univalent* in $\mathbb{D}$ if both f and f^{-1} are univalent in $\mathbb{D}$. In 1967, Lewin [14] introduced the class σ of bi-univalent analytic functions and showed that the second coefficient of every $f \in \sigma$ satisfy the inequality $|a_2| \leq 1.51$. Let σ_1 be the class of all functions $f = \phi \circ \psi^{-1}$ where ϕ, ψ map $\mathbb{D}$ onto domain containing $\mathbb{D}$ and $\phi'(0) = \psi'(0)$. In 1969, Suffridge [22] gave a function in $\sigma_1 \subset \sigma$ satisfying $a_2 = 4/3$ and conjectured that $|a_2| \leq 4/3$ for all functions in σ. Netanyahu [16] in 1969 proved this conjecture for the subclass of σ_1. Later in 1981, Styer and Wright [21] disproved the conjecture of Suffridge [22] by showing $a_2 > 4/3$ for some function in σ. See [4] also for an

example to show $\sigma \neq \sigma_1$. For results on bi-univalent polynomial, see [13,18]. Branan [5] in 1967 conjectured that $|a_2| \leq \sqrt{2}$ for $f \in \sigma$. Kedzierawski [12, Theorem 2] in 1985 proved this conjecture for a special case when the function f and f^{-1} are starlike functions. The best known bound $|a_2| \leq 1.485$ is proved by Tan [23]. For some open problems and survey, see [11, 19].

For $0 \leq \alpha < 1$, a function $f \in \sigma$ is in the class $\mathcal{S}^*_\sigma(\alpha)$ of *bi-starlike function of order* α, or $\mathcal{K}_\sigma(\alpha)$ of *bi-convex function of order* α if both f and f^{-1} are respectively starlike or convex functions of order α. For $0 < \alpha \leq 1$, the function $f \in \sigma$ is *strongly bi-starlike function of order* α if both the functions f and f^{-1} are strongly starlike functions of order α. The class of all such functions is denoted by $\mathcal{S}^*_{\sigma,\alpha}$. These classes were introduced by Branan and Taha [7] in 1985 (see also [6]). They obtained estimates on the initial coefficients a_2 and a_3 for functions in these classes. Recently, Ali *et al.* [2] extended the results of Branan and Taha [7] by generalizing their classes using subordination. For some related results for special cases, see [10, 20, 24]. Recall that an analytic function f is *subordinate* to an analytic function g, written $f \prec g$, if there is an analytic function w with $|w(z)| \leq |z|$ such that $f = g \circ w$. If g is univalent, then $f \prec g$ if and only if $f(0) = g(0)$ and $f(\mathbb{D}) \subseteq g(\mathbb{D})$. For the various applications of subordination one can refer to [1, 3, 9, 15, 17] and the references cited therein.

Throughout this paper, we assume that φ is an analytic univalent function with positive real part in $\mathbb{D}$, $\varphi(\mathbb{D})$ is symmetric with respect to the real axis and starlike with respect to $\varphi(0) = 1$, and $\varphi'(0) > 0$. The Taylor's series expansion of such function is of the form

$$\varphi(z) = 1 + B_1 z + B_2 z^2 + B_3 z^3 + \cdots \text{ with } B_1 > 0. \tag{1.3}$$

With this assumption on φ, we now introduce a class of functions investigated in the paper.

Definition 1.1. *Let $\lambda \geq 0$. A function $f \in \sigma$ given by (1.1) is in the class $\mathcal{R}_\sigma(\lambda, \varphi)$, if it satisfies*

$$(1-\lambda)\frac{f(z)}{z} + \lambda f'(z) \prec \varphi(z) \quad \text{and} \quad (1-\lambda)\frac{F(w)}{w} + \lambda F'(w) \prec \varphi(w), \quad (F = f^{-1}).$$

The class $\mathcal{R}_\sigma(\lambda, \varphi)$ includes many earlier classes, which are mentioned below:

(1) $\mathcal{R}_\sigma(\lambda, (1+(1-2\beta)z)/(1-z)) = \mathcal{R}_\sigma(\lambda, \beta)$ $(\lambda \geq 1;\ 0 \leq \beta < 1)$ [10, Definition 3.1]
(2) $\mathcal{R}_\sigma(\lambda, ((1+z)/(1-z))^\alpha) = \mathcal{R}_{\sigma,\alpha}(\lambda)$ $(\lambda \geq 1;\ 0 < \alpha \leq 1)$ [10, Definition 2.1]
(3) $\mathcal{R}_\sigma(1, \varphi) = \mathcal{R}_\sigma(\varphi)$ [2, p. 345].
(4) $\mathcal{R}_\sigma(1, (1+(1-2\beta)z)/(1-z)) = \mathcal{R}_\sigma(\beta)$ $(0 \leq \beta < 1)$ [20, Definition 2]
(5) $\mathcal{R}_\sigma(1, ((1+z)/(1-z))^\alpha) = \mathcal{R}_{\sigma,\alpha}$ $(0 < \alpha \leq 1)$ [20, Definition 1]

Motivated by Ali *et al.* [2], we investigate the estimates for the initial coefficients a_2 and a_3 of bi-univalent functions belonging to the class $\mathcal{R}_\sigma(\lambda, \varphi)$ introduced above as well as to the classes $\mathcal{S}^\lambda_\sigma(\varphi)$ and $N^\lambda_{\sigma,\gamma}(\varphi)$ defined later. We also obtain an estimate for a_4 for functions belongs to $\mathcal{R}_\sigma(\lambda, \varphi)$. Our results generalize several well-known results in [2, 10, 20] and these are pointed out.

2. Coefficient estimates

Our first result provides estimates for the coefficients a_2, a_3 and a_4 for functions belonging to the class $\mathcal{R}_\sigma(\lambda, \varphi)$.

Theorem 2.1. *If $f \in \mathscr{R}_\sigma(\lambda,\varphi)$, then*

$$|a_2| \le \frac{B_1\sqrt{B_1}}{\sqrt{|(1+2\lambda)B_1^2+(1+\lambda)^2(B_1-B_2)|}}, \tag{2.1}$$

$$|a_3| \le \frac{B_1^2}{(1+\lambda)^2}+\frac{B_1}{1+2\lambda} \tag{2.2}$$

and

$$|a_4| \le \frac{3B_1+2|B_2|+|B_3|}{1+3\lambda}. \tag{2.3}$$

Proof. Since $f \in \mathscr{R}_\sigma(\lambda,\varphi)$, there exists two analytic functions $r,s:\mathbb{D}\to\mathbb{D}$, with $r(0)=0=s(0)$, such that

$$(1-\lambda)\frac{f(z)}{z}+\lambda f'(z)=\varphi(r(z)) \text{ and } (1-\lambda)\frac{F(w)}{w}+\lambda F'(w)=\varphi(s(z)). \tag{2.4}$$

Define the functions p and q by

$$p(z)=\frac{1+r(z)}{1-r(z)}=1+p_1z+p_2z^2+p_3z^3+\cdots \text{ and } q(z)=\frac{1+s(z)}{1-s(z)}=1+q_1z+q_2z^2+q_3z^3+\cdots, \tag{2.5}$$

or equivalently,

$$r(z)=\frac{p(z)-1}{p(z)+1}=\frac{1}{2}\left(p_1z+\left(p_2-\frac{p_1^2}{2}\right)z^2+\left(p_3+\frac{p_1}{2}\left(\frac{p_1^2}{2}-p_2\right)-\frac{p_1p_2}{2}\right)z^3+\cdots\right) \tag{2.6}$$

and

$$s(z)=\frac{q(z)-1}{q(z)+1}=\frac{1}{2}\left(q_1z+\left(q_2-\frac{q_1^2}{2}\right)z^2+\left(q_3+\frac{q_1}{2}\left(\frac{q_1^2}{2}-q_2\right)-\frac{q_1q_2}{2}\right)z^3+\cdots\right). \tag{2.7}$$

It is clear that p and q are analytic in $\mathbb{D}$ and $p(0)=1=q(0)$. Also p and q have positive real part in $\mathbb{D}$, and hence $|p_i|\le 2$ and $|q_i|\le 2$. In the view of (2.4), (2.6) and (2.7), clearly

$$(1-\lambda)\frac{f(z)}{z}+\lambda f'(z)=\varphi\left(\frac{p(z)-1}{p(z)+1}\right) \text{ and } (1-\lambda)\frac{F(w)}{w}+\lambda F'(w)=\varphi\left(\frac{q(w)-1}{q(w)+1}\right). \tag{2.8}$$

Using (2.6) and (2.7) together with (1.3), it is evident that

$$\begin{aligned}\varphi\left(\frac{p(z)-1}{p(z)+1}\right)&=1+\frac{1}{2}B_1p_1z+\left(\frac{1}{2}B_1\left(p_2-\frac{1}{2}p_1^2\right)+\frac{1}{4}B_2p_1^2\right)z^2\\&\quad+\left(\frac{B_1}{2}\left(2p_3+p_1\left(\frac{p_1^2}{2}-p_2\right)-p_1p_2\right)+\frac{B_2p_1}{2}\left(p_2-\frac{p_1^2}{2}\right)+\frac{B_3p_1^3}{8}\right)z^3+\cdots.\end{aligned} \tag{2.9}$$

and

$$\begin{aligned}\varphi\left(\frac{q(w)-1}{q(w)+1}\right)&=1+\frac{1}{2}B_1q_1w+\left(\frac{1}{2}B_1\left(q_2-\frac{1}{2}q_1^2\right)+\frac{1}{4}B_2q_1^2\right)w^2\\&\quad+\left(\frac{B_1}{2}\left(2q_3+q_1\left(\frac{q_1^2}{2}-q_2\right)-q_1q_2\right)+\frac{B_2q_1}{2}\left(q_2-\frac{q_1^2}{2}\right)+\frac{B_3q_1^3}{8}\right)w^3+\cdots.\end{aligned} \tag{2.10}$$

Since $f \in \sigma$ has the Maclaurin series given by (1.1), a computation shows that its inverse $F = f^{-1}$ has the expansion given by (1.2). It follows from (2.8), (2.9) and (2.10) that

$$(1+\lambda)a_2 = \frac{1}{2}B_1 p_1, \tag{2.11}$$

$$(1+2\lambda)a_3 = \frac{1}{2}B_1\Big(p_2 - \frac{1}{2}p_1^2\Big) + \frac{1}{4}B_2 p_1^2, \tag{2.12}$$

$$(1+3\lambda)a_4 = \frac{B_1}{2}\left(2p_3 + p_1\Big(\frac{p_1^2}{2} - p_2\Big) - p_1p_2\right) + \frac{B_2p_1}{2}\left(p_2 - \frac{p_1^2}{2}\right) + \frac{B_3p_1^3}{8}, \tag{2.13}$$

$$-(1+\lambda)a_2 = \frac{1}{2}B_1 q_1, \tag{2.14}$$

$$(1+2\lambda)(2a_2^2 - a_3) = \frac{1}{2}B_1\left(q_2 - \frac{1}{2}q_1^2\right) + \frac{1}{4}B_2 q_1^2 \tag{2.15}$$

and

$$\begin{aligned} -(1+3\lambda)(5a_2^2 - 5a_2a_3 + a_4) = {} & \frac{B_1}{2}\left(2q_3 + q_1\Big(\frac{q_1^2}{2} - q_2\Big) - q_1q_2\right) \\ & + \frac{B_2q_1}{2}\left(q_2 - \frac{q_1^2}{2}\right) + \frac{B_3q_1^3}{8}. \end{aligned} \tag{2.16}$$

From (2.11) and (2.14), it follows that

$$p_1 = -q_1 \tag{2.17}$$

and

$$8(1+2\lambda)^2a_2^2 = B_1^2(p_1^2 + q_1^2). \tag{2.18}$$

Now (2.12), (2.15) and (2.18) yield

$$a_2^2 = \frac{(p_2+q_2)B_1^3}{4[(1+2\lambda)B_1^2 + (1+\lambda)^2(B_1 - B_2)]}. \tag{2.19}$$

Thus the desired estimate on $|a_2|$ as asserted in (2.1), follows at once using the fact that $|p_2| \leq 2$ and $|q_2| \leq 2$.

By subtracting (2.12) from (2.15) and a computation using (2.19) and (2.11) finally lead to

$$a_3 = \frac{B_1^2p_1^2}{4(1+\lambda)^2} + \frac{(q_2-p_2)B_1}{4(1+2\lambda)},$$

which in turn yields the estimate given in (2.2).

By adding (2.13) and (2.16) and a computation using (2.19) leads to

$$-5(1+3\lambda)(a_2^2 - a_2a_3) = \frac{B_1}{2}(p_3+q_3) - \frac{B_1}{2}(p_1p_2 - q_1q_2) + \frac{B_2}{2}(p_1p_2 + q_1q_2). \tag{2.20}$$

Now subtracting (2.16) from (2.13), will yield

$$\begin{aligned} 5(1+3\lambda)(a_2^2 - a_2a_3) + 2(1+3\lambda)a_4 = {} & B_1(p_3 - q_3) + \frac{B_1}{4}(-2p_1p_2 + 2q_1q_2 + p_1^3) \\ & + \frac{B_2}{2}(2p_1p_2 + 2q_1q_2 - p_1^3) + \frac{B_3p_1^3}{4}. \end{aligned} \tag{2.21}$$

Again the equations (2.20) and (2.21) lead to

$$2(1+3\lambda)a_4 = B_1p_3 + \frac{B_1}{4}(-4p_1p_2+p_1^3) - \frac{B_2}{2}(2p_1p_2-p_1^3) + \frac{B_3p_1^3}{4}. \tag{2.22}$$

Now the equation (2.22) can be rewritten as

$$\begin{aligned} 2(1+3\lambda)a_4 = B_1p_3 + \frac{B_1}{4}\left(-2p_1p_2 + 2p_1\Big(\frac{p_1^2}{2}-p_2\Big)\right) \\ - B_2p_1\Big(p_2-\frac{p_1^2}{2}\Big) + \frac{B_3p_1^3}{4}. \end{aligned} \tag{2.23}$$

Finally an application of the known result,

$$|p_i| \le 2 \quad \text{and} \quad \left|p_2 - \frac{p_1^2}{2}\right| \le 2 - \frac{|p_1|^2}{2} \le 2$$

in (2.23), yields the desired estimate given by (2.3) for a_4. ∎

Remark 2.1. For $\lambda = 1$, Theorem 2.1 reduces to a result of Ali *et al.* [2, Theorem 2.1].

For $\varphi(z) = (1+Cz)/(1+Dz)$, $-1 \le D < C \le 1$, Theorem 2.1 leads to the following result:

Corollary 2.1. *Let $-1 \le D < C \le 1$. If $f \in \mathscr{R}_\sigma(\lambda, (1+Cz)/(1+Dz))$, then*

$$|a_2| \le \frac{C-D}{\sqrt{(1+2\lambda)(C-D)+(1+\lambda)^2(1+D)}},$$
$$|a_3| \le \frac{(C-D)^2}{(1+\lambda)^2} + \frac{C-D}{1+2\lambda}, \quad \textit{and} \quad |a_4| \le \frac{(C-D)(3+2|D|+D^2)}{1+3\lambda}.$$

For $C = 1-2\beta$ with $0 \le \beta < 1$ and $D = -1$, Corollary 2.1 reduces to the following result [10, Theorem 3.1], as well as it gives an estimate for $|a_4|$.

Example 2.1. Let $0 \le \beta < 1$ and $\lambda \ge 0$. If $f \in \mathscr{R}_\sigma(\lambda, \beta)$, then

$$|a_2| \le \sqrt{\frac{2(1-\beta)}{1+2\lambda}}, \quad |a_3| \le \frac{4(1-\beta)^2}{(1+\lambda)^2} + \frac{2(1-\beta)}{1+2\lambda}, \quad \text{and} \quad |a_4| \le \frac{12(1-\beta)}{1+3\lambda}.$$

For $\lambda = 1$ and $\varphi(z) = (1+z)/(1-z)$, Theorem 2.1 gives the following coefficient estimates for $f \in \mathscr{R}_\sigma(0)$:

$$|a_2| \le \sqrt{\frac{2}{3}} \approx 0.816, \ |a_3| \le \frac{5}{3} \approx 1.667 \text{ and } |a_4| \le 3.$$

Since the estimate on $|a_2|$ for $f \in \mathscr{R}_\sigma(0)$ is improved over the conjectured estimate $|a_2| \le \sqrt{2} \approx 1.414$ for $f \in \sigma$, the functions in $\mathscr{R}_\sigma(0)$ are not the candidate for the sharpness of the estimate in σ.

When $\varphi(z) = ((1+z)/(1-z))^\alpha$, $0 < \alpha \le 1$ in Theorem 2.1, we get the following corollary. The estimates for a_2 and a_3 is the same as [10, Theorem 2.1] while the estimate for $|a_4|$ is new.

Corollary 2.2. *Let $0 < \alpha \le 1$ and $\lambda \ge 0$. If $f \in \mathscr{R}_\sigma(\lambda, \alpha)$, then*

$$|a_2| \le \frac{2\alpha}{\sqrt{(1+\lambda)^2+\alpha(1+2\lambda-\lambda^2)}},$$

$$|a_3| \leq \frac{4\alpha^2}{(1+\lambda)^2} + \frac{2\alpha}{1+2\lambda}, \quad \textit{and} \quad |a_4| \leq \frac{4\alpha(\alpha^2+3\alpha+5)}{3(1+3\lambda)}.$$

Definition 2.1. *Let $\lambda \geq 0$. A function $f \in \sigma$ is in the class $\mathscr{S}_\sigma^\lambda(\varphi)$, if it satisfies*

$$\left(\frac{f(z)}{z}\right)^{\lambda-1} f'(z) \prec \varphi(z) \quad \textit{and} \quad \left(\frac{F(w)}{w}\right)^{\lambda-1} F'(w) \prec \varphi(w) \quad (F = f^{-1}).$$

Note that for a suitable choice of λ and φ, the class $\mathscr{S}_\sigma^\lambda(\varphi)$, reduces to the following known classes:

(1) $\mathscr{S}_\sigma^0((1+(1-2\beta)z)/(1-z)) = \mathscr{S}_\sigma^*(\beta) \quad (0 \leq \beta < 1)$.
(2) $\mathscr{S}_\sigma^0(((1+z)/(1-z))^\alpha) = \mathscr{S}_{\sigma,\alpha}^* \quad (0 < \alpha \leq 1)$.
(3) $\mathscr{S}_\sigma^1((1+(1-2\beta)z)/(1-z)) = \mathscr{R}_\sigma(\beta) \quad (0 \leq \beta < 1)$.
(4) $\mathscr{S}_\sigma^1(((1+z)/(1-z))^\alpha) = \mathscr{R}_{\sigma,\alpha}^* \quad (0 < \alpha \leq 1)$.

Theorem 2.2. *If $f \in \mathscr{S}_\sigma^\lambda(\varphi)$, then*

$$|a_2| \leq \frac{\sqrt{2B_1}B_1}{\sqrt{|(\lambda^2+3\lambda+2)B_1^2 + 2(\lambda+1)^2(B_1-B_2)|}} \tag{2.24}$$

and

$$|a_3| \leq \frac{2(B_1+|B_2-B_1|)}{\lambda^2+3\lambda+2}. \tag{2.25}$$

Proof. Since $f \in \mathscr{S}_\sigma^\lambda(\varphi)$, there are analytic functions $r,s : \mathbb{D} \to \mathbb{D}$, with $r(0) = s(0) = 0$, satisfying

$$\left(\frac{f(z)}{z}\right)^{\lambda-1} f'(z) = \varphi(r(z)) \text{ and } \left(\frac{F(w)}{w}\right)^{\lambda-1} F'(w) = \varphi(s(z)). \tag{2.26}$$

Let p and q be defined as in (2.5), then it is clear from (2.26), (2.6) and (2.7) that

$$\left(\frac{f(z)}{z}\right)^{\lambda-1} f'(z) = \varphi\left(\frac{p(z)-1}{p(z)+1}\right) \text{ and } \left(\frac{F(w)}{w}\right)^{\lambda-1} F'(w) = \varphi\left(\frac{q(z)-1}{q(z)+1}\right). \tag{2.27}$$

It follows from (2.27), (2.9) and (2.10) that

$$(1+\lambda)a_2 = \frac{1}{2}B_1 p_1, \tag{2.28}$$

$$-\frac{(1-\lambda)(\lambda+2)}{2}a_2^2 + (\lambda+2)a_3 = \frac{1}{2}B_1\left(p_2 - \frac{1}{2}p_1^2\right) + \frac{1}{4}B_2 p_1^2, \tag{2.29}$$

$$-(1+\lambda)a_2 = \frac{1}{2}B_1 q_1 \tag{2.30}$$

and

$$\frac{(\lambda+2)(\lambda+3)}{2}a_2^2 - (\lambda+2)a_3 = \frac{1}{2}B_1\left(q_2 - \frac{1}{2}q_1^2\right) + \frac{1}{4}B_2 q_1^2. \tag{2.31}$$

The equations (2.28) and (2.30) yield

$$p_1 = -q_1 \tag{2.32}$$

and

$$2(1+\lambda)^2 a_2 = \frac{1}{4}B_1^2(p_1^2+q_1^2). \tag{2.33}$$

From (2.29), (2.31), (2.32) and (2.33), it follows that

$$a_2^2 = \frac{B_1^3(p_1^2+q_1^2)}{2[(\lambda^2+3\lambda+2)B_1^2+2(B_1-B_2)(\lambda+1)^2]}, \tag{2.34}$$

which yields the desired estimate on $|a_2|$ as described in (2.24). Similarly, it can be obtained from (2.29), (2.31) and (2.32) that

$$a_3 = \frac{B_1(p_2(\lambda+3)+q_2(1-\lambda))+2(B_2-B_1)p_1^2}{4(\lambda^2+3\lambda+2)},$$

which eventually leads to the desired estimate (2.25) on a_3. ∎

Remark 2.2. If $\lambda = 0$, then the Theorem 2.2 reduces to [2, Corollary 2.1] and when $\varphi(z) = (1+(1-2\beta)z)/(1-z)$ $(0 \le \beta < 1)$, it reduces to [7, Theorem 3.1] .

Definition 2.2. *Let $0 \neq \gamma \in \mathbb{C}$ and $\lambda \ge 0$. A function f given by (1.1) is said to be in the class $N_{\sigma,\gamma}^{\lambda}(\varphi)$, if f and $F = f^{-1}$ satisfy the subordinations*

$$1+\frac{1}{\gamma}\left(\frac{zf'(z)+\lambda z^2 f''(z)}{\lambda z f'(z)+(1-\lambda)f(z)}-1\right) \prec \varphi(z)$$

and

$$1+\frac{1}{\gamma}\left(\frac{wF'(w)+\lambda w^2 F''(w)}{\lambda wF'(w)+(1-\lambda)F(w)}-1\right) \prec \varphi(w).$$

Note that by choosing appropriate values for λ and γ, the class $N_{\gamma}^{\lambda}(\varphi)$ reduces to different classes:

(1) $N_{\sigma,1}^{0}((1+(1-2\beta)z)/(1-z))) = \mathscr{S}_{\sigma}^{*}(\beta) \quad (0 \le \beta < 1)$.
(2) $N_{\sigma,1}^{1}(((1+(1-2\beta)z)/(1-z))) = \mathscr{K}_{\sigma}(\beta) \quad (0 \le \beta < 1)$.
(3) $N_{\sigma,1}^{0}(((1+z)/(1-z))^{\delta}) = \mathscr{S}_{\sigma,\delta}^{*} \quad (0 < \delta \le 1)$.

Theorem 2.3. *If $f \in N_{\sigma,\gamma}^{\lambda}(\varphi)$, then*

$$|a_2| \le \frac{|\gamma|B_1\sqrt{B_1}}{\sqrt{|(1+2\lambda-\lambda^2)B_1^2\gamma^2+(1+\lambda)^2(B_1-B_2)|}} \quad \textit{and} \quad |a_3| \le \frac{|\gamma|(B_1+|B_2-B_1|)}{|1+2\lambda-\lambda^2|}.$$

The proof is omitted as it is similar to the proof of Theorem 2.2.

Remark 2.3. If we set $\gamma = 1$ and $\varphi(z) = (1+(1-2\beta)z)/(1-z)$ $(0 \le \beta < 1)$ in Theorem 2.3, then for $\lambda = 0$ and $\lambda = 1$, it respectively reduces to [7, Theorem 3.1] and [7, Theorem 4.1].

References

[1] R. M. Ali, N. E. Cho, N. Jain and V. Ravichandran, Radii of starlikeness and convexity of functions defined by subordination with fixed second coefficients, Filomat, accepted

[2] R. M. Ali, S. K. Lee, V. Ravichandran and S. Supramaniam, Cofficient estimates for bi-univalent function Ma-Minda starlike and convex functions, Appl. Math. Lett., **25** (2012), 344–351.

[3] R. M. Ali, S. Nagpal and V. Ravichandran, Second-order differential subordination for analytic functions with fixed initial coefficient, Bull. Malays. Math. Sci. Soc. (2) **34** (2011), no. 3, 611–629.

[4] D. Bshouty, W. Hengartner and G. Schober, Estimates for the Koebe constant and the second coefficient for some classes of univalent functions, Canad. J. Math. **32** (1980), no. 6, 1311–1324.
[5] A. Brannan and J. G. Clunie, Aspects of contemporary complex analysis Proceedings of the NATO Advanced Study Institute held at the University of Durham, Durham, July 120, 1979, Academic Press New York, London, 1980.
[6] D. A. Brannan and T. S. Taha, On some classes of bi-univalent functions, in *Mathematical analysis and its applications (Kuwait, 1985)*, 53–60, KFAS Proc. Ser., 3 Pergamon, Oxford.
[7] D. A. Brannan and T. S. Taha, On some classes of bi-univalent functions, Studia Univ. Babeş-Bolyai Math. **31** (1986), no. 2, 70–77.
[8] Sh. Chen, S. Ponnusamy and X. Wang, Coefficient estimates and Landau-Bloch's constant for planar harmonic mappings, Bull. Malays. Math. Sci. Soc. (2) **34** (2011), no. 2, 255–265.
[9] N. E. Cho and O. S. Kwon, A class of integral operators preserving subordination and superordination, Bull. Malays. Math. Sci. Soc. (2) **33** (2010), no. 3, 429–437.
[10] B. A. Frasin and M. K. Aouf, New subclasses of bi-univalent functions, Appl. Math. Lett. **24** (2011), no. 9, 1569–1573.
[11] A. W. Goodman, An invitation to the study of univalent and multivalent functions, Internat. J. Math. Math. Sci. **2** (1979), no. 2, 163–186.
[12] A. W. Kedzierawski, Some remarks on bi-univalent functions, Ann. Univ. Mariae Curie-Skłodowska Sect. A **39** (1985), 77–81 (1988).
[13] A. Kedzierawski and J. Waniurski, Bi-univalent polynomials of small degree, Complex Variables Theory Appl. **10** (1988), no. 2-3, 97–100.
[14] M. Lewin, On a coefficient problem for bi-univalent functions, Proc. Amer. Math. Soc. **18** (1967), 63–68.
[15] J.-L. Liu, Certain sufficient conditions for strongly starlike functions associated with an integral operator, Bull. Malays. Math. Sci. Soc. (2) **34** (2011), no. 1, 21–30.
[16] E. Netanyahu, The minimal distance of the image boundary from the origin and the second coefficient of a univalent function in $|z| < 1$, Arch. Rational Mech. Anal. **32** (1969), 100–112.
[17] S. Supramaniam, R.M. Ali, S. K. Lee and V. Ravichandran, Convolution and differential subordination for multivalent functions, Bull. Malays. Math. Sci. Soc. (2) **32** (2009), no. 3, 351–360.
[18] H. V. Smith, Bi-univalent polynomials, Simon Stevin **50** (1976/77), no. 2, 115–122.
[19] H. V. Smith, Some results/open questions in the theory of bi-univalent functions, J. Inst. Math. Comput. Sci. Math. Ser. **7** (1994), no. 3, 185–195.
[20] H. M. Srivastava, A. K. Mishra and P. Gochhayat, Certain subclasses of analytic and bi-univalent functions, Appl. Math. Lett. **23** (2010), no. 10, 1188–1192.
[21] D. Styer and J. Wright, Result on bi-univalent functions, Proc. Amer. Math. Soc., Vol.82, No 2, 1981, 243–248.
[22] T. J. Suffridge, A coefficient problem for a class of univalent functions, Michigan Math. J. 16(1969), 33-42.
[23] D. L. Tan, Coefficient estimates for bi-univalent functions, Chinese Ann. Math. Ser. A **5** (1984), no. 5, 559–568.
[24] Q.-H. Xu, Y.-C. Gui and H. M. Srivastava, Coefficient estimates for a certain subclass of analytic and bi-univalent functions, Appl. Math. Lett. **25** (2012), 990–994.

Fabrication of nanocrystalline CdS electrode via chemical bath deposition technique for application to cholesterol sensor

2012 J. Phys.: Conf. Ser. 358 012008

(http://iopscience.iop.org/1742-6596/358/1/012008)

Fabrication of nanocrystalline CdS electrode via chemical bath deposition technique for application to cholesterol sensor

Hemant Dhyani[1], Saurabh Srivastava[2], Md. Azahar Ali[2], B.D. Malhotra[2, 3] and Prasenjit Sen[1]

[1] School of Physical Sciences, Jawaharlal Nehru University, New Delhi-110067, India
[2]Department of Science and Technology Centre on Biomolecular Electronics, National Physical Laboratory, Dr. K. S. Krishnan Marg, New Delhi-110012, India
[3]Deapartment of Biotechnology, Delhi Technological University, Shahbad Daulatpur, Main Bawana Road, Delhi, 110042, India

E-mail: "Prasenjit Sen" psen.jnu@gmail.com

Abstract. A nanocystalline CdS electrode has been fabricated by chemical bath deposition (CBD) technique onto hydrolyzed indium tin oxide (ITO) coated glass substrate at 78^0C for the immobilization of cholesterol oxidase (ChOx). The prepared Nano-CdS based electrode has been characterized using UV-visible, X-ray diffraction (XRD), Fourier transform-infrared (FTIR) and scanning electron microscopy (SEM). The ChOx/Nano-CdS/ITO bioelectrode shows the detection range of cholesterol from 50 to 400 mg/dl with improved sensitivity of 1.35 μA/mgdl^{-1}/cm^2, low detection limit (6.1 mg/dl) and low K_m (0.45mM) value indicating strong enzyme (cholesterol oxidase)-matrix (CdS) affinity.

1. Introduction

In recent years semiconductor quantum dots (Qdots) have attracted much interess in the different fields of science due to their unique optical, electronic and electrochemical properties. These properties especially large absorption spectra but narrow emission bands, excellent photostability, high quantum yield and size dependent photoluminescence make them desirable fluorescence probes for the sensing of biological samples [1-4]. Apart from optical sensing, other platforms comprising of quantum dots have recently been explored for the sensing of biological analytes using the electrochemical technique .In this context, it has been reported that the semiconductor Qdots can be used to obtain enhanced charge transfer in enzymatic electrochemical biosensor [5-9]. The Qdots deposited onto desired substrate, have been used for H_2O_2 estimation [10]. Vastarella *et. al.* have fabricated enzyme-core/shell nanoparticle hybrid material and enzyme/semiconductor nanocluster for the amperometric biosensing [11]. Among the various semiconductors Qdots, the CdS nanocrystals have attracted considerable attention due to their good chemical stability, photo-electrochemistry, intrinsic properties of a narrow band gap and excellent electro-catalysts for the sulfide/polysulfide redox couple [12-14]. The good electron transport behavior of CdS quantum dots due to higher charge detaching efficiency [15] and high enzyme affinity to the hexagonal nanocystalline surface area has recently been reported for electrochemical sensing [16,17]. There are several methods to deposit the semiconductor CdS onto a substrate such as electrodeposition, vacuum evaporation, photochemical

[1] To whom any correspondence should be addressed.

deposition, spray pyrolysis, sputtering , Chemical bath deposition (CBD) etc. The CBD technique is an easy process to achieve high quality crystalline films by adjusting the temperature, reagent concentration and pH for large area industrial applications with low cost.

We report results of the studies relating to preparation of nanocystalline CdS film onto indium tin oxide coated glass substrate by chemical bath deposition (CBD) technique for the immobilization of cholesterol oxidase used for cholesterol estimation.

2. Experimental

2.1. Fbrication of the nano-CdS/ITO electrode

The CdS quantum dots have been prepared and deposited simultaneously onto ITO substrate by chemical bath deposition (CBD) technique reported in literature [18] with some modifications. For the synthesis of CdS, 36.60mg cadmium chloride, 152.24mg thiourea and 1.2gm ammonium nitrate are dissolved separately in 10 ml water. After this we dissolved 701.25mg KOH in 25 ml water and then mixed the cadmium chloride and ammonium nitrate with KOH and raised the temperature of the bath at kept at 78^0C with constant stirring. For deposition , the desired area of pre-cleaned ITO substrate is suspended into the bath and mixed with 10 ml solution of thiourea to form CdS. The observed yellowish color indicates formation of nanocrytalline CdS . After about 40 minutes the suspended electrode is taken out, washed with distilled water and stored in a refrigerator.

2.2. Immobilization of ChOx onto nano-CdS/ITO electrode

Cholesterol oxidase is immobilized via physical adsorption onto the surface of prepared Nano-CdS/ITO electrodes. 30 µl of ChOx (1mg/dl) solution is spread onto the Nano-CdS/ITO electrode surface and the electrode is then left inside a humid chamber for about 4h for immobilization of ChOx on electrode surface and stored in 4°C when not in use. The ChOx binds with the CdS quantum dots via electrostatic interaction.

2.3. Instrumentations

Surface morphology and structural properties of electrode (Nano-CdS/ITO) and bioelectrode (ChOx/Nano-CdS/ITO) has been characterized using scanning electron microscopy (SEM, Zeiss EVO 40) and Fourier transform infra-red (FT-IR) spectroscopy (Perkin–Elmer ,model ‘‘Spectrum BX’’ using ATR accessory), UV–visible spectrophotometer (Model 2200DPCV, Phoenix) and X-ray diffraction(PAN alytical X’Pert PRO). Electrochemical investigations (CV and EIS) of the prepared electrodes have been carried out using an Autolab Potentiostat/Galvanostat (Eco Chemie, Netherlands) in a conventional three-electrode electrochemical cell consisting of Ag/AgCl as reference electrode and platinum foil as the counter electrode. Electrochemical impedance spectroscopy (EIS) studies have been performed in the frequency range, 0.01–10^5 Hz with amplitude of 5 mV in PBS solution.

3. Results and discussion

3.1. UV-visible and X-ray diffraction

The UV-visible absorption spectra of the Nano-CdS/ITO electrode is shown in Fig. 1(a). the characteristic absorption peak assigned to the first excitonic state of the CdS electrode is located at 450 nm with the broad range of 425-500 nm. The blue-shift is observed for the absorption band of Nano-CdS as compared to the 520nm of the bulk CdS. This indicates quantum confinement effect and presence of CdS nanoparticles/crystallites in the fabricated electrode[19]. The X-ray diffraction (XRD) pattern of the Nano-CdS/ITO electrode is shown in the Fig.1(b). The XRD pattern indicates polycrystalline nature of the Nano-CdS film deposited onto ITO glass. The CdS exists in two crystallographic forms, hexagonal (Wurtzite) and cubic (Zincblend). The presence of the peaks with 2θ values at 30.55˚, 45.56˚ and 50.93˚ may be associated with cubic planes (111), (220) and (311) or with the hexagonal lattice planes (101), (110) and (200), respectively. The extra peaks seen at 35.80

and 60.6 are due to the ITO substrates. The average grain size (D) of the CdS is found to be as 12 nm, calculated using Scherrer formula $D=0.94\lambda/\beta \cos\theta$, where λ is the X-ray wavelength, β is the full width at half maximum and θ is the Bragg angle.

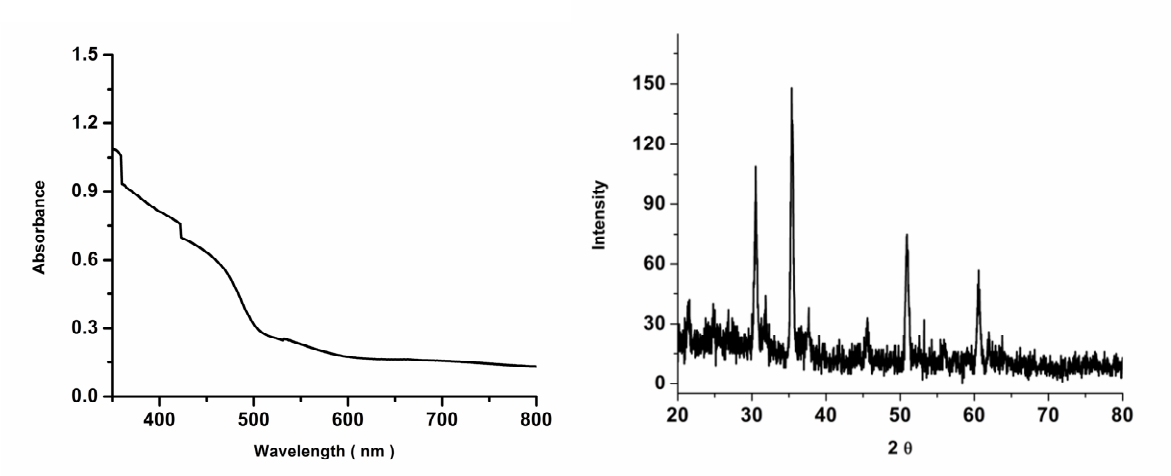

Figure 1. (a) UV-Visible spectra of Nano-CdS/ITO electrode & (b) XRD pattern of Nano-CdS/ITO.

3.2. Scanning electron microscopy studies

The scanning electron micrographs (SEM) of the Nano-CdS/ITO electrode shows the uniform and continuous crystallization during the film formation (Fig. 2(a)). The homogeneous crystalline granular and nanoporous structure of CdS with size distribution of 50- 100 nm can be seen on the ITO surface. The SEM image of the cholesterol oxidase (ChOx) immobilized onto the electrode surface Fig. 2(b) demonstrates the covered and packed granular structure indicating immobilization of ChOx via electrostatic interactions.

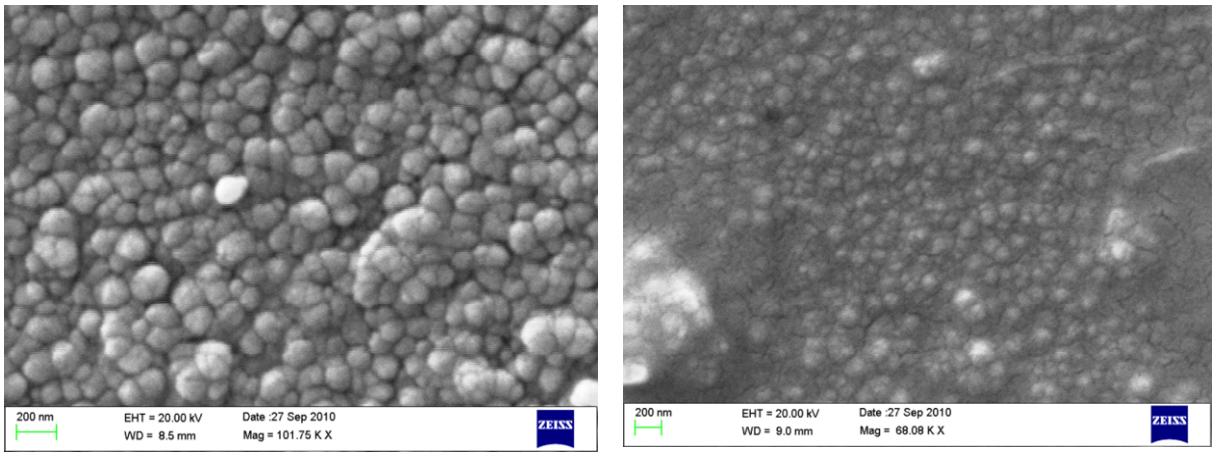

Figure 2. (a) SEM micrograph of Nano-CdS/ITO electrode & (b) ChOx/Nano-CdS/ITO bioelectrode.

3.3. Fourier transform infra-red spectroscopy studies

FT-IR spectra of Nano-CdS/ITO electrode is shown in Fig. 3(a). The peak seen at 671 cm^{-1} in the fingerprint region, corresponds to Cd-S vibrational band. The peaks observed at 1187 cm^{-1} , 1363 cm^{-1} and 1450 cm^{-1} are assigned to O-C=O (symmetric and asymmetric stretching band) due to strong physical absorption of CO_2 and H_2O on the electrode surface. The spectra [Fig. 3(b)] shows the broad

peak at 1100 cm^{-1} confirms the immobilization of ChOx with the peak found at 1630 cm^{-1} is due to amide bonds showing the presence of ChOx[20].

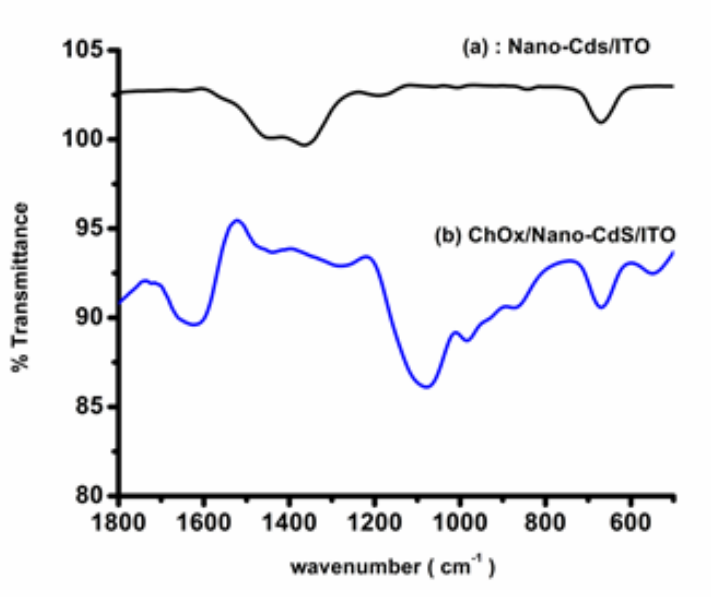

Figure 3. FT-IR spectra of (a) Nano-CdS/ITO electrode and (b) ChOx/Nano-CdS/ITO bioelectrode

3.4. Cyclic voltammetry studies

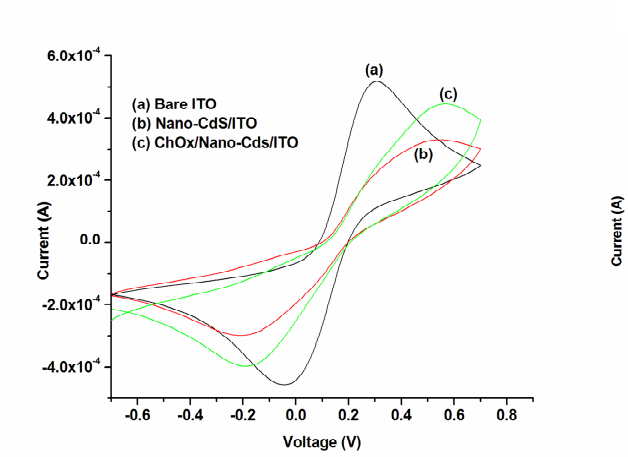

Figure 4. Cyclic Voltammetric (CV) of bare ITO (a), Nano-CdS/ITO electrode (b) and ChOx/Nano-CdS/ITO bioelectrode at scan rate 20 mV/s in PBS (50mM, pH 7.0, 0.9% NaCl) containing $[Fe(CN)_6]^{3-/4-}$ (5mM).

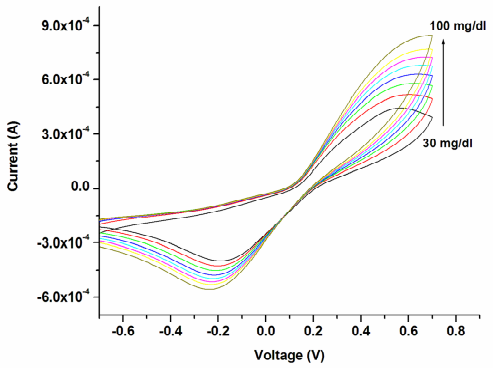

Figure 5. Cyclic Voltammetric (CV) of ChOx/Nano-CdS/ITO bioelectrode at different scan rate 30-100 mV/s in PBS containing $[Fe(CN)_6]^{3-/4-}$ (5mM).

Fig. 4 shows results of cyclic voltammetric (CV) studies conducted on bare ITO (a), Nano-CdS/ITO electrode (b) and ChOx/Nano-CdS/ITO bioelectrode (c) at scan rate 20 mV/s with potential range -7.0V to +7.0V in PBS (50mM, pH 7.0, 0.9% NaCl) containing $[Fe(CN)_6]^{3-/4-}$ (5mM). It can be seen that the magnitude of the peak current for Nano-CdS/ITO electrode (3.29×10^{-4}A) decreases as compared to bare ITO (5.1710^{-4}A) and the peak is shifted toward the higher potential. This is due to

the semiconducting CdS that obstructs the electron transfer between the CdS QDs electrode and the solution. The peak current is found to be higher for ChOx/Nano-CdS/ITO bioelectrode (c) as compared to that of the Nano-CdS/ITO electrode (b) indicating that Nano-CdS quantum dots perhaps act as mediator resulting in enhanced electron transfer between enzyme and electrode.

Fig. 5 shows cyclic voltammogrammes obtained for ChOx/Nano-CdS/ITO bioelectrode in PBS containing $[Fe(CN)_6]^{3-/4-}$ recorded at different scan rates (30–100mVs^{-1}). It can be seen that the anodic potential shifts towards positive side and the cathodic peak potential (Fig.6A) shifts in the reverse direction. The peak-to-peak separation potential ΔE ~0.37 V increases with increasing scan rate resulting in uniform facile charge transfer kinetics. The magnitude of current of both anodic peak (I_a) and cathodic peak (I_c) observed for ChOx/Nano-CdS/ITO bioelectrode increases linearly with the scan rate indicating quasi reversible diffusion controlled behavior. The values of the slope, intercept and correlation coefficient given as

I_a [ChOx/Nano-CdS/ITO]= -1.3μA + 0.8μA (s/mV) × scan rate (mV/s) with r^2=.993 (Eq.1)

I_c[ChOx/Nano-CdS/ITO]= -0.002μA -0.35μA (s/mV) × scan rate (mV/s) with r^2=.998 (Eq.2)

3.5. Cyclic voltammetry studies

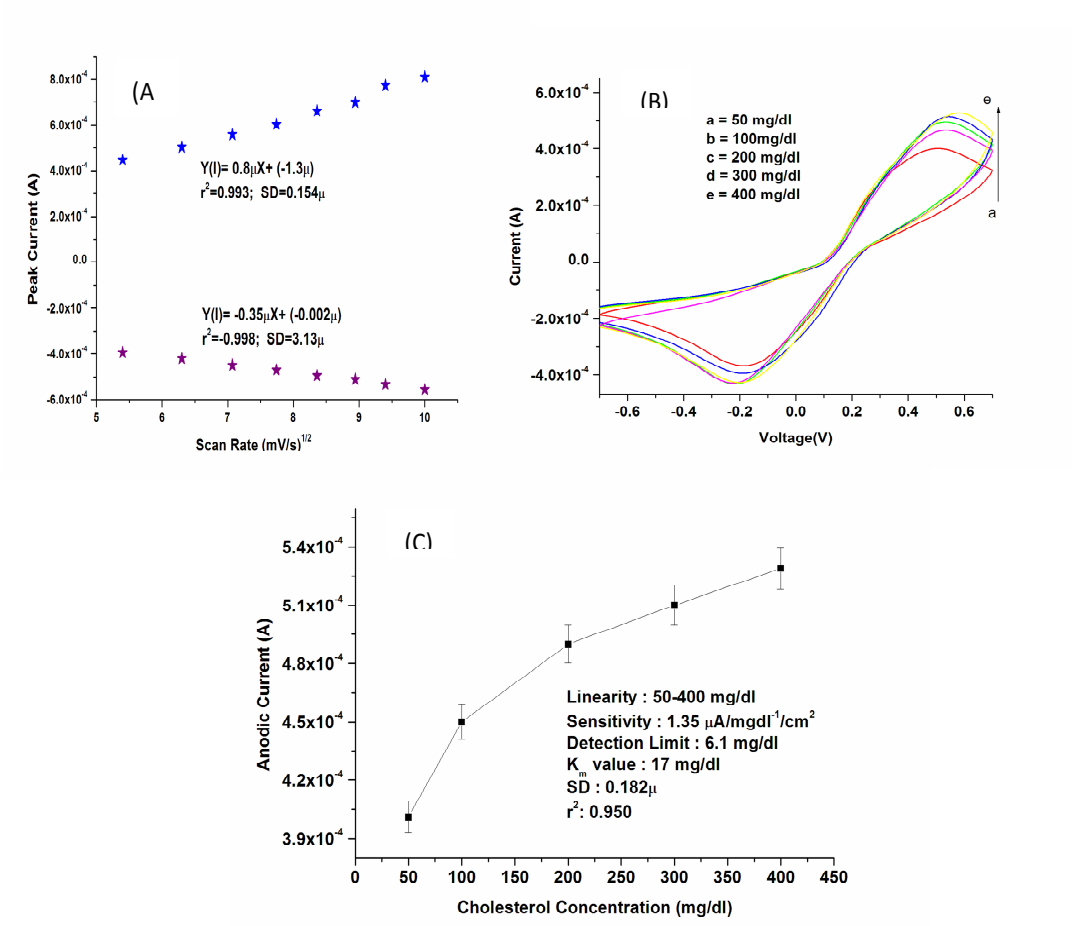

Figure 6. (A) Anodic peak current and cathodic peak current vs square root of scan rate of ChOx/Nano-CdS/ITO bioelectrode from CV studies, (B) CV response at different cholesterol concentration (50-400 mg/dl) at scan rate 20 mV/s in PBS (50mM, pH 7.0, 0.9% NaCl) containing $[Fe(CN)_6]^{3-/4-}$ (5mM) and (C) Sensor response curve plot between current vs cholesterol concentration.

The results of response studies of the ChOx/Nano-CdS/ITO bioelectrode for different cholesterol concentrations in phosphate buffer (50mM, pH 7.0, 0.9% NaCl) containing $[Fe(CN)_6]^{3-/4-}$ are shown in Fig. 6(B). The peak current of CV response increases with adding cholesterol indicating increase in the H_2O_2 concentration produced due to the interaction of ChOx with cholesterol during the biochemical reaction [Fig. 6C]. The ChOx/Nano-CdS/ITO bioelectrode shows linearity as 50–400 $mgdl^{-1}$ and the detection limit as 6.1 mg dl^{-1}. This biosensor shows high sensitivity as 1.35 $\mu A/mgdl^{-1}/cm^2$ with linear regression (r^2) 0.950. The Michaelis–Menten constant (K_m), that gives an indication of the enzyme-substrate kinetics, can be obtained from the Lineweaver–Burke plot . The K_m value for the ChOx/Nano-CdS/ITO bioelectrode has been calculated using the formula 3×SD/m, where SD is standered deviation and m is the slope of the curve and it is found to be 17.0 $mgdl^{-1}$ indicating high affinity for cholesterol.

3.6. Effect of interferents of the ChOx/Nano-CdS/ITO bioelectrode

The effect of interferents (lactic acid, ascorbic acid, uric acid, glucose and urea) on the response of this cholesterol sensor has been evaluated by adding the solution containing (1:1) ratio of cholesterol ($100mgdl^{-1}$) and interferents such as glucose (5 mM), ascorbic acid (0.05 mM), uric acid (0.1 mM), lactic acid (0.5mM) and urea (1 mM) (data not shown). The results indicate negligible effect of these interferents on the CV response of ChOx/Nano-CdS /ITO bioelectrode.

4. Conclusions

We have fabricated the nanocystalline CdS electrode using chemical bath deposition technique. The UV-Visible and X-ray diffraction studies confirms that the quantum confinement effect during the formation of CdS favors its deposition as homogeneous nanocrystals and helps in ChOx loading. FT-IR and SEM studies reveal the successful immobilization of ChOx onto Nano-CdS/ITOelectrode surface. The ChOx/Nano-CdS/ITO bioelectrode exhibits linear range of 50–400 mg/dl and improved sensitivity 1.35 $\mu A/mgdl^{-1}/cm^2$. It has been found that the CdS Qdots based bioelectrode shows the detection limit of 6.1 mg/dl and low K_m(0.45mM) value indicating strong enzyme-matrix affinity. Efforts should be made to control the shape and size of Nano-CdS and to utilize this electrode for estimation of total cholesterol, triglycerides and low density lipoproteins (LDL) etc.

Acknowledgements

The authors thank Director NPL, New Delhi India for providing the facilities. We also thank the Advanced Instrumentation and Research facility (AIRF), JNU, New Delhi for the XRD and SEM analysis. Hemant Dhyani, Saurabh Srivastava and Md. Azahar Ali thank CSIR-India for the award of Senior Research Fellowships.

References

[1] Hu M, Tian J, Lu H T, Weng L and Wang L H 2010 *Talanta* **82** 997-1002
[2] Frasco M F and Chaniotakis N 2009 *Sensors* **9** 7266-7286
[3] Jaiswal J K, Mattoussi H, Mauro J M and Simon S M 2003 *Nat. Biotechnol.* **21** 47-51
[4] Huang S, Xiao Q, Li R, Guan H L, Liu J, Liu X R, He Z K and Liu Y 2009 *Anal. Chim. Acta* 645-78
[5] Du P, Li H, Mei Z and Liu S 2009 *Bioelectrochemistry* **75** 37-43
[6] Liu Q, Lu X, Li L, Yao X and Li J 2007 *Biosens. & Bioelectron.* **22** 3203-3209
[7] Huang Y, Zhang W, Xiao H and Li G 2005 *Biosens. & Bioelectron.* **21** 817-821
[8] Zhao J, Chen G, Zhu L and Li G 2011 *Electro. Commu.* **13** 31-33
[9] Hansen J A, Wang J, Kawde A N, Xiang Y, Gothelf K V and Collin G 2006 *J. Am. Chem. Soc.* **128** 2228–2229
[10] Won Y H, Aboagye D, Jang H S, Jitianu A and Stanciu L A 2010 *J. Mater.Chem*. **20** 5030-5034
[11] Vastarella W and Nicastri R 2005 *Talanta* **66** 627-633
[12] Li Y, Kotzeva V P and Fray D J 2006 *Materials letters* **60** 2743-2746

[13] Prabhakar S, Suryanarayanan N, Rajasekar K, Srikanth S and Kathirvel D 2009 *Chalcogenide Letters* **6** 309-313
[14] Ramaiah K S, Pilkington R D, Hill A E, Tomlinson R D and Bhatnagar A K 2001 *Materials chemistry and physics* **68** 22-30
[15] Liu M, Shi G, Zhang L, Cheng Y and Jin L 2006 *Electrochem. Commu.* **8** 305-310
[16] Dhyani H, Ali A, Pandey M K, Malhotra B D and Sen P 2012 *J. Mater. Chem.* **22** 4970-4976
[17] Wang K, Liu Q, Guan Q M, Wu J, Li H N and Yan J J 2011 *Biosens. & Bioelectron.* **26** 2252-2257
[18] Flores A O, Perez P B, Rodr´ıguez R C and Oliva A I 2006 *Rev. Mex. Fis.* **52** 15–19
[19] Majumdar M, Chakraborty A K and Mallik B 2010 *Journal of Luminescence* **130** 1497-1503
[20] Solanki P, Kaushik A, Ansari A and Malhotra B D 2009 *Appl. Phys. Lett.* **94** 143901

India–Japan Workshop on Biomolecular Electronics & Organic Nanotechnology for Environment Preservation

2012 J. Phys.: Conf. Ser. 358 011001

(http://iopscience.iop.org/1742-6596/358/1/011001)

Preface

The 'India–Japan Workshop on Biomolecular Electronics & Organic Nanotechnology for Environment Preservation' (IJWBME 2011) will be held on 7–10 December 2011 at EGRET Himeji, Himeji, Hyogo, Japan. This workshop was held for the first time on 17–19 December 2009 at NPL, New Delhi. Keeping in mind the importance of organic nanotechnology and biomolecular electronics for environmental preservation and their anticipated impact on the economics of both the developing and the developed world, IJWBME 2009 was jointly organized by the Department of Biological Functions, Graduate School of Life Sciences and Systems Engineering, the Kyushu Institute of Technology (KIT), Kitakyushu, Japan, and the Department of Science & Technology Centre on Biomolecular Electronics (DSTCBE), National Physical Laboratory (NPL).

Much progress in the field of biomolecular electronics and organic nanotechnology for environmental preservation is expected for the 21st Century. Organic optoelectronic devices, such as organic electroluminescent devices, organic thin-film transistors, organic sensors, biological systems and so on have especially attracted much attention. The main purpose of this workshop is to provide an opportunity for researchers interested in biomolecular electronics and organic nanotechnology for environmental preservation, to come together in an informal and friendly atmosphere and exchange technical knowledge and experience. We are sure that this workshop will be very useful and fruitful for all participants in summarizing the recent progress in biomolecular electronics and organic nanotechnology for environmental preservation and preparing new ground for the next generation.

Many papers have been submitted from India and Japan and more than 30 papers have been accepted for presentation. The main topics of interest are as follows:

- Bioelectronics
- Biomolecular Electronics
- Fabrication Techniques
- Self-assembled Monolayers
- Nano-sensors
- Environmental Monitoring
- Organic Devices
- Organic Functional Materials

We would like to express our sincere thanks to the organizing committee members of this workshop and the many organizations such as the Japan Society for the Promotion of Science (JSPS), Japan, the Department of Science & Technology (DST), India, the Society of Organic Nanometric Interfacial Controlled Electronic (NICE) Devices, the Japan Society of Applied Physics, Himeji City, Himeji Convention & Visitors Bureau, Delhi Technological University, Delhi, India and the University of Hyogo for their financial support. Thanks are also given to The Japan Society of Applied Physics, Division of

Molecular Electronics and Bioelectronics, The Japan Society of Applied Physics (M & BE), the Technical Committee on Dielectric and Electrical Insulation Materials of the Institute of Electrical Engineering in Japan (IEEJ), the Technical Group on Organic Molecular Electronics, Electronics Society of the Institute of Electronics, Information and Communication Engineers (IEICE), and the IEEE Dielectrics and Electrical Insulation Society, Japan Chapter, for their cooperation.

Finally, we hope that the many young and active researchers who are participating will enjoy stimulating discussions and exchange ideas with each other at IJWBME 2011, Himeji, Japan.

IJWBME 2011 Chairs
7 April 2011

Mitsuyoshi Onoda
Graduate School of Engineering, University of Hyogo, Himeji, Japan

Bansi D Malhotra
Department of Biotechnology, Delhi Technological University, Delhi, India

Caption: Participants of the India–Japan Workshop on Biomolecular Electronics & Organic Nanotechnology for Environment Preservation 2011, December 7–10 2011, EGRET Himeji, Japan

Japan Society for the Promotion of Science (JSPS), Japan

Department of Science & Technology (DST), India

Centre on Biomolecular Electronics, and Department of Science & Technology National Physical Laboratory (Council of Scientific & Industrial Research) India

Delhi Technological University, India

The Society of Organic NICE Devices
The Japan Society of Applied Physics

University of Hyogo, Japan

Himeji City, Japan

Himeji Convention & Visitors Bureau, Japan

Technical Committee on Dielectric and Electrical Insulation Materials
The Institute of Electrical Engineers of Japan

Division of Molecular Electronics and bioelectronics
The Japan Society of Applied Physics

Technical Group on Organic Molecular Electronics, The Institute of Electronics Information and Communication Engineers

IEE Dielectrics and Electrical Insulation Society Japan Chapter

Opportunities in nano-structured metal oxides based biosensors

2012 J. Phys.: Conf. Ser. 358 012007

(http://iopscience.iop.org/1742-6596/358/1/012007)

Opportunities in nano-structured metal oxides based biosensors

B D Malhotra*[1, 2] Maumita Das[1] and Pratima R Solanki[1]
[1]Department of Science & Technology Centre on Biomolecular Electronics, Biomedical Instrumentation Section, National Physical Laboratory, Dr. K. S. Krishnan Marg, New Delhi 110012, India
[2]Department of Biotechnology, Delhi Technological University, Shahbad Daulatpur, Main Bawana Road, Delhi 110042, India

E-mail: bansi.malhotra@gmail.com or bansi.malhotra@dce.ac.in

Abstract. Nanomaterials are presently at the critical stage of the next technological revolution in solid-state electronics and are emerging as new structural materials, to serve as systems for controlled drug delivery, biomolecular electronics and are considered to have considerable impact in practically all domains of science. Among the various types of nanomaterials that have been developed, nanostructured metal oxides (NSMOs) have recently aroused much interest as immobilizing matrices for biosensors development. The unique properties of NSMOs offer excellent prospects for interfacing biological recognition events with electronic signal transduction and for designing a new generation of bioelectronics devices that may exhibit novel functions. Among the NSMOs, biocompatible zirconia (ZrO_2) and its composite especially with chitosan and carbon nanotubes are technologically important exhibits high bioactivity for biomolecules with rapid rand enhanced electrochemical signal. Efforts are being continuously made to explore the prospects and future challenges of NSMOs for the development of biosensing devices.

1. Introduction

Nano-structured materials can be grouped as (i) inorganic, (ii) organic and (iii) inorganic-organic nanocomposites. Inorganic nanostructures especially nano-structured metal oxides (NSMOs) e.g. iron oxide (Fe_2O_3), zirconium oxide (ZrO_2), zinc oxide (ZnO), nickel oxide (NiO), cerium oxide (CeO_2) silicon dioxide (SiO_2) etc, have opened new opportunities for a plethora of applications due to their unique properties (Figure 1) [7-11]. Electron transport properties of NSMOs are very important for electrical and electronic applications as well as for understanding the unique one-dimensional carrier transport mechanism. Besides this, metal oxide nanoparticles have high thermal stability, chemical inertness, non-toxicity, large surface-to-volume ratio, high surface reaction activity, biocompatibility and tunable electron transport properties. However, these NSMOs are difficult to functionalize that can perhaps be addressed by combining them with organic nanostructures which are otherwise not stable alone, as they interact with the moieties present in the environment. There is, thus a synergic effect between the inorganic and organic nanostructure and these inorganic-organic nanocomposite

* To whom any correspondence should be addressed.

offer excellent prospects for interfacing biological recognition events with electronic signal transduction and for designing new biosensor devices [12-15].

According to IUPAC, a biosensor is a self-contained integral device that is capable of providing specific quantitative or semi-quantitative analytical information using a biological element. Biosensor has three major components: (i) a bio-recognition element such as DNA, enzyme, antibody etc. for recognition of an analyte also called bioreceptor (ii) an immobilization surface such as a nanomaterial/conducting polymer/sol–gel film/self-assembled monolayer, etc., used for the immobilization of a biomolecule and (iii) a transducer for conversion of a biochemical reaction product into a recognizable signal.

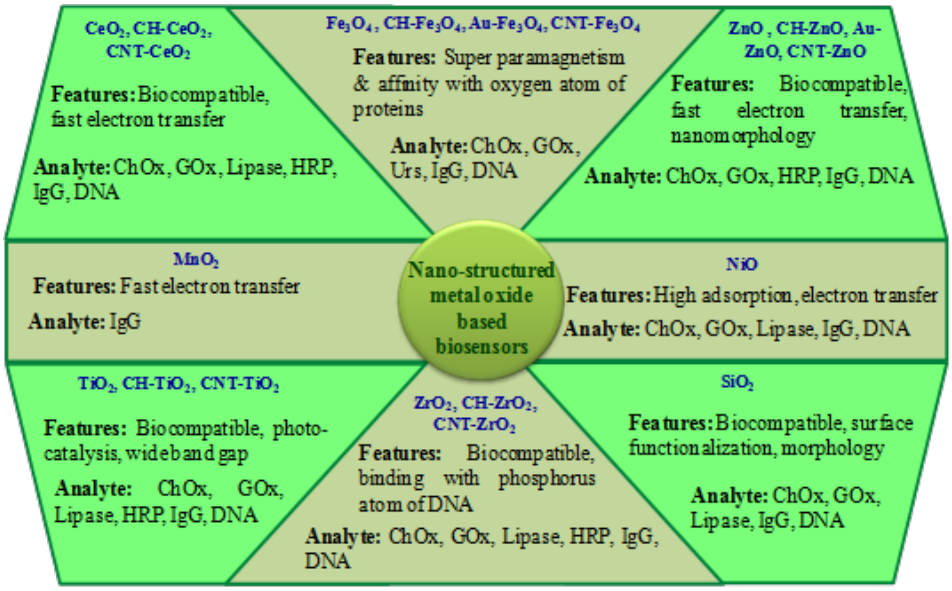

Figure 1. Properties of some NSMOs used for the fabrication of biosensors.

2. Importance of NSMOs for biosensing

Biosensor is based on the interaction of a biomolecule in conjunction with an electrode where the redox reaction could be monitored electrochemically by measurement of the loss or formation of a substrate or product, by the use of a small mediator species that shuttles between the biomolecule and the electrode, or less commonly by direct electron transfer (ET) between biomolecule redox site and the electrode. Direct ET can be difficult to achieve, since the redox site of a biomolecule is often hidden deep inside the biomolecule. Recent advances in achieving direct ET have been made by the modification of biomolecules or electrode surface through the use of novel NSMO as a mediator and the design of functional biointerface (Figure 2), which has extended throughout the field of bioelectrochemistry [16-19].

The NSMOs have recently become important as immobilization matrices for the fabrication of biosensors, as they provide excellent optical and electrical properties due to electron and phonon confinement, high surface-to-volume ratio, high surface reactivity and catalytic activity along with strong adsorption ability resulting in enhanced sensing characteristics. The adsorption of biomolecules directly onto the bare surface a of bulk material may frequently result in their denaturation and loss of bioactivity. However, the adsorption of such biomolecules onto a given NSMO surface may perhaps retain the bioactivity because of the non-toxicity NSMO and their biocompatible composites with carbon nanotubes (CNT), chitosan (CHIT) etc using electrostatic and other interactive forces.

The interface formed between an NSMO and a biomolecule is of utmost importance as the surface area, surface energy, roughness, porosity etc. affect the performance of a biosensor. So, the judicious selection of NSMO is the key success for the development of an effective biosensor [20].

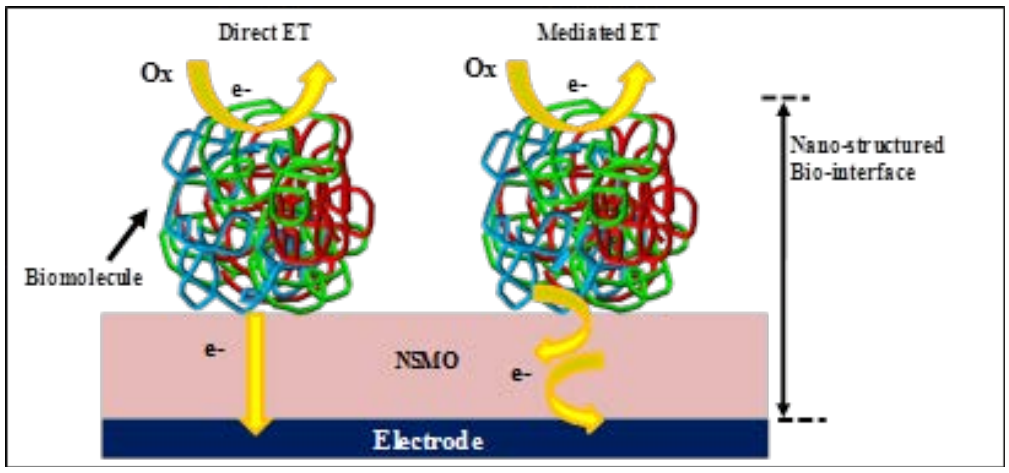

Figure 2. Scheme of ET process of nanostructured bio-interfaces on the electrode surface.

An effective NSMO biointerface helps a biomolecule, to retain its biological activity with high stability by establishing a biocompatible microenvironment, and also faster rate of electron transfer. There is thus, a considerable opportunity for the development of biosensors with improved sensitivity and detection limits, as well as lower cost and extended shelf life, through the use of NSMOs.

3. Electrochemical DNA biosensor using nano-structured biocompatible ZrO_2 based matrices

Fascinating electrochemistry and unique hybridization behaviour of desired nucleic acid and the excellent prospects for interfacial biological recognition event with electronic signal transduction using NSMOs, has stimulated much interest for designing new generation bioelectronic devices that may exhibit novel applications especially in the field of DNA biosensors. The high sensitivity, specificity for target analyte, faster response, ability to operate in turbid or colored solutions, easy handling, low cost, compatibility with micro-fabrication technology and portability has aroused increased interest for the fabrication of DNA biosensors [21-23].

For the fabrication of an electrochemical DNA biosensor, immobilization of DNA onto a nanocrystalline transparent metal oxide based matrices like ZrO_2 have drawn considerable attention due to their unique physical, chemical, and optical properties that make them promising matrices for sensing applications. Moreover, the nanostructures provide increased surface area for DNA immobilization that may lead to the improved limit of detection. Besides this, it is found to be thermally stable, chemically inert, non-toxic, and has affinity for groups containing oxygen that facilitates covalent immobilization of biomolecules without using any cross-linker that may limit sensitivity of a biosensor. The biocompatibility of ZrO_2 is anticipated to offer conducive environment to the fabricated biosensor which may perhaps result in enhanced stability and reusability.

Solanki et.al have utilized sol–gel-derived nano-structured ZrO_2 film for immobilization of 17-base ssDNA identified from the 16srRNA coding region of *Escherichia coli*. This bioelectrode exhibits high selectivity and sensitivity for hybridization, with linearity in the range of 10^{-6} to 10^{6} pM of complementary DNA [24]. *Zuo et al.* have fabricated a DNA biosensor by immobilizing ssDNA with a terminal 5'-phosphate group to a ZrO_2 surface utilizing the strong affinity between the oxygen atoms of the phosphoric group and zirconium. This biosensor has been found to have high sensitivity and selectivity for hybridization detection (≤20 nM complementary DNA) [25]. Yang et al. have fabricated a DNA biosensor using a composite comprising of Nano ZrO_2-CNT-CHIT and observed

that the bioelectrode can effectively detect the complementary DNA 1.49×10^{-10} – 9.32×10^{-8} using differential pulse voltammetry [26].

Inspired by the characteristics of nano ZrO_2, *Das et.al* have fabricated electrochemical DNA biosensor for *M. tuberculosis* detection using nano-structured ZrO_2, from an aqueous solution of zirconium oxychloride ($ZrOCl_2$) onto gold coated glass plate (Au) (Figure 3). They have observed that ssDNA-NanoZrO_2/Au electrode can detect target analyte from 640-0.065 ng.μL^{-1}, with lower detection limit of 0.065 ng.μL^{-1}(20nM) and 1 ng.μL^{-1} for genomic DNA indicating that it can be used for rapid and early detection of *M. tuberculosis* [27].

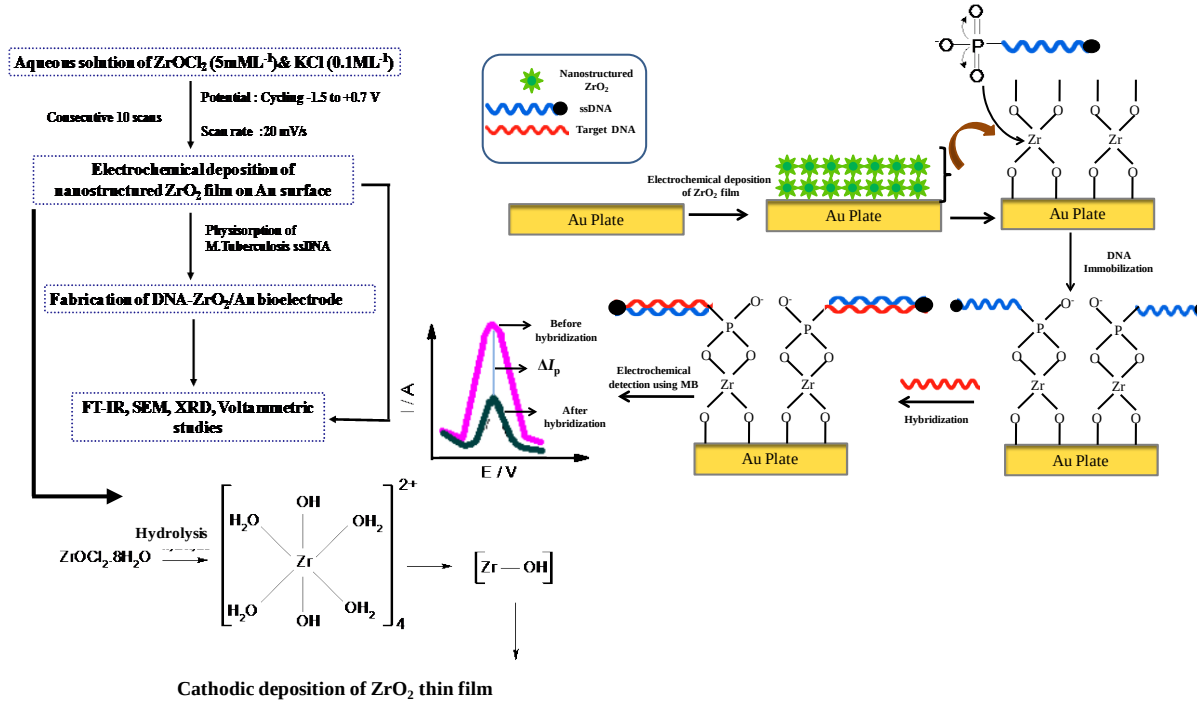

Figure 3. Proposed schematic for the fabrication of NanoZrO_2/Au based DNA biosensor.

In spite of being an interesting matrix for biomolecule immobilization, nano-structured ZrO_2 based electrode suffers from the problems of cracking and aggregation leading to limited application of ZrO_2 nanoparticles to biosensing. This problem can perhaps be addressed by modifying ZrO_2 nanoparticles with CHIT. CHIT has been found to be an interesting biopolymer for immobilization of biomolecules because of its excellent film-forming ability, high permeability, biocompatibility, low cost etc. Moreover, chemical modification of amino groups of CHIT provides hydrophilic environment for the biomolecules. *Feng et al.* have reported nanoporous CeO_2/CHIT composite film as the immobilization matrix for fabrication of electrochemical DNA biosensor for colo-rectal cancer detection [28]. This biocomposite matrix can be used for increased loading of probe DNA to obtain enhanced biosensor response. *Kaushik et al.* have developed a nucleic acid sensor based on Fe_2O_3/CHIT hybrid matrix for pyrethroid detection [29].

We have proposed chitosan-zirconium-oxide (CHIT-NanoZrO_2) nanocomposite, deposited via electrophoretic deposition of onto indium-tin-oxide(ITO) coated glass plate from a colloidal suspension of CHIT-NanoZrO_2 in acetonitrile, to reveal its application in DNA biosensor for *M. tuberculosis* detection. Efforts have been directed to propose a mechanism for the electrophoretic deposition of CHIT-NanoZrO_2 colloidal particles onto given ITO plate in presence of DC electric field. A key characteristic of CHIT, used for the preparation of CHIT-NanoZrO_2 composite film fabrication, is its unique response to applied electrical stimuli. When applied voltage is sufficient for protons to be

reduced at the cathode surface, a localized pH gradient is generated, resulting in cathodic electrodeposition of thin CHIT-NanoZrO_2 film (180 nm) with ZrO_2 molecules entrapped within CHIT chains due to strong electrostatic interactions between these oppositely charged moieties [30].

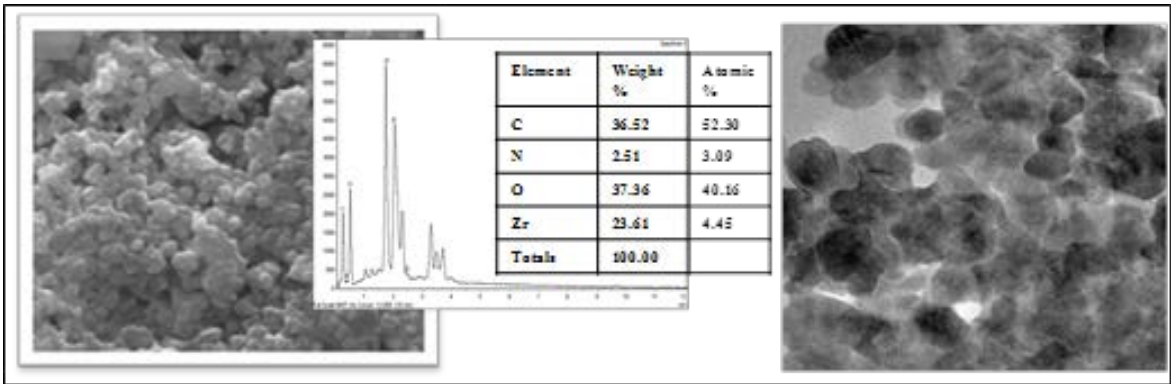

Figure 4. SEM and TEM analysis of CHIT-NanoZrO_2 composite

The morphological studies carried out using SEM and TEM techniques clearly reveal incorporation of the hexagonal grains of ZrO_2 (30-50 nm) in the amorphous network of CHIT (Figure 4). Interestingly, the nano grained ZrO_2 have been found to be inter-linked and well-dispersed into the CHIT matrix, corroborating the homogeneous nanobiocomposite formation. This has been attributed to electrostatic interactions between cationic CHIT and surface charged ZrO_2 nanoparticles. The DNA/CHIT-NanoZrO_2/ITO bioelectrode, fabricated by covalent immobilization of biotinylated probe DNA specific to *M. tuberculosis* onto this nanobiocomposite matrix, has been found to be selective and can detect complementary target up to 0.78 nM with sensitivity of 6.38×10^{-6} A μM^{-1}.

Contemporary interest in metal and metal oxide/CNT composites stems from their utilization as an emitter in field emission displays, a thermal interface material, a super capacitor, interconnects in large scale integrated circuits etc [31-32]. Keeping in view, the advantages of CNT-metal oxide composites in various emerging fields, there is an augmented interest in exploring the synergy of electroactive CNT and biocompatible metal oxides in the potential field of biomolecular electronics. In this context, bio-functional devices based on CNT/ZrO_2 nanocomposites have recently gained much attention [33-35]. In the fabrication of a biosensing device composed of CNT/ZrO_2, the thickness and the morphology of the ZrO_2 coating is considered to play a critical role. The uniform, dense pin-hole free thin coating provides large surface area that can be useful for biosensor applications. In this context, electrophoretic technique has achieved much interest for deposition of the uniform, dense and electrochemically reversible films from colloidal suspension [36]. In addition, this technique provides a unique strategy to prepare nano-patterned composite film with nanoporosity and densely packed structure with controlled thickness and morphology.

Electrophoretic deposition of ZrO_2 grafted CNT, has been obtained by *Das et al.* via isothermal hydrolysis of zirconium oxychloride ($ZrOCl_4$) in presence of CNT, onto ITO coated glass plate (Figure 5). The structural characterization of this nanocomposite (Figure 6) divulge that there is transition of crystal structure of ZrO_2 from its pristine monoclinic to deviated monoclinic arrangement with increased unit cell volume of 163 $Å^3$. The high resolution TEM and SEM studies reveal that the ZrO_2 is present in and around the nanotubes resulting in deviated monoclinic crystalline arrangement having crystallite size of 28.63 nm. The change in the crystalline structure provides increased surface area to immobilize the biomolecules required for the fabrication of an effective biosensor.

Based on this idea, an impedimetric genosensor (ssDNA-NanoZrO_2-CNT/ITO) is fabricated by *in-situ* entrapment of 21-mer DNA probe specific to *Mycobacterium tuberculosis* [37].

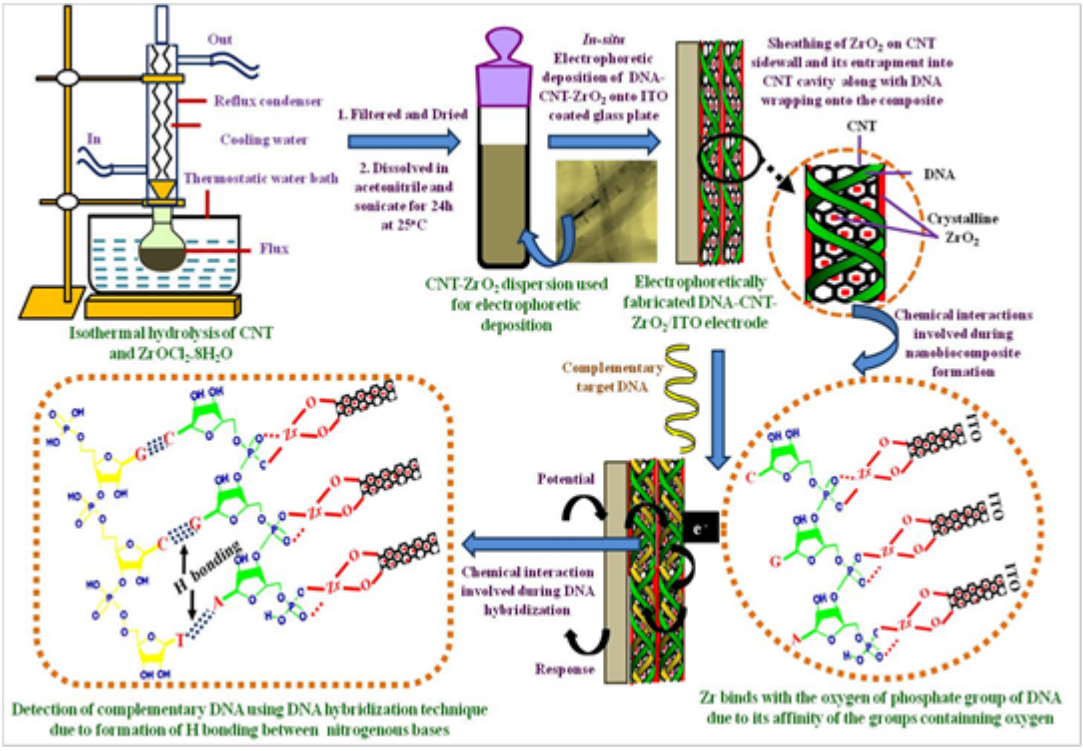

Figure 5. Electrophoretic fabrication of CNT/ZrO_2 nanocomposite and the interaction between DNA and the nanocomposite.

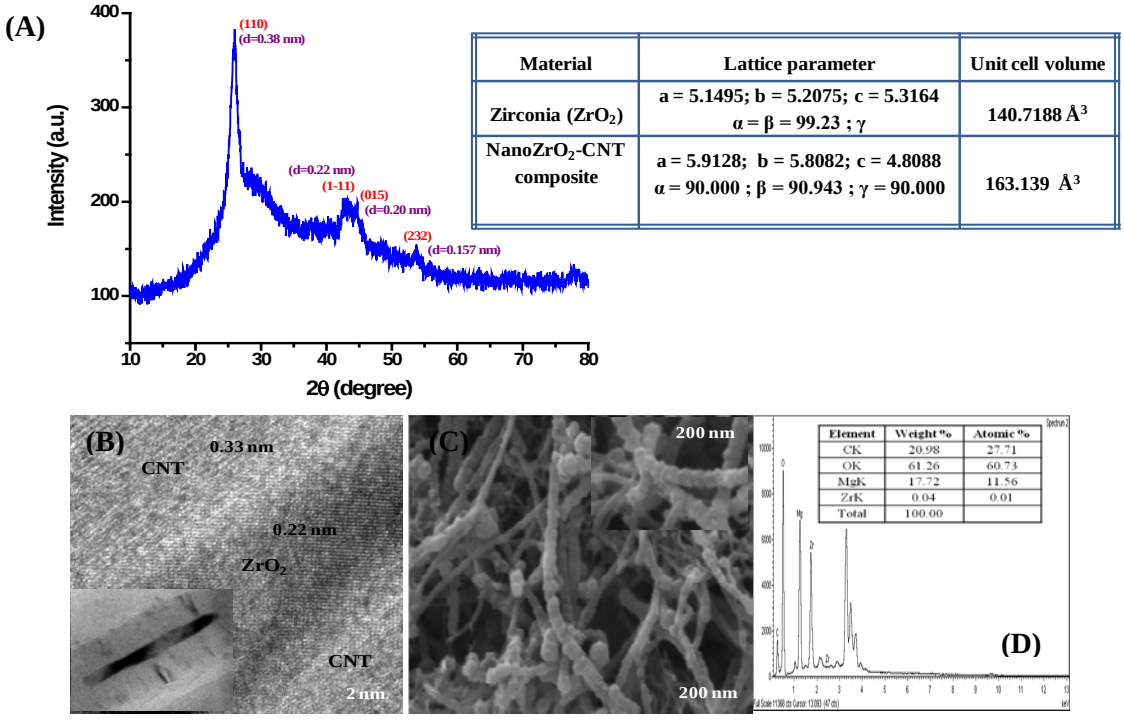

Material	Lattice parameter	Unit cell volume
Zirconia (ZrO_2)	a = 5.1495; b = 5.2075; c = 5.3164 α = β = 99.23 ; γ	140.7188 Å^3
NanoZrO_2-CNT composite	a = 5.9128; b = 5.8082; c = 4.8088 α = 90.000 ; β = 90.943 ; γ = 90.000	163.139 Å^3

Element	Weight %	Atomic %
CK	20.98	27.71
OK	61.26	60.73
MgK	17.72	11.56
ZrK	0.04	0.01
Total	100.00	

Figure 6. (A) XRD; (B) TEM ; (C) SEM and (D) EDX pattern of NanoZrO_2-CNT composite.

The ssDNA-NanoZrO_2-CNT/ITO electrode is capable of detecting DNA hybridization process by showing the variation in charge transfer resistance (R_{CT}) obtained from the diameter of the semicircle of the Nyquist plot. The results of DNA hybridization with the complementary target DNA strands reveal wider detection range of target DNA concentration (1×10^{-2} mM to 1×10^{-8} mM) and exhibit detection limit as low as 1×10^{-8} mM or 0.01 nM with storage stability of 24 weeks.

Table 1 exhibits the various biosensing characteristics obtained for the fabrication of DNA biosensors for *M. tuberculosis* detection using ZrO_2 and its composite by *Das et al*.

Table 1. Various biosensing parameter obtained using ZrO_2 and its composite with CHIT and CNT

Biosensing characteristics / Matrix	Film fabrication method	Detection limit	Reusability	Stability
NanoZrO_2	**Electrochemical**	**20 nM**	**10-12 times**	**16 weeks**
NanoZrO_2-CHIT	**Electrophoretic**	**0.78 nM**	**10-12 times**	**18 weeks**
NanoZrO_2-CNT	**Electrophoretic**	**0.01 nM**	**~ 15 times**	**24 weeks**

4. Conclusions

With the rapid emergence of nanotechnology, hybrid bio/nanostructures with well-defined morphologies have been popularly employed to modern materials science. Capitalizing the properties of NSMOs, novel composite nano-scale materials have opened up a new horizon in materials science with a synergistic effect of the individual components. The highly sensitive detection protocol for the fabrication of biosensor using NSMOs especially with ZrO_2, suggest that future interdisciplinary research is likely to lead to a new generation of electrochemical biosensors for the detection of infectious agent in an early stage.

References

[1] Gooding J J 2006 *Small* **2** 313
[2] Caruso F 2001 *Adv. Mater.***13** 11
[3] Rosenholm J M, Meinander A, Peuhu E, Niemi R, Eriksson J E, Sahlgren C and Linden M 2009 *ACS Nano* **3** 197
[4] Ghadiali J E and Stevens M M 2008 *Adv. Mater.* **99** 1
[5] Forzani E S, Zhang H Q, Nagahara L A, Amlani I, Tsui R and Tao N J 2004 *Nano Lett.* **4** 1785
[6] Wang J X, Sun X W, Wei A, Lei Y, Cai X P, Li C M and Dong Z L 2006 *Appl. Phys. Lett.* **88**, 233106.
[7] Liu Z, Liu Y, Yang H, Yang Y, Shen G and Yu R 2005 *Electroanalysis* **17** 1065
[8] Wei H and Wang E 2008 *Anal. Chem.* **80** 2250
[9] Kim H J, Yoon S H, Choi H N, Lyu Y K and Lee W Y 2006 *Bull. Korean Chem. Soc.***27** 65
[10] Xiao X, Luan Q, Yao X and Zhou K 2009 *Biosens. Bioelectron.* **24** 2447
[11] Feng K J, Yang Y H, Wang Z J, Jiang J H, Shen G L and Yu R Q 2006 *Talanta* **70** 561
[12] Hook F, Kasemo B, Grunze M and Zauscher S 2008 *ACS Nano* **2** 2428
[13] Hu c and Hu S 2009 *J. Sens.* **1** 1
[14] Nel A E Mädler L, Velegol D, Xia T, Hoek Eric M V, Somasundaran P, Klaessig F, Castranova V and Thompson M 2009 *Nat. Mater*. **8** 543
[15] Rahman M M, Ahammad A J S, Jin J H, Ahn S J and Lee J J 2010 *Sensors* **10** 4855
[16] Katz E, Willner I and Wang J 2004 *Electroanalysis* **16** 19
[17] Hartmann M 2005 *Chem. Mater.* **17** 4577
[18] Herna´ndez-Santos D, Gonzalez-Garcıa M B and Garcıa A C 2002 *Electroanalysis* **14** 1225

[19] Wang J 2005 *Electroanalysis* **17** 7
[20] Solanki P R, Kaushik A, Agrawal V V and Malhotra B D 2011 *NPG Asia Mater.* **3** 17
[21] Vaníková M, Lehotay J, Imárik J and Labuda J 2005 *Bioelectrochemistry* **66** 125
[22] Palecek E andFojta M 2001 *Anal. Chem.* **73** 74A
[23] Burda C, Chen X, Narayanan R and El-Sayed M A 2005 *Che.Rev.* **105** 1025
[24] Solanki P R, Kaushik A, Chavhan P M, Maheshwari S N and Malhotra B D 2009 *Electrochem. Commun.* **11** 2272
[25] Zuo S-H, Zhang L F, Yuan H H, Lan M B, Lawrance G A and Wei G 2009 *Bioelectrochemistry* **74** 223
[26] Yang Y, Wang Z, Yang M, Li J, Zheng F, Shen G and Yu R 2007 *Anal. Chim. Acta.* **584** 268
[27] Das M, Sumana G, Nagarajan R and Malhotra B D 2010 *Appl.Phs. Lett.* **96** 133703
[28] Feng K J, Yang Y H, Wang Z J, Jiang J H, Shen G L and Yu R Q 2006 *Talanta* **70** 561
[29] Kaushik A, Solanki P R, Ansari A A, Malhotra B D and Ahmad S 2009 *Biochem. Eng. J.* **46** 132
[30] Das M, Dhand C, Sumana G, Srivastava A K, Nagarajan R, Nain L, Iwamoto M, Manaka T and Malhotra B D 2011 *Biomacromolecules* **12** 540
[31] Weizmann Y, Chenoweth D M and Swager T M 2011 *J. Am. Chem. Soc.***133** 3238
[32] Nugent J M, Santhanam K S V, Rubio A and Ajayan P M 2001*Nano Lett.* **1** 87
[33] Kim I H, Kim J H, Cho B W, Lee Y H and Kim K B J 2006 *Electrochem. Soc.***153** A989
[34] Brasse G, Restoin C, Soule D and Blondy J M 2011 *J. Phys.Chem.C.* **115** 248
[35] Meighan M M, Vasquez J, Dziubcynski L, Hews S and Hayes M A 2011 *Anal. Chem.* **83** 368
[36] Tada K and Onoda M *Adv Funct Mater.*, 2002 **2** 420
[37] Das M, Dhand C, Sumana G, Srivastava A K, Vijayan N, Nagarajan and Malhotra B D 2011 *Appl.Phy. Lett.* **99** 143702

PERFORMANCE EVALUATION OF IMAGE COMPRESSION TECHNIQUES

Vinod Kumar, Asheesh Kumar, Abhishek Bhardwaj
Dept of computer Engineering Delhi Technological University
(Formerly Delhi College of Engg.), Delhi, India

ABSTRACT

The purpose of image compression is to achieve a very squat bit rate representation, while preserving a soaring visual quality of decompressed images. Compression reduces the storage and finds its potency and limitations. Transmission burdens of raw information by reducing the ubiquitous redundancy without losing its entropy significantly. The image manipulation that occupies a significant position in multimedia technology necessitated the development of JPEG compression technique, which has proved its usefulness until recently; to minimize the blocking artifact, inherently present in JPEG at higher compression ratios. In this work, a new approach to JPEG compression technique is proposed that enhanced the compression performances in comparison with aforesaid JPEG techniques. The new technique considers DCT, SVD, and BTC. A rigorous comparison of the various compressions through quality components (PSNR, MSE).

Keywords

Discrete cosinetransform (DCT), Singular Value Decomposition (SVD), Block Truncation Code (BTC), Standard Deviation (STD).

I.INTRODUCTION

Now a day, the usage of digital image in various applications is growing rapidly. Video and television transmission is becoming digital and more and more digital image sequences are used in multimedia applications. A digital image is composed of pixels, which can be thought of as small dots on the screen and it becomes more complex when the pixels are colored[6]. An enormous amount of data is produced when a two dimensional light intensity function is sampled and quantized to create a digital image. In fact, the amount of data generated may be so great that it results in impractical storage, processing and communications requirements. Image compression addresses the problem of reducing the amount of data required to represent a digital image. It is a process intended to yield a compact representation of an image, thereby reducing the image storage/transmission requirements.[1] A common characteristic of most images is that the neighboring pixels are interrelated and therefore contain redundant information. The foremost task then is to find less correlated representation of the image. Two fundamental components of compression are redundancy and irrelevancy reduction.

Redundancies reduction aims at removing duplication from the signal source (image/video).

Irrelevancy reduction omits parts of the signal that will not be noticed by the signal receiver, namely the Human Visual System.

In this work, the two main compression techniques, SVD and BTC associates DCT in JPEG as baseline coding system .A careful comparison of proposed method with the existing one is made to find its potential and limitation.

II. DCT IN COMPRESSION

The Discrete Cosine Transform (DCT) attempts to decorrelate the image data. After decorrelation each transform coefficient can be encoded independently without losing compression efficiency.

The following is a general overview of the JPEG process.

1. The image is broken into 8x8 blocks of pixels.
2. Working from left to right, top to bottom, the DCT is applied to each block.
3. Each block is compressed through quantization.
4. The array of compressed blocks that constitute the image is stored in a drastically reduced amount of space.
5. When desired, the image is reconstructed through decompression, a process that uses the Inverse Discrete Cosine transform

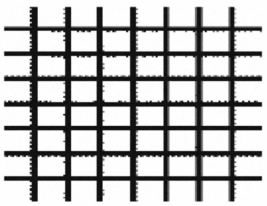

Fig.1 The basic function of 8x8 matrix.

II.a THE DCT EQUATION

The DCT equation (Eg. 1) computes the i, j^{th} entry of the DCT of an image.

$$D(i,j) = \frac{1}{\sqrt{2N}} C(i)C(j) \sum_{x=0}^{N-1} \sum_{y=0}^{N-1} p(x,y) \cos\left[\frac{(2x+1)i\pi}{2N}\right] \cos\left[\frac{(2y+1)j\pi}{2N}\right] \quad 1$$

$$C(u) = \begin{cases} \frac{1}{\sqrt{2}} & \text{if } u = 0 \\ 1 & \text{if } u > 0 \end{cases} \quad 2$$

P(x, y) is the x, yth elements of the image represented by the matrix p.N is the Size of the block that the DCT is done on. The equation calculates one entry of the transformed image from the Pixel value Of Original image Matrix. For the Standard 8x8 block that JPEG Compression uses N equals 8 and x & y range from 0 to 7.

$$D(i,j) = \frac{1}{4} C(i)C(j) \sum_{x=0}^{7} \sum_{y=0}^{7} p(x,y) \cos\left[\frac{(2x+1)i\pi}{16}\right] \cos\left[\frac{(2y+1)j\pi}{16}\right] \quad 3$$

Because the DCT use cosine functions, the resulting matrix depends on the horizontal, diagonal, and vertical frequencies[3]. Therefore and image black with a lot of change in frequency has a very random looking resulting matrix, while and image matrix of just one color, has a resulting matrix of a large value for the first element and zeroes for the other elements.

$$T_{ij} = \begin{cases} \frac{1}{\sqrt{N}} & \text{if } i = 0 \\ \sqrt{\frac{2}{N}} \cos\left[\frac{(2j+1)i\pi}{2N}\right] & \text{if } i > 0 \end{cases} \quad 4$$

it should be noted that the pixel values of a black & white image range from 0 to 255 in step of 1, where pure black is represented by 0 and pure white by 255. Thus it can be seen how a photo, illustration etc. can be accurately represented by these 256 shades of gray.

III. SVD IN COMPRESSION

Image compression is achieved by using Singular Value Decomposition (SVD) technique on the image matrix. The advantage of using the SVD is the property of energy compaction and its ability to adapt to the local statistical variations of an image. Further, the SVD can be performed on any arbitrary, square, reversible and non reversible matrix of m x n size.[8]

Singular Value Decomposition (SVD) is said to be a significant topic in linear algebra by many renowned mathematicians. SVD has many practical and theoretical values; Special feature of SVD is that it can be performed on any real (m, n) matrix. Let's say we have a matrix A with m rows and n columns, with rank r *and* $r \leq n \leq m$. Then the A can be factorized into three matrices:

$$A = USV^T \quad 5$$

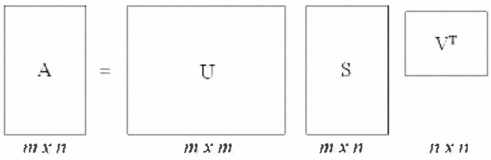

FIGURE 2. Illustration of Factoring *A* to *USV*^{t}

Actually, calculation of SVD consist of finding the Eigen Values & Eigen vector of AA_H & A_HA .Eigen vector of AA_H make up the columns of U & A^HA make up the columns of V. The Eigen Value of A^HA or AA_H is the squares of the singular values for A.

VI. BTC IN COMPRESSION

Block Truncation Coding (BTC) is a well-known compression scheme proposed in 1979 for the grayscale images. It was also called the moment-preserving block truncation [2]-[4] because it preserves the first and second moments of each image block. The BTC algorithm involves the following steps:[7]

• **Step1**: The given image is divided into non overlapping rectangular regions. For the sake of simplicity the blocks were let to be square regions of size m x m.

• **Step 2**: For a two level (1 bit) quantizer, the idea is to select two luminance values to represent each pixel in the block. These values are the mean x and standard deviation σ.

$$\bar{x} = \frac{1}{n} \sum_{i=1}^{n} x_i \quad 6.$$

$$\sigma = \sqrt{\frac{1}{n} \sum_{i=1}^{n} (x_i - \bar{x}_i)^2} \quad 7.$$

Where x_i represents the i^{th} pixel value of the image block and n is the total number of pixels in that block.

• **Step3**: The two values x and σ are termed as quantizers of BTC. Taking $\bar{x}$ as the threshold value a two-level bit plane is obtained by comparing each pixel value x_i with the threshold. A binary block, denoted by B, is also used to represent the pixels. We can use "1" to represent a pixel whose gray level is greater than or equal to $\bar{x}$ and "0" to represent a pixel whose gray level is less than $\bar{x}$

$$B = \begin{cases} 1 & x_i \geq \bar{x} \\ 0 & x_i \prec \bar{x} \end{cases} \qquad 8.$$

By this process each block is reduced to a bit plane. For example, a block of 4 x 4 pixels will give a 32 bit compressed data, amounting to 2 bit per pixel (bpp).

• **Step 4**: In the decoder an image block is reconstructed by replacing '1's in the bit plane with H and the '0's with L, which are given by:

$$H = \bar{x} + \sigma\sqrt{\frac{p}{q}} \qquad 9.$$

$$L = \bar{x} - \sigma\sqrt{\frac{q}{p}} \qquad 10.$$

Where p and q are the number of 0's and 1's in the compressed bit plane respectively.

V.PURPOSED WORK

In this work, a new approach to image compression technique is projected that enhanced the compression performance, the two main compression techniques, SVD and BTC associates DCT in JPEG. In this approach we select the compression technique on the decision parameter of the image .In this work the decision parameter of image is its Standard Deviation (STD).

V.a PROPOSED TECHNIQUE

The proposed algorithm incorporates DCT, SVD and BTC compression techniques. Depending on the image properties a simple decision making criterion is choose. The decision making criterion is based on the observation of standard deviation (STD) of the source STD of an image is larger when it has many abrupt changes in intensity than when the image has Smoothly varying intensity. The technique is based on the following algorithm.

1. Input an image which is processed according to the selected compression technique and selection based on the STD of the image.

2. The STD of current image is computed and for the compression technique if STD is lesser than the decision making parameter, the DCT is used to compute the transform coefficients. Conversely if the standard deviation is more than the decision making parameter the SVD transform is used. However if the STD is lying between 35 to 45 then BTC is used even though the results of compression for BTC depends on the block size of image here we are considering to be 8x8. This is done because DCT is computationally efficient and achieves good performance for images characterized by high correlation. In contrast, SVD provides optimal energy packing efficiency for less correlated images.
3. The image quality factors are given as the output.

VI. IMAGE QUALITY MEASUREMENTS

In objective measures of image quality metrics, some statistical indices are calculated to indicate the image quality. In our work we will focus in objective measures such as Peak Signal to Noise Ratio (PSNR) and mean square error (MSE).
The PSNR is most generally used as a measure of excellence of reconstruction of lossy compression .It is an striking measure for the loss of image quality due to its simplicity and mathematical convenience .Peak signal-to-noise ratio (PSNR) is a qualitative measure based on the mean-square-error of the reconstructed image .If the reconstructed image is quite similer to the original image, then MSE is small and PSNR takes a large value .PSNR is dimensionless and is expressed in decibel .Peak Signal-to-Noise Ratio (PSNR) avoids this problem by scaling the MSE according to the image range .PSNR is defined as follow:

$$MSE = \frac{1}{MN}\sum_{i=1}^{M}\sum_{j=1}^{N}\left[y(i,j) - x(i,j)\right]^2$$

$$PSNR = 10 \log\left(\frac{L^2}{MSE}\right)$$

Where L is the dynamic range of the pixel values (255 for 8-bit grayscale images).

VII. EXPERIMENTAL RESULTS

VII.I INPUT IMAGE-LENA.BMP

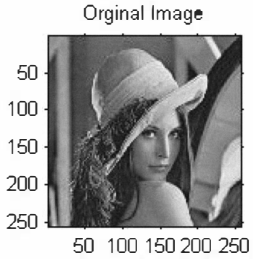

Algorithm	PSNR	MSE	SD
DCT	30.70271	55.31073	52.59425
SVD	33.97248	26.0515	52.59425
BTC	30.08119	63.82063	52.59425

VII.II. INPUT IMAGE-HRITHIK.BMP

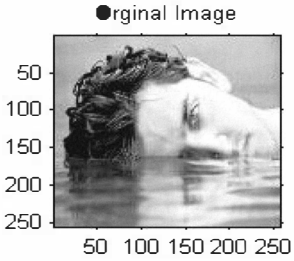

Algorithm	PSNR	MSE	SD
DCT	31.86982	42.27641	69.02297
SVD	38.79564	8.580566	69.02297
BTC	30.73738	54.87093	69.02297

VII.III. INPUT IMAGE-CIRCLE.BMP

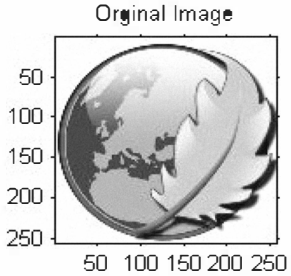

Algorithm	PSNR	MSE	SD
DCT	29.3267	75.92943	66.34601
SVD	33.07188	32.05476	66.34601
BTC	28.8524	84.69154	66.34601

VIII. CONCLUSION

The analysis, of all the obtained experimental results, demonstrates that the incorporation of SVD and BTC in image compression along with DCT in an adaptive manner enhances the compression performance significantly. The proposed technique perform perform the best technique in terms of PSNR and MSE. But it requires slightly longer time that makes it suitable for large bandwidth channel only.In this research compression technique is selected on the basis of its standard deviation used as decision parameter for compression. Compression techniques other then wavelet transformation can be divided as SVD for the image having large standard deviation (greater than 45). If the standard deviation lies between 35 to 45 BTC compressions is selected and lesser standard deviation DCT is selected.

REFERENCES

1. K. Ramchandran, A. Ortega, K. Metin Uz, and M. Vetterli, "Multiresolution broadcast for digital HDTV using joint source/channel coding." *IEEE Journal on Selected Areas in Communications*, 11(1):6–23, January 1993.

2. M. W. Garrett and M. Vetterli, "Joint Source/Channel Coding of Statistically Multiplexed Real Time Services on Packet Networks," *IEEE/ACM Transactions on Networking*, 1993.

3. S. McCanne and M. Vetterli, "Joint source/channel coding for multicast packet video," International Conference on Image Processing (Vol. 1)-Volume 1, October 1995, Washington D.C.

4. K. Sayood and J. C. Borkenhagen, "Use of residual redundancy in the design of jointsource/channel coders," *IEEE Transactions on Communications*, 39(6):838-846, June
1991.

5. E. J Delp., Saenz, M., and Salama, P., 2000, Block Truncation Coding (BTC), Handbook of Image and Video Processing, edited by Bovik A. C., Academic Press, pp. 176-181.

6. Tinku Acharya, Ajoy.K.Ray, "IMAGE PROCESSING –Principles and Applications", Hoboken, New Jersey, A JOHN WILEY & SONS, MC. , Publication, 2005.

7. Doaa Mohammed,"Image compression using BTC", "*Multidisciplinary Journal in Science & technology, JSAT, Feb 2011".*

8. Nusrat Ahmed Surobhi, "Amalgamation of SVD to JPEG for Enhanced performance, "*International conference on Information & communication Technology-2007*".

Sensor architecture allows real-time auto emissions monitoring, Pt. 1

Ravindra Arora, Manmohan Rana, and Sunil Deep Maheshwari Freescale Semiconductor

4/12/2012 12:03 AM EDT

As opposed to current periodic emission-control system testing—sensors, MCUs, and memory come together in an updated approach to real-time exhaust monitoring for improved pollution control.

"Green" is the buzzword these days. Globally, various organizations are striving to make their processes as eco-friendly as possible, with the automotive industry one of the leaders in this endeavor.

Vehicle-emissions are being strictly monitored and emission-norms being revised regularly to ensure a "greener" and pollution-free environment. However, present vehicle pollution-checking is still dependent on old mechanisms of manual-regular-checking of the auto-exhaust. The exhausts are sensed and analyzed by a machine and a pollution certificate is issued.

This article highlights inherent limitations of this traditional approach and proposes a real-time exhaust monitoring solution to enforce better pollution control for a greener future."

The challenges of emission pollution control
Probably, pollution is one of the biggest problems which humankind is facing today and the worst part is that the pollution has reached such a level that we have ourselves stuck in a vicious cycle of this evil and auto emission is one of the biggest contributors. Automobiles used worldwide produce vast amount of harmful exhausts including carbon dioxide, carbon monoxide, nitrogen oxides (NOX), and un-burned hydrocarbons. All these add to greenhouse gases and are significant contributors to global warming.

Taming this devil has become one of the biggest challenges for the governments worldwide. Adoption of cleaner fuels like compressed natural gas and commercial development of hydrogen-based automobiles is one of the priorities for many agencies. However, before we can reach such a long-term, fool-proof solution, probably the easiest and the cheapest solution is to keep the pollution emissions of the current automobiles in check.

In every country, the emission norms are regulated by the respective pollution control regulatory body. Vehicles are checked for their emissions and if exhaust is within the specified limit, a certificate might be issued for the vehicle, which may come with an expiry date. However, this system has its own loopholes—the system only checks for the emissions on the date of the test, not in between the two test dates. Also, the data is not under load conditions, which might change according to the age and condition of the vehicle. Besides, many factors like engine-tuning, adulteration of fuel, etc might increase the pollution temporarily and may move it to an unacceptable level.

Instead, we can have some mechanism in place which would signal the real-time pollution level data of the vehicle to the owner/driver and also, if required, to the monitoring and controlling authority (via wireless communication). This way, we can implement a rather strict pollution check regime.

In such a case, there might not be any need for regular pollution checks and issuance of vehicle fitness certificates. The authority may take appropriate action against repetitively defaulting vehicle/owners. This would ensure better upkeep of the vehicles and as a result, good upkeep of the environment! The rest of this article deals with the technical implementation of the above mentioned system/regime.

Proposed solution architecture

The basic blocks required for above mentioned real-time monitoring mechanism include: Profiling of the exhaust gases, conversion of this data into digital form, storing and processing the data, display of the result, and transmission of the data. Each of these blocks works together to generate the desired results. The micro-level architecture of the proposed solution is shown below. Discussion of the operation of the above mentioned blocks follows.

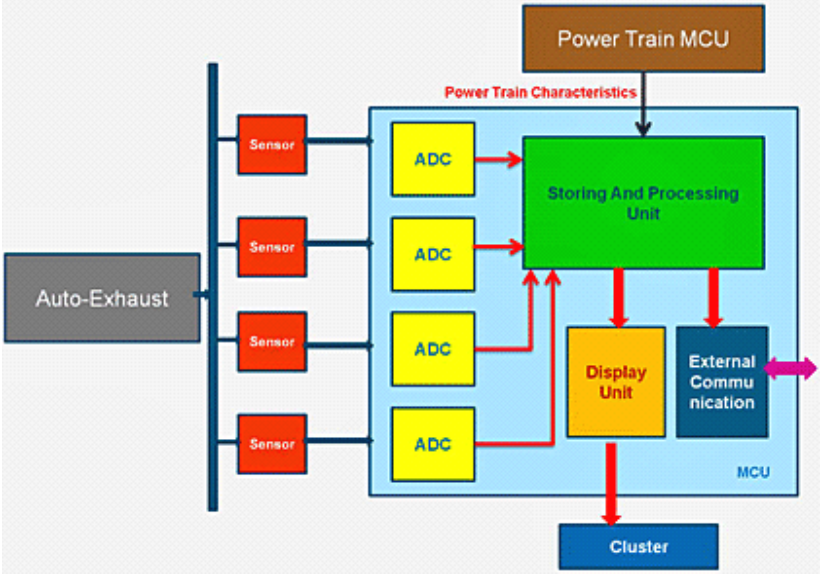

Profiling the exhaust gases

An array of sensors can be used to sense the amount of various components of the exhaust. These sensors would be giving real-time information of the exhaust components such as carbon monoxide, nitrous oxide, etc. The sensors can give either digital output or analog output.

If sensors with digital outputs are used, then they can be interfaced with some timer module of the MCU (microcontroller) to quantify the output. In case the sensors are of the analog output type, then the next mentioned block (converter, next page) would be used to make the output usable by the MCU.

Another alternative could be to use the data from the engine control and management unit (ECMU). This information could serve to replace the network of sensors. However, this method may suffer from relative inaccuracy because sensors directly sense the exhaust, and thus are able to give more accurate results as compared to the ECMU data. But again, that statement is based upon the assumption that the

array would give fairly accurate results and the fact that the array would be sitting right at the exhaust, sensing the real-time information.

Data conversion, storage, and processing and display controllers

Converting analog data to digital format

To enable the sensors' data to be processed by the MCUs, one needs to convert this data into digital format. ADCs (analog-to-digital converters) can be used to convert the sensors' output into digital format, making it easier for the processing unit to store and process it.

Given the type of application, one would not require constant or very frequent exhaust-profile data gathering. Therefore, one can easily multiplex various sensors' outputs on one or two ADCs so that each of them could be sampled one-by-one, therefore, saving the BOM (bill of material) of the solution.

One may also use those intervals when the MCU is not very active or when its ADCs are free to sample the sensors' output so that effective cost of the overall solution might be reduced. This way, data would be available as and when the core is free to process the data, on a lower priority basis. This way, higher MCU throughput can also be achieved.

For such a system, the overall accuracy of the solution would be heavily dependent upon the sensors accuracy and the performance of the ADCs.

Storage and processing unit

The storage and processing unit also becomes very important for systems which would be catering to this proposed solution on as-and-when-free basis. This approach would require one to have a processor of good processing speed and able to support various MAC (multiply and accumulate)/DSP instructions to quickly manipulate the pool of data required for this solution (which also includes data coming in from the power-train MCU giving the engine loading information).

Another point to note is that the pollution control and monitoring application is an additional feature being extracted out of almost the same already-being-used hardware. Therefore, this application would be sharing its memory space with the already existing applications. As a result, there would be an additional demand for memory to meet all the requirements.

Now adding such functions to the 'as-and-when-free' model of the application, one may be required to be more stringent with the access speed of the memory and more liberal with the on-chip memory. A situation may also arise where the on-chip memory is not sufficient for the needs of the overall system. Therefore, depending upon the already existing application requirement of the memory and the size of the data to be stored by the pollution control and monitoring unit, one may require additional amount of memory or interface for external memory along with fast access speed.

Without fast memory access, the whole calculations and report-generation may become a very slow operation. However, techniques like data pre-fetch from such an external memory might be able to overcome such limitations to a reasonable extent.

Display controllers

Display controllers are required to transmit data to the automobile dashboard/cluster so that the driver could take appropriate action. For example, if the pollution increased due to over-loading, the same can

be calculated using the data from the power-train MCU and displayed as a flag on the cluster so that loading could be decreased (see below). This visual sharing of information can be achieved in two ways—on-chip display drivers or interfacing this MCU with an external display controller using communication peripherals like I2C, SPI, SCI, Flexbus, Ethernet, USB, etc.

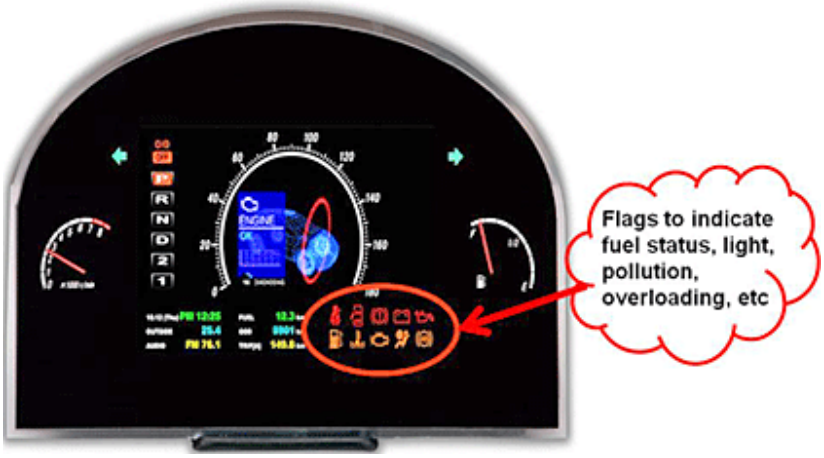

Part 2 of this series discusses communications between the emissions monitoring system and the driver, the sensor array, and future challenges.

References:

1. Inspection of Car's Emission Using Infrared Spectrum Technique, M Kong,Z Luo, Y Lu and W j Fan
2. http://www.vehicletest.state.ma.us/
3. http://www.implats.co.za/implats/Emission-standards.asp
4. http://www.theicct.org
5. http://lh3.ggpht.com/_SHPVwr-0FwA/SdYvlpbGPzI/AAAAAAAAA5s/k0mv_xc08wg/s800/96749.jpg

About the authors:

Ravindra Arora has worked at Freescale Semiconductor as senior design engineer for about six years. He has worked on automotive cluster and safety architecture MCUs. He earned his M.Tech (Instrumentation) from N.I.T Kurukshetra and B.Tech from R.E.C Kurukshetra (India).

Manmohan Rana has worked at Freescale as senior design engineer for about five years. He has worked on memory circuit design, analog and mixed signal design and simulation for various SoC architectures. He earned his BE (Electronics and Communications) from Delhi College of Engineering (Delhi University, India).

Sunil Deep Maheshwari has worked at Freescale as senior design engineer for about five years. He has worked on architectures ranging from motor control, power train, and metering to auto safety. He earned his BE (Electronics and Communications) from Netaji Subhas Institute of Technology (Delhi University, India).